Impact of green interventions on outdoor temperatures, indoor temperatures and energy usage across various building typologies

Master thesis

Joram Nottrot

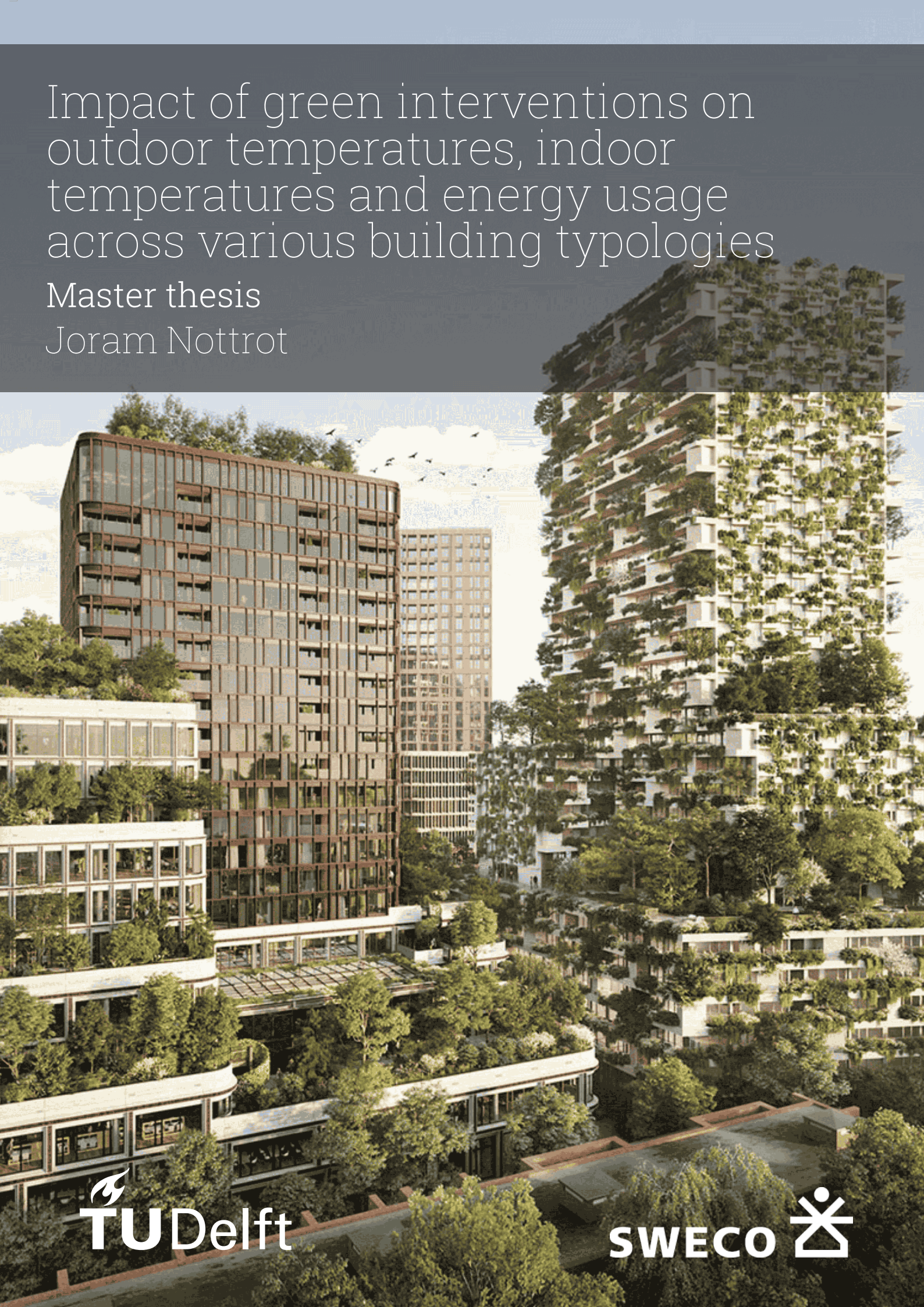

Impact of green interventions on outdoor temperatures, indoor temperatures and energy usage across various building typologies

by

Joram Nottrot

Student Name	Student Number
Joram Nottrot	4964551

Supervisors:	Arjan Droste & Marjolein van Esch & Henk Jonkers & Jart Ligterink (Sweco)
Project Duration:	February, 2025 - October, 2025
Faculty:	Faculty of Civil Engineering and Geosciences, Delft
Msc program:	Environmental Engineering
Track:	Atmospheric Environment Engineering

Cover:	Representation of Sweco office and residential building Wonderwoods Utrecht, Netherlands, source Wonderwoods development/Vero Digital

TU Delft

SWECO

Abstract

Rising global temperatures, combined with increasingly dense urban environments, raise concerns regarding outdoor thermal comfort and indoor liveability. As cities become warmer, both energy demand and health risks increase, urging the need for effective climate adaptation strategies. This thesis investigates how different green interventions affect outdoor and indoor temperatures in the Netherlands, and how these measures influence building cooling loads during heatwaves. Green interventions used in this study are trees, green roofs, green walls, shrubs, and grass. Within 10 m of the buildings, green is implemented to represent realistic opportunities for greening in private gardens and immediate surroundings. As a result, the simulated cooling effects reflect local-scale interventions rather than district-wide greening strategies. The Dutch heatwave from 23–27 August 2019 served as a reference event to assess three representative Dutch building typologies: low-rise, mid-rise, and high-rise.

A one-way coupled approach between an urban climate model (UCM) and a building energy model (BEM) is applied. For both the UCM and BEM, different model options were considered and compared. The selected models were then further evaluated against findings from literature to assess their suitability and accuracy. The outdoor microclimate was simulated with the ENVI-met model, which provides detailed outputs of air temperature, wind speed, and Physiological Equivalent Temperature (PET) at pedestrian height (1.5 m). Indoor thermal conditions and cooling energy demand were then evaluated using the building energy model IES-VE, with the microclimatic outputs from ENVI-met serving as boundary conditions. This coupling provides a more realistic estimation of the benefits of green infrastructure compared to building energy modelling that relies on standardised weather data.

The results show that the coupled ENVI-met–IES-VE framework successfully reproduced outdoor and indoor temperature reductions within the range reported in the literature, though typically at the lower end. This is expected, as the relatively small amount of greenery applied was intentionally chosen to isolate and quantify the local effect of greening around buildings. Among all interventions, trees produced the strongest cooling effect due to their shading capacity and evapotranspiration, with the largest impact observed when trees were combined with other types of greenery. Across all typologies, reductions of up to 1.17 °C in average outdoor air temperature, 3.92 °C in local maximum air temperature, and 13.45 °C in maximum PET were observed. Indoors, green interventions reduced peak air temperatures by up to 1.20 °C and cooling loads by as much as 32%. The relative effectiveness differed across building typologies: low-rise dwellings benefited most due to their closer interaction with the modified microclimate, whereas high-rise buildings showed more limited improvements.

This thesis provides a coupled UCM–BEM framework applicable to multiple Dutch building typologies, offering new insights into the role of vegetation in a temperate maritime climate. The modelling approach can be used to test different greening scenarios across building typologies. Future research should validate this framework with on-site measurements to further improve accuracy. Furthermore, combinations with shading devices and adaptive occupant behaviour should be explored in future research. The insights gained can guide municipalities, urban planners, and property owners in designing greener, more comfortable, and energy-efficient urban environments.

Preface

Before you lies my master thesis, "*Impact of green interventions on outdoor temperatures, indoor temperatures and energy usage across various building typologies*", which marks the completion of my Master of Science in Environmental Engineering at Delft University of Technology.

This research has been an inspiring and insightful journey. This allowed me to explore how vegetation influences the urban environment, deepening my understanding of the urban atmosphere while also teaching me much about myself and the way I work.

I would like to express my sincere gratitude to my supervisors, Arjan Droste, Jart Ligterink, Marjolein van Esch, and Henk Jonkers, for their expertise, constructive feedback, and encouragement throughout the process. Their enthusiasm and inspiring guidance have been invaluable.

I am also thankful to Sweco for giving me the opportunity to conduct my thesis within the organisation. The internship provided me with both a professional and enjoyable experience, and I am grateful to my colleagues for their support, the opportunities they provided me, and the many pleasant moments at the office. I would also like to thank all interviewees, whose input led to many insightful and inspiring conversations. My thanks further go to the Student IT Desk of Architecture for their practical assistance during this research.

On a more personal note, I want to thank my girlfriend, family, and roommates for their continuous support and my friends for all the memorable moments during my studies. A special word of thanks goes to Simon, with whom I shared countless hours of study and work. His companionship, together with all friends in the master's program, made this journey not only more productive but also much more enjoyable.

I hope that this thesis will, in its own way, contribute to creating greener and more sustainable living environments. Above all, I hope it inspires others to see the value of integrating nature into our built environment, helping us create cities that are resilient, healthy, and pleasant to live in.

Joram Nottrot
Delft, October 2025

Contents

List of Figures

List of Tables

Nomenclature

Abbreviations

Table 1: Table of abbreviations

Abbreviation	Definition
UHI	Urban Heat Island
SDG	Sustainable Development Goal
NAS	Nationale Klimaatadaptatie Strategie (Dutch National Climate Adaptation Strategy)
UCM	Urban Climate Model
BEM	Building Energy Model
PET	Physiological Equivalent Temperature (°C)
UCL	Urban Canopy Layer
UBL	Urban Boundary Layer
SEB	Surface Energy Balance
RSL	Roughness Sublayer
CFD	Computational Fluid Dynamics
UWG	Urban Weather Generator
WRF	Weather Research and Forecasting model
UMEP	Urban Multi-scale Environmental Predictor
GIS	Geographic Information System
MD-USEM	Multi-Domain Urban Surface Energy Model
UBEM	Urban Building Energy Model
TMY	Typical Meteorological Year
EPW	EnergyPlus Weather file format
LAI	Leaf Area Index (m^2 leaf area per m^2 ground)
ACH	air changes per hour
NSE	Nash–Sutcliffe Efficiency (model performance metric)
RMSE	Root Mean Square Error
MBE	Mean Bias Error
MRT	Mean Radiant Temperature (°C)
SW	Shortwave (Radiation)
LW	Longwave (Radiation)
Q25	25th percentile (lower quartile)
Q75	75th percentile (upper quartile)
BPS	Building Performance Simulation
VPD	Vapour Pressure Deficit (kPa)
Area 1	10 m zone from the north and south façades of the building, used for outdoor outputs
Area 2	20 m zone around all façades of the building, used for outdoor outputs
T_{mrt}	Mean Radiant Temperature (°C)
IES-VE	Integrated Environmental Solutions Virtual Environment (building simulation software)
ENVI-met	ENVI-met microclimate simulation software

Scenario Abbreviations

Table 2: Table of scenario coding

Abbreviation	Definition
LOW-	Prefix for low-rise scenarios
MID-	Prefix for mid-rise scenarios
HIGH-	Prefix for high-rise scenarios
REF	Reference scenario (no greening)
GR-EXT	Extensive green roof
GR-INT	Intensive green roof
GW-N	Green wall on north façade
GW-S	Green wall on south façade
GW-S-N	Green wall on both façades
GRASS	50% grass scenario
SHRUBS	50% shrubs scenario
TREE-6m	Trees of 6 m height (young trees)
TREE-11m	Trees of 11 m height (medium-aged trees)
N(x)S(y)	Tree placement: distance of x m north and y m south of the building
INTEGRATED	Combination of multiple greening interventions (trees, grass, shrubs, façades, roofs)

Symbols

Table 3: Table of symbols used in the main report

Symbol	Definition	Unit
T_a	Outdoor air temperature	[°C]
T_s	Surface temperature	[°C]
T_m	Mean temperature between air and surface ($T_m = (T_a + T_s)/2$)	[K]
T_{dew}	Dew-point temperature	[°C]
RH	Relative humidity	[%]
v_s	Wind speed measured 1 m from façade	[m s^{-1}]
A_{eff}	Effective open window area	[m^2]
Q_{window}	Airflow rate through opening	[m^3 s^{-1}]
q_{equip}	Internal heat gain from equipment	[W]
Q^*	Net radiation (sum of net shortwave and longwave)	[W m^{-2}]
Q_F	Anthropogenic heat flux from human activities	[W m^{-2}]
Q_H	Sensible heat flux from surface to atmosphere	[W m^{-2}]
Q_E	Latent heat flux due to evapotranspiration and evaporation	[W m^{-2}]
Q_G	Ground heat flux via conduction into substrate	[W m^{-2}]
ΔQ_S	Net storage heat flux in built environment	[W m^{-2}]
ΔQ_A	Net advective heat flux due to air mass movement	[W m^{-2}]
Q_{SW}	Shortwave radiation gains (solar radiation through glazing or absorbed)	[W]
Q_{LW}	Longwave radiation exchange between surfaces	[W]
Q_{int}	Internal heat gains (occupants, lighting, appliances)	[W]
Q_{vent}	Heat exchange due to ventilation and air infiltration	[W]
Q_{cond}	Conductive heat transfer through envelope (walls, roof, floors)	[W]
Q_{conv}	Convective heat flux at interior/exterior surfaces	[W]
Q_{HVAC}	Heating or cooling load supplied by HVAC system	[W]
Q_{lat}	Latent heat flux from evaporation/condensation	[W]
h_c	Convective heat transfer coefficient	[W m^{-2} K^{-1}]
h_r	Radiative heat transfer coefficient (from Stefan–Boltzmann law)	[W m^{-2} K^{-1}]
h_e	Total external heat transfer coefficient	[W m^{-2} K^{-1}]
R_e	External resistance	[m^2 K W^{-1}]
ε	Surface emissivity	[–]
σ	Stefan–Boltzmann constant (5.67×10^{-8})	[W m^{-2} K^{-4}]

1 Introduction

1.1. Background

Increasing global temperatures and more densely populated areas exacerbate local climate issues, particularly in urban areas. Globally, the percentage of people living in cities is expected to increase from 46.7 % in 2000 to 60.4 % in 2030, and in the Netherlands, from 76.8 % to 95.8 % (UN-Habitat, 2024). This rapid urban growth intensifies environmental problems, such as air pollution and the urban heat island (UHI) effect (Singh et al., 2020), while also posing threats to biodiversity (Seto et al., 2012).

The UHI effect describes the phenomenon where urban areas experience higher temperatures than their rural surroundings (Oke et al., 2017; Santamouris, 2014). Despite the temperate maritime Cfb climate in the Netherlands, the UHI is a significant issue (Köppen, 1931; Peel et al., 2007). Dutch cities experience a mean daily maximum UHI of 2.3 °C, with a 95th percentile of 5.3 °C (Steeneveld et al., 2011).

Climate change is expected to exacerbate these conditions. Under a high-emissions scenario, the number of tropical nights in the Netherlands increases from 0.3 per year in the current climate to 3 by 2050 and 19 by 2100. Similarly, the number of summer days ($T_{\mathrm{a,max}} \geq 25\,^{\circ}\mathrm{C}$) rises from 28 currently to 49 in 2050 and 89 in 2100 (KNMI, 2023).

Rising urban temperatures increase cooling energy demand, stressing electricity systems and increasing greenhouse gas emissions (Manso et al., 2021). In addition, urban heat reduces indoor thermal comfort, reduces the efficiency of cooling systems, and poses serious public health risks during heat waves (KNMI, 2023; Lundgren-Kownacki et al., 2018; Schinasi et al., 2018). Mechanical cooling systems, such as air conditioning, mitigate indoor heat exposure but simultaneously can exacerbate the urban heat island effect through the release of waste heat into the outdoor environment (Brousse et al., 2024; Jin et al., 2020). In the Netherlands, higher rates of hospital admission and mortality are recorded during heatwaves, particularly among vulnerable groups, such as the elderly (Huynen et al., 2001; Rovers et al., 2015; van Loenhout et al., 2018).

Expanding urban greenery can mitigate urban heat both outdoors and indoors (Balany et al., 2020). Moreover, it yields other beneficial effects, such as improved air quality, reduced noise pollution, enhanced biodiversity, and lower building energy demand (Manso et al., 2021). In addition, green urban policies contribute to achieving several Sustainable Development Goals (SDG3, SDG11, SDG13, SDG15, and SDG16) (Tate et al., 2024). The Dutch government has the national goal of becoming nearly energy-neutral by 2050, underlining the need for strategies that simultaneously improve climate resilience and reduce energy demand (Ministerie van Klimaat en Groene Groei, 2025).

1.2. Problem statement

In the Dutch context, the National Climate Adaptation Strategy (NAS) identifies heat stress as a key climate risk. It proposes measures such as reflective materials, improved ventilation, and urban redesign, while highlighting urban greenery as an important strategy for reducing heat stress (Ministerie van Infrastructuur en Waterstaat, 2016). Numerous studies have examined the effects of green interventions on outdoor or indoor temperatures, but only a limited number have focused specifically on the Netherlands. This study builds on existing Dutch studies on green roofs, green walls, and ground-level vegetation (Kluck et al., 2020; Ottelé & Perini, 2017; Solcerova et al., 2022; van der Velde et al., 2023).

However, combining both indoor and outdoor effects remains challenging because models are typically designed for either outdoor or indoor analysis. Furthermore, only a few studies have simultaneously measured both indoor

and outdoor thermal conditions, and the spatial coverage of urban monitoring stations is limited (Li et al., 2019; Nguyen et al., 2014). Recently, the coupling of urban climate models (UCM) with building energy models (BEM) has emerged as a promising approach, as building energy models that ignore microclimatic conditions are no longer sufficient (Allegrini et al., 2015). Although coupling UCM with BEM has been demonstrated in other countries, no study has applied such a coupled approach specifically to assess the impact of urban green interventions on typical Dutch housing (Pasandi et al., 2024).

Therefore, this study applies a coupled UCM–BEM framework to systematically analyse different greening scenarios across representative Dutch building typologies. By evaluating the effects on both outdoor and indoor temperatures, as well as building energy demand, this study aims to identify the most effective types of green interventions.

1.3. Research objective

This study explores different methods of incorporating greenery around buildings and assesses their effects on outdoor and indoor climates. Additionally, it examines the impact of these measures on energy usage for maintaining comfortable indoor conditions. This is investigated through the following research question:

What is the impact of green roofs, green walls, trees, shrubs and grass on outdoor temperatures, indoor temperatures and energy usage across various building typologies?

To answer this question, each green intervention is modelled independently for low, mid and high-rise building typologies. This enables conclusions to be drawn regarding the optimal type and amount of green intervention. To determine which combination of green interventions results in the maximum temperature decrease, the different types of greenery are analysed in various combinations.

For each building typology, a generic building representation is used to minimise the influence of individual morphological differences. The study employs typical Dutch buildings arranged in a strip formation, which means a row of houses for each typology. Green infrastructure is applied exclusively in the immediate surroundings of buildings to isolate and assess the effect of greening. The surroundings are modelled as standard soil. The low-rise (three storeys) typology is represented by a typical Dutch terraced house from the 1970s, whereas the mid-rise (five storeys) typology corresponds to a simplified residential block commonly found in Dutch inner cities. The high-rise (eight storeys) typology is represented by a simplified gallery-access apartment block commonly found in Dutch cities.

The outdoor air temperature and Physiological Equivalent Temperature (PET) are evaluated at 1.5 m above the surface to capture conditions at pedestrian level. This height is the standard measurement level for air temperature at meteorological stations in the Netherlands and is commonly used in thermal comfort studies to derive thermal comfort indices such as the PET (Höppe, 1999a; KNMI, n.d.-b).

The model outputs from the UCM include air temperature, surface temperature, relative humidity, and wind speed, which are subsequently used as inputs for the BEM. This model simulates the indoor climate of a building without mechanical cooling and the energy demand of a building equipped with cooling to maintain thermal comfort. A maximum indoor temperature of 25 °C is adopted as the comfort threshold (RIVM, 2022; RVO, 2018).

1.3.1. Research hypotheses

The main research question leads to three hypotheses which are evaluated in this study.

- Hypothesis 1: Green interventions reduce local outdoor air temperature and PET.
- Hypothesis 2: Green interventions maintain indoor temperatures within the comfort range.
- Hypothesis 3: Green interventions (partly) reduce the need for mechanical cooling by limiting indoor overheating.

These hypotheses are formulated based on previous studies that demonstrated the potential of green interventions to mitigate outdoor heat and improve outdoor thermal comfort, indoor thermal comfort, and reduce cooling energy demand (Balany et al., 2020; Manso et al., 2021; Santamouris et al., 2017). Hypothesis 1 builds on findings that vegetation lowers outdoor air temperature and PET through shading and evapotranspiration. Hypothesis 2 follows from findings that some vegetation can reduce solar heat gain or improve insulation and thus lower indoor temperatures (Morakinyo & Lam, 2016). Hypothesis 3 is based on the expected link between reduced indoor overheating and decreased energy use for mechanical cooling. Each hypothesis reflects a distinct modelling component namely outdoor, indoor, and energy-usage, together covering the main research question.

2

Theoretical Framework

This chapter outlines the theoretical background of this study. First, the concepts of urban climate, UHI effect, and urban energy balance are introduced, including how these can be modelled. Second, the mechanisms of building energy exchange are described, followed by an explanation of how building energy is represented in models. Third, different coupling approaches between UCMs and BEMs are discussed to assess which method is most appropriate for this research. Finally, the types of green infrastructure considered in this study are introduced, and their effects on outdoor and indoor temperatures are discussed. Together, these elements provide the necessary background to address the main research question.

2.1. Urban microclimate and the urban heat island

This section provides the basis for Hypothesis 1 by explaining how the urban heat island effect and microclimatic processes influence outdoor air temperature. To understand the effect of green interventions, it is essential to first consider the urban microclimate and the urban heat island phenomenon. PET is used in this study as it provides a more comprehensive measure of human thermal comfort than air temperature alone, accounting for wind speed, humidity, radiation, and thermal properties of the environment. A more detailed explanation of PET is provided in Appendix A. Urban areas develop distinct microclimates compared to their rural surroundings due to impervious surfaces with high heat capacity, reduced vegetation, anthropogenic heat emissions, and compact building configurations (Oke et al., 2017; Santamouris et al., 2015). These factors contribute to the UHI effect, which elevates urban temperatures, increases energy use, and reduces outdoor thermal comfort, with potential implications for public health (Lundgren-Kownacki et al., 2018; Manso et al., 2021; Schinasi et al., 2018).

Oke et al. (2017) distinguishes four UHI types: (1) the **surface UHI**, indicating surface temperature differences between rural and urban surfaces; (2) the **subsurface UHI**, representing underground thermal differences caused by urban materials; (3) the **canopy layer UHI**, referring to air temperature variation within the Urban Canopy Layer (UCL)—the zone from ground to rooftop where human exposure is highest; and (4) the **boundary layer UHI**, which affects the Urban Boundary Layer (UBL) above roof and treetops, up to roughly 1,500 m in height where the urban landscape no longer influences the atmosphere (van Hove et al., 2011). For a representation of the daytime and nighttime UCL and UBL, see Figure 2.1a.

The surface UHI peaks during the day because of solar heat storage in urban materials with low albedo and high thermal mass (Erell et al., 2014; Peng et al., 2012). The canopy layer UHI is strongest at night, as rural areas cool faster (Oke et al., 2017). In the Netherlands, UHI intensities of 5.3 °C are common, with extremes exceeding 8 °C during heat events (van Hove et al., 2011). Factors such as vegetation, street layout, building geometry, and sky view factor modulate these gradients (Allegrini et al., 2012; Morakinyo & Lam, 2016). An example of the urban heat island effect for different land-use categories is visualised in Figure 2.1b.

Urban morphology also alters wind flow patterns. Buildings obstruct prevailing winds and reduce mean wind speeds in the UCL, limiting convective cooling and increasing microclimatic heterogeneity (Allegrini et al., 2015; Oke et al., 2017). Consequently, thermal comfort declines, particularly in poorly ventilated areas. Furthermore, anthropogenic heat emissions from buildings, traffic, and other human activities increase urban temperatures.

These urban thermal conditions directly impact buildings. Energy demand rises by 0.5–8.5% per degree increase in outdoor air temperature (Santamouris et al., 2015). Cities such as London and Athens show double the cooling loads compared to rural areas (Santamouris, 2001; Watkins et al., 2002). Recently, López-Guerrero et al. (2022) reviewed 53 studies and found that the UHI impact on cooling loads and consumption ranged from 20% to 345%,

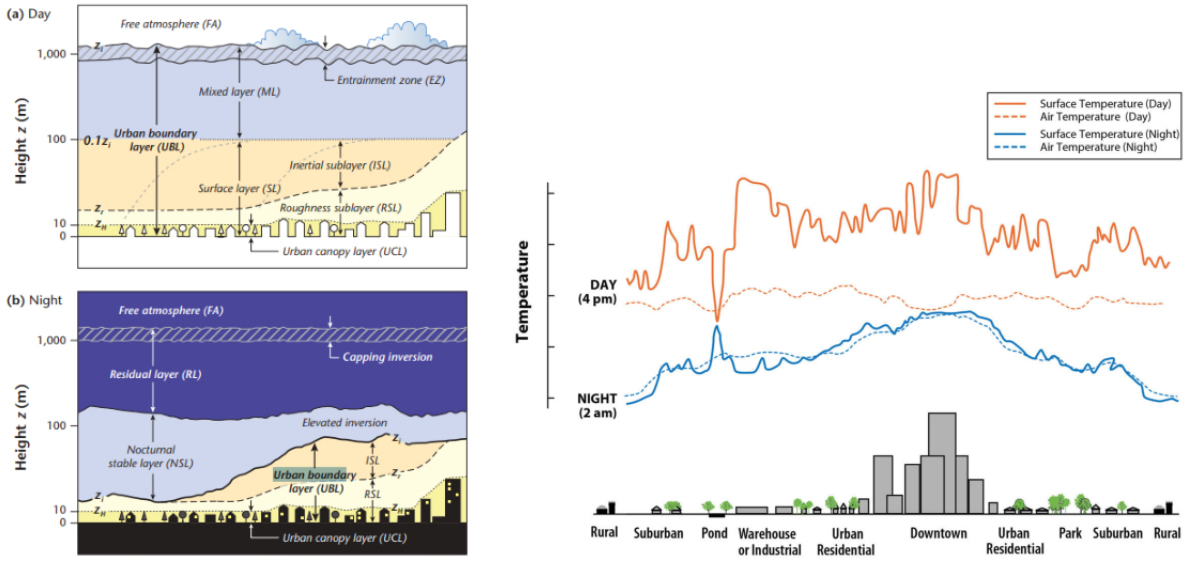

(a) Typical atmospheric layering over a city during the day and night. The UBL height varies from 1000 m during the day to 100 m at night (Oke et al., 2017).

(b) U.S. EPA illustration showing how land use affects air and surface temperatures (U.S. Geological Survey, 2022).

Figure 2.1: Urban atmospheric layers and land use influence on urban air temperature.

with an overall average of 23.2%. In Europe, 10 studies reported variation between 10% and 120% with a median of 30% (Li et al., 2019). Climate change will further increase this cooling load; for example, in London, cooling loads could increase by a factor of 2.4 between year 2000 and 2050 (Kolokotroni et al., 2012).

Green interventions, including green roofs, façades, and vegetation at street level, can lower surface and air temperatures through shading, reflection, and evapotranspiration (Manso et al., 2021; Peng et al., 2012; Steeneveld et al., 2011). This study focuses on the UCL UHI effect and the influence of green interventions.

2.1.1. Urban energy balance

The urban energy balance links radiative, convective, and storage heat fluxes to outdoor air temperature, forming the physical basis for Hypothesis 1. The Urban Heat Island (UHI) effect can be explained by comparing the surface energy balance (SEB) between rural and urban environments. The schematic in Figure 2.2 illustrates the fluxes in the SEB of both systems. These fluxes are defined over a control volume extending from the top of the roughness sublayer (RSL) to a subsurface depth at which no net conduction occurs over the time period of interest (Oke et al., 2017).

The urban SEB can be described by the following general equation:

$$Q^* + Q_F = Q_H + Q_E + \Delta Q_S + \Delta Q_A \tag{2.1}$$

where:

- Q^*: net radiation, the sum of net shortwave (diffuse and direct) and net longwave radiation [Wm^{-2}]
- Q_F: anthropogenic heat flux from human activities such as transportation, heating, and industry [Wm^{-2}]
- Q_H: turbulent sensible heat flux from the surface to the atmosphere [Wm^{-2}]
- Q_E: turbulent latent heat flux due to evapotranspiration and evaporation [Wm^{-2}]
- ΔQ_S: net storage heat flux in the built environment (e.g., buildings, roads) [Wm^{-2}]
- ΔQ_A: net advective heat flux due to horizontal movement of air masses [Wm^{-2}]

Although the same fluxes exist in both rural and urban environments, their relative magnitudes differ. The main factors contributing to this difference are:

1. **Surface albedo**: Urban materials typically have a lower albedo than vegetated surfaces, leading to increased absorption of solar radiation. This results in higher Q_H and ΔQ_S values and elevated (surface) temperatures

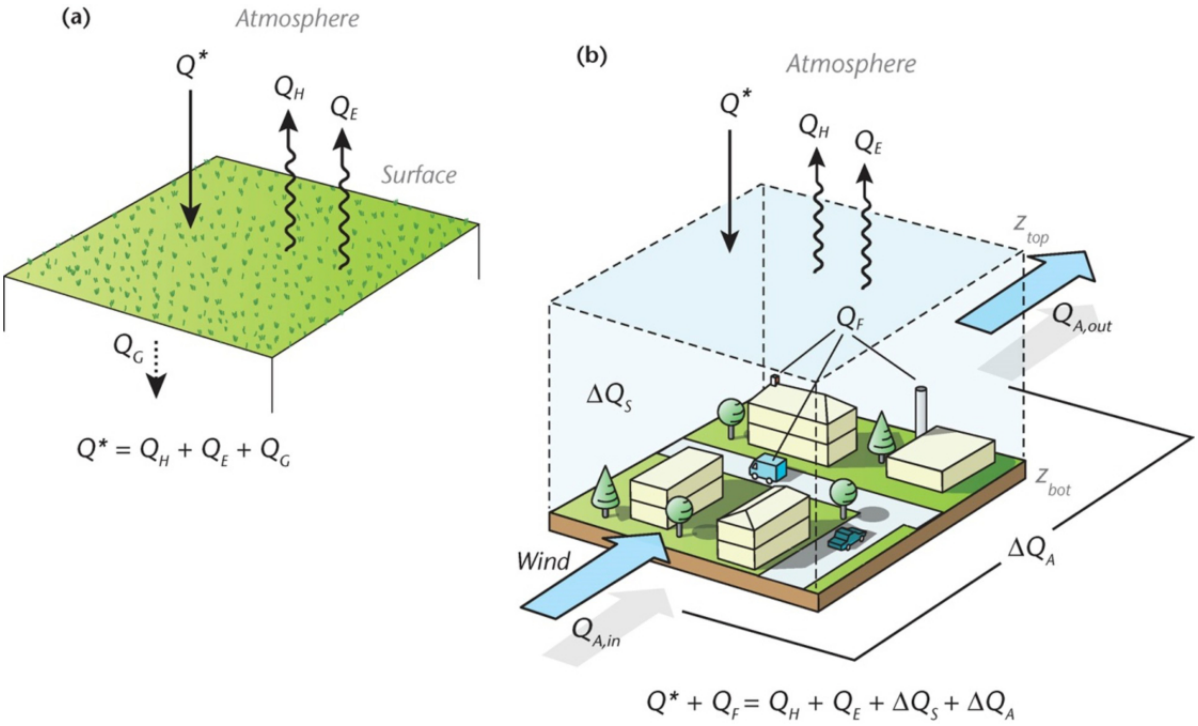

Figure 2.2: Schematic of the fluxes in the Surface Energy Balance of (a) a rural and (b) an urban building-soil-air volume. The urban volume extends from the top of the RSL (z_{top}) down to a depth where there is no net conduction over the period of interest (z_{bot}). The arrows are drawn in the direction in which the corresponding flux is considered positive. For ΔQ_S and ΔQ_A, they are positive if the internal energy of the volume increases (Oke et al., 2017). All fluxes are in [Wm^{-2}].

(Oke et al., 2017).

2. **Evapotranspiration**: In urban areas, vegetation is often not present and soils are sealed, decreasing evapotranspiration Q_E. Consequently, more energy from Q^* is partitioned into Q_H and ΔQ_S, enhancing the UHI effect (Oke et al., 2017).
3. **Anthropogenic heat**: Activities such as heating, cooling, traffic, and industrial processes contribute additional heat (Q_F) to the urban system, particularly during winter and nighttime.
4. **Urban geometry and sky view factor**: Tall and dense building configurations reduce the sky view factor, limiting longwave radiative cooling to the sky and increasing Q^*. Additionally, urban morphology affects turbulent exchange processes, influencing both Q_H and Q_E (Arnfield, 2003).
5. **Thermal properties of urban materials**: Materials commonly used in urban environments, such as concrete, asphalt, and brick, typically exhibit high heat capacity and thermal admittance. These properties enable them to absorb large amounts of heat during the day and gradually release it at night. This enhances the net storage heat flux ΔQ_S, prolongs elevated surface temperatures, and amplifies the UHI effect (Mirzaei & Haghighat, 2010; Oke et al., 2017).

This study focuses on how green interventions alter the urban energy balance by increasing latent heat flux through evapotranspiration and providing shading, while also modifying albedo and sky view factor.

2.1.2. Urban climate modelling

This subsection supports Hypothesis 1 by describing how UCMs simulate outdoor temperature and PET responses to green interventions. Several UCMs have been developed to model the urban climate, providing a clear advantage over meteorological station data by generating spatially explicit information on temperature, wind, humidity, and radiation at fine resolutions (Pasandi et al., 2024; Toparlar et al., 2017). The urban environment is highly complex, and standard weather station data can differ significantly from the local microclimate due to the combined effects of urban form, materials, vegetation, and atmospheric conditions (Arnfield, 2003; Huang & Li, 2017; Mosteiro-Romero et al., 2020). Furthermore, weather stations are predominantly situated outside urban environments in the Netherlands (Habib et al., 2025). UCMs are used to capture microclimatic variability;

therefore, the most relevant model options are introduced in this section.

Prognostic Computational Fluid Dynamics (CFD) models, such as ENVI-met, Fluent, OpenFOAM, and PALM-Urban, are widely used to analyse microclimates in high spatial detail. They can simulate scenarios at scales ranging from single buildings to entire districts, under different climatic and temporal conditions (Blocken, 2014; Maronga et al., 2015; Mirzaei & Haghighat, 2010; Pasandi et al., 2024). These models explicitly account for processes such as radiative exchanges, heat and moisture fluxes, and the influence of vegetation, which makes them well-suited for evaluating outdoor thermal comfort and the energy demand of buildings (Sola et al., 2018; Vurro & Carlucci, 2024).

Other model categories provide more simplified approaches. SEB models, including SOLWEIG, Solene-microclimat, and RayMan, concentrate on radiative and thermal exchanges at the surface, but do not resolve airflow or indoor conditions (Ding et al., 2024; Matzarakis et al., 2007; Pasandi et al., 2024; Vurro & Carlucci, 2024). Some, like Solene, can be coupled with CFD modules to extend their capabilities (Musy et al., 2015). Urban Weather Generators (UWG) take a different approach by producing urbanised meteorological time series, adjusting regional weather data to reflect urban heat island effects (Xu et al., 2022). At a larger scale, mesoscale atmospheric models such as the Weather Research and Forecasting model (WRF) include urban canopy parameterisations to capture the interaction between regional weather and urban form. However, their resolution remains too coarse to reproduce the detailed processes that shape local microclimates (Chen et al., 2011).

Furthermore, tools such as UMEP (Urban Multi-scale Environmental Predictor) offer integrated frameworks combining pre-processing, simulation, and post-processing capabilities, often embedded in GIS platforms for ease of use (Lindberg et al., 2018). SOLWEIG could be a module in UMEP calculation. Recently, data-driven and machine learning approaches have shown promise in accelerating microclimate predictions with reasonable accuracy (Yang et al., 2023).

Note that Pasandi et al. (2024) list additional UCMs beyond those considered here. In this section, only the models used in the model selection are stated. In chapter 3, one model is selected for this study, and its accuracy in modelling the urban climate and green interventions is discussed.

2.2. Building energy balance

This section is required for Hypotheses 2 and 3, as it outlines how internal and external heat sources influence indoor temperature and energy usage. A building can be described as a complex thermodynamic system, with both internal and external heat sources affecting indoor temperature (Sadineni et al., 2011). The boundaries of this system are defined by the building envelope, which consists of walls, windows, roofs, and floors. The building energy balance quantifies the heat exchange between the indoor environment and its surroundings, incorporating sources from conductive, convective, radiative, and latent heat transfers, as well as internal heat gains. The building energy balance is visualised in Figure 2.3.

In its general form, the building energy balance can be expressed as (Hensen & Lamberts, 2019):

$$Q_{\text{total}} = Q_{\text{SW}} + Q_{\text{int}} + Q_{\text{vent}} + Q_{\text{cond}} + Q_{\text{conv}} + Q_{\text{HVAC}} + Q_{\text{LW}} + Q_{\text{lat}}$$

where:

- Q_{SW}: shortwave radiation gains, primarily solar radiation transmitted through windows and absorbed by exterior surfaces [W]
- Q_{int}: internal heat gains from occupants, lighting, and electrical appliances [W]
- Q_{vent}: heat exchange due to ventilation and air infiltration [W]
- Q_{cond}: conductive heat transfer through the building envelope (walls, roofs, floors) [W]
- Q_{conv}: convective heat transfer at interior and exterior surfaces [W]
- Q_{HVAC}: heating or cooling provided by the HVAC system [W]
- Q_{LW}: longwave radiation exchange between building surfaces and the surroundings [W]
- Q_{lat}: latent heat associated with evaporation and condensation processes within the building [W]

Solar radiation is an important factor in this balance, depending on façade orientation, shading, and seasonal sun paths. For instance, east- and west-facing façades typically receive more solar gains during summer, leading to

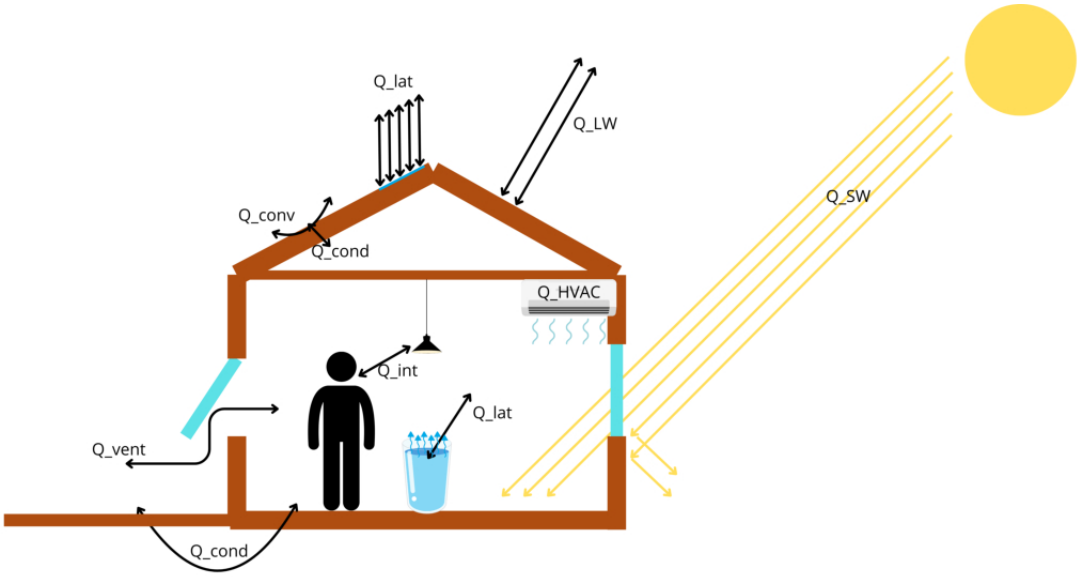

Figure 2.3: Building energy balance, Q_i is the sensible convective internal heat gain such as people, cooking or lighting. Q_vent is the amount of ventilation. Q_v and Q_c are convection and conduction together responsible for transmission losses. Q_HVAC is the cooling or heating load by the HVAC system, Q_LW is the net longwave radiation on the building, Q_lat is heat gain/loss from moisture evaporation / condensation.

higher cooling loads, whereas south-facing façades may optimise winter solar gains and reduce heating demand. Variations in building orientation, shading, thermal mass, wall thermal resistance, and ventilation strategies have a substantial effect on the indoor energy budget and temperature (Csáky & Kalmár, 2015; Rosenfelder et al., 2016; Tamerius et al., 2013).

Greening, such as green roofs and walls, affects the thermal resistance and exterior surface temperature of walls and roofs, thereby reducing conductive heat transfer. Outdoor green interventions reduce the amount of energy reaching the building by lowering the outdoor temperature and providing shade.

2.2.1. Building energy modelling

This section is required for Hypotheses 2 and 3 to show how BEMs can be used to model the indoor climate. BEMs are the primary tools used to calculate a building's energy balance and evaluate its energy performance (Hensen & Lamberts, 2019; Pan et al., 2023). These models numerically solve the heat balance equations, accounting for conduction, convection, shortwave and longwave radiation, ventilation, moisture balance, and internal gains (Allegrini et al., 2015).

A range of BEMs is available, each with different levels of physical detail, spatial resolution, and integration with other modelling environments. Commonly used tools include VABI Elements, IES-VE, EnergyPlus, IDA ICE, DOE-2, TRNSYS, e_Quest, umi, CityBEM, ESP-r, and DesignBuilder (Hensen & Lamberts, 2019; Pan et al., 2023; Sezer et al., 2023). Even more models are reported in the literature (Pasandi et al., 2024). Some models operate as standalone tools, while others can be coupled with simulation frameworks such as CFD or WRF to incorporate microclimatic influences into indoor energy predictions.

Within the context of Multi Domain Urban Scale Energy Modelling (MD-USEM) frameworks, BEMs range from detailed, physics-based models for single buildings to reduced-order Urban Building Energy Models (UBEMs) applied at the district scale (Pasandi et al., 2024; Sezer et al., 2023). Although detailed BEMs provide high-resolution results, their computational demands limit their feasibility for large-scale two-way coupling (Frayssinet et al., 2018). UBEM approaches, often based on archetypes and simplified thermal equations, offer a trade-off between accuracy and computational efficiency. The ability to couple with microclimate models also varies between BEMs, with some tools offering direct coupling options, whereas others require a customised coupling data framework.

In standalone operation, BEMs typically rely on standardised weather files (for example, TMY or EPW), thereby neglecting spatial and temporal variability in urban microclimates. Therefore, in this study, a coupled approach between a UCM and a BEM is used to more accurately capture the interactions between buildings and their surrounding climate.

2.3. Coupling BEM with UCM

To include microclimatic effects in BEMs for Hypotheses 2 and 3, a coupled UCM-BEM approach is used. In recent years, there has been growing attention to coupling BEMs with UCMs, as it has become increasingly clear that simulating building energy use without considering the local microclimate is insufficient (Allegrini et al., 2015). By coupling UCMs with BEMs, researchers gain better insights into how urban features such as street geometry, materials, and vegetation influence both indoor and outdoor conditions (Manapragada & Natanian, 2025; Pasandi et al., 2024; Sezer et al., 2023; Zhang et al., 2018). Standalone BEMs typically use averaged climate inputs, whereas using microclimate simulations as input has a noticeable impact on the thermal behaviour of buildings (Lauzet et al., 2019; Manapragada & Natanian, 2025).

Studies show that factors such as the height-to-width ratio of street canyons and the presence of shading vegetation significantly affect cooling and heating loads. These effects vary considerably depending on whether a single building or an entire district is modelled (Mosteiro-Romero et al., 2020). Coupling at the district scale remains challenging, mainly because of the substantial computational resources required (Frayssinet et al., 2018). Traditional BEMs tools are primarily designed for individual buildings, whereas UBEMs are increasingly used for large-scale simulations (Gobakis & Kolokotsa, 2017; Reinhart & Cerezo Davila, 2016).

Pasandi et al. (2024) reviewed 35 studies, most of which were conducted in the past decade. These studies coupled BEMs and UCMs within the so-called Multi-Domain Urban Scale Energy Modelling (MD-USEM) frameworks. Another review by Sezer et al. (2023) explained different coupling strategies in detail. Lauzet et al. (2019) analysed eight coupling studies and noted that, because most BEMs were originally developed around mesoscale weather files, UCMs outputs for air temperature, humidity, and wind can be imported via a "local climatic file." However, integrating short- and long-wave radiative exchanges remains challenging due to geometric mismatches between UCMs and BEMs representations. Another study by Manapragada and Natanian (2025) reviewed 30 studies, most of which were also conducted in the past decade. They showed that most studies typically modify weather file data or heat transfer coefficients to incorporate localised microclimate effects. Among these studies, 54% revised only weather file data, 14% modified heat transfer coefficients exclusively, and 21% employed both approaches. The coupling approaches ranged from one-way coupling, in which microclimate outputs feed into the BEM, to two-way coupling that also accounts for heat and moisture released by buildings. The latter provides more realistic interactions but requires significantly more computational resources (Pasandi et al., 2024; Sezer et al., 2023). No two-way coupling has yet been reported for ENVI-met (Pasandi et al., 2024).

These methods are becoming more common, but fully integrated platforms remain rare and are often too computationally demanding for district-scale studies. Consequently, most applications still rely on simplified coupling, which provides only low spatial and temporal details of the feedback between buildings and their microclimate.

2.4. Influence of urban green

Hypotheses 1–3 require knowledge of the types and effects of green interventions. Urban green interventions affect the microclimate around buildings and therefore influence indoor thermal conditions and energy demand. Vegetation cools the surrounding air through shading and evapotranspiration, thereby reducing the surface temperatures of building envelopes (Wong et al., 2010). The degree of these effects depends on the plant type, coverage, orientation, and maintenance, as well as the surrounding urban form. For every type of vegetation used in this study, reference studies are provided.

2.4.1. Green walls

In this study, a direct green wall with Hedera helix is used. Other types include indirect green walls, indirect green walls combined with planter boxes, and living wall systems (Perini & Rosasco, 2013). The main difference is that direct systems allow plants to climb directly on the façade, while indirect systems use a supporting structure that creates an air gap between the wall and the vegetation. Traditional green walls with climbing species such as Hedera helix reduce outside wall surface temperatures by an average of 3.7 °C and indoor wall temperatures by an average of 0.9 °C (Hoelscher et al., 2016). Another study reports a 7.3 °C reduction in outdoor wall surface temperature (Cameron et al., 2014). A further study shows that after 8 hours of heating, the outside wall surface temperature decreases by 1.7 °C, with no indoor effects (Ottelé & Perini, 2017).

A review by Balany et al. (2020) on green walls reports that the addition of 50% green walls in a target area results in an outdoor air temperature reduction of up to 1.86 °C. A review of case studies by Spanjar et al. (2023) shows

that, close to the wall (< 1 m), an outdoor air temperature reduction between 0 and 4 °C can be achieved, with a PET effect between 1 and 7 °C. However, because the number of available studies is low and the variation in types and sizes of green walls is high, conclusions regarding their cooling ability should be drawn with caution.

2.4.2. Green roofs

In this study a sedum green roof and an intensive green roof are used to assess the effect of green roofs on outdoor and indoor heat. A review by Balany et al. (2020) shows inconsistent results for the effect of green roofs. Some studies show air temperature reductions between 0 and 1.8 °C, while others report almost no effect on air temperature or PET. A review by Berardi et al. (2014) finds that an outdoor air temperature reduction between 0.3 and 3 °C can be expected, with higher impact in the hottest and driest climates. In Amsterdam, 27% green roof coverage results in an outdoor air temperature decrease at street level of approximately 0.3 °C (Solcerova et al., 2022). Another review by Mihalakakou et al. (2023) shows a significant reduction of up to 70% in building cooling load and a decrease in indoor air temperature between 0.4 and 3.5 °C for green roofs depending on type, climate, and study.

Experimental data with (blue-)green roofs also show promising results (Langewen et al., 2022). All indoor measurements indicate small but systematic influences of blue-green and green roofs on indoor temperature. The increased insulation values for (blue-)green roofs suggest that the additional (blue-)green layer contributes to this. In this study a blue-green roof shows a potential resistance value increase of 1–1.3 m^2 K W^{-1}. The comparison in resistance is not made for the green roof in that study. Furthermore, an effect of 0.6 °C on indoor air temperature is reported for a green roof, and 1.5 °C for the blue-green roof. Although the authors state that the exact effect of the blue-green roof on indoor air temperature and, consequently, thermal comfort is unclear and needs further study, this study shows promising results. Another study with a green roof reports a reduction in indoor air temperature in the room under the green roof of 0.5–1 °C at 1.5 m above the floor (Parizotto & Lamberts, 2011). Although the green roof has a lower surface temperature and higher insulation than the reference roof, the overall cooling effects remain relatively small.

2.4.3. Green at surface level

Trees

The influence of trees depends on their size and number. A review shows reductions in outdoor air temperature between 0.2 °C and 2.27 °C, with a median of 1 °C (Balany et al., 2020). Another review finds that urban trees and hedges decrease peak outdoor temperatures by between 0.1 °C and 7 °C, with a median maximum drop close to 1.5 °C (Santamouris et al., 2017). For Cfb climates, Li et al. (2024) report an outdoor air temperature difference between +0.6 and –6 °C across 13 studies. A study discussing the effect of different types of trees finds an outdoor air temperature difference ranging from –2.6 °C to 0.7 °C. In the shade of each tree canopy, PET is reduced by 14.8 °C to 23.7 °C (van der Velde et al., 2023).

The potential of urban street trees to reduce building cooling demand is directly related to their foliage density and planting pattern (Tsoka et al., 2021). Energy savings of up to 54% are achieved when trees form a continuous shading canopy. Higher Leaf Area Density values result in greater reductions in cooling energy needs.

Shrubs

Balany et al. (2020) find that in some cases, shrubs only slightly improve the microclimate. However, they can reduce soil surface temperature. The overall positive effect is smaller than for trees. Another study shows that increasing shrub height by 0.5 m decreases the average outdoor air temperature of a small green space by approximately 0.2 °C (Sun et al., 2024). Another study reports an increase in PET due to decreased wind speeds (Li, Zheng, Ouyang, et al., 2021). For shrubs, few studies are available, so firm conclusions are difficult. Based on shading and evapotranspiration effects, shrubs are expected to have a small cooling effect, though generally much lower than that of trees.

Grass

Grass has a much lower effect on outdoor air temperature and PET than trees. PET reductions of up to 4 °C are reported, while effects on air temperature are negligibly. Combining grass with other green interventions yields better results than using grass alone (Armson et al., 2012; Balany et al., 2020). The effect of grass on air temperature is assumed to be low. During a heatwave, the effect of soil and grass evaporation decreases over time, lowering the evaporative cooling effect (Teuling et al., 2010).

3

Model selection and validation

This chapter provides an overview of the selection and validation of urban climate models (UCMs) and building energy models (BEMs). It serves as an intermediate step between the theoretical framework and the methodology, offering a clear justification for the model choices made in this research. Presenting model selection and validation separately keeps the methodology concise and makes the rationale behind the chosen models transparent. First, several UCMs are reviewed. Then, the selected model is introduced and validated to demonstrate its suitability for the research objectives and sub-questions. Subsequently, several BEMs are compared, leading to the selection of one model that is likewise validated for this research context.

3.1. Urban climate model selection

UCM selection is based on three criteria: (i) ability to couple with indoor models, (ii) accuracy in representing green-intervention effects, and (iii) provision of detailed spatial outputs. The list of UCMs presented by Sezer et al. (2023) forms the starting point for the comparison. In principle, these models can be coupled with BEMs. In addition, WRF is included to assess the possibility of analysing larger-scale effects, PALM-4U for its large-eddy simulation capabilities, CityFFD for its reduced-complexity CFD approach, and SOLWEIG and RayMan as representative surface energy balance (SEB) models. The final shortlist is:

- ENVI-met
- Fluent
- OpenFOAM
- CityFFD
- SOLWEIG
- Solene
- RayMan
- PALM-4U
- UWG
- WRF

Detailed vegetation modelling is crucial, because evaporation and shading must be represented as accurately as possible. ENVI-met and Fluent are currently the only models in this selection that comprehensively simulate green roofs, green walls, and evaporative cooling (Vurro & Carlucci, 2024). Vegetation in ENVI-met can be parameterised in detail, including location, type, height, leaf area index (LAI), and photosynthesis and evaporative properties. In Fluent, vegetation representation is limited to location and photosynthesis/evaporative characteristics. Moreover, Fluent requires a significant amount of computational time (Jamei & Rajagopalan, 2019). ENVI-met is also characterised by a substantial computational time. Other models, such as PALM-4U, OpenFOAM, Solweig, UWG, and CityFFD, are less favourable in this respect, although integrated vegetation modelling has been demonstrated in OpenFOAM (Manickathan et al., 2018). Solene has similar capabilities as ENVI-met (Musy et al., 2015). UWG is designed to adjust meteorological inputs to account for urban heat island effects at neighbourhood to city scales, but it cannot resolve vegetation impacts at the fine spatial resolution needed here (Bueno et al., 2012).

The ability to produce detailed spatial outputs is also important for coupling. Solweig, ENVI-met, and PALM-4U can simulate surface and air temperature, relative humidity, wind speed and direction, and long- and short-wave radiation (Vurro & Carlucci, 2024). RayMan, OpenFOAM, CityFFD and UWG do not provide all of these parameters in their standard configuration, although in OpenFOAM and CityFFD they can be obtained through additional boundary conditions or model coupling. Solene can provide most of these parameters when coupled with its CFD module, but in its base radiative configuration it does not simulate airflow and humidity directly (Musy et al., 2015). Regarding scale, WRF typically operates at 33 m (often >100 m), which is too coarse to capture the 1–5 m microclimatic variations required here (Chen et al., 2011; Wang et al., 2023).

The qualitative assessment above is summarised in Table 3.1, where models are ranked using relative scores for their ability to couple with BEMs, represent vegetation, and provide detailed spatial outputs. Based on this analysis, ENVI-met is selected as the most suitable model. It offers the necessary spatial resolution, detailed vegetation modelling capabilities, and outputs that are well-suited for coupling with indoor-environment simulations.

Table 3.1: Evaluation of UCMs against selection criteria

Model	Coupling with BEM	Vegetation modelling	Detailed spatial outputs
ENVI-met	+	++	++
Fluent	+	+	+
OpenFOAM	+	+-	+-
CityFFD	+	-	+-
SOLWEIG	+	-	+
Solene	+	+	+
RayMan	+-	–	-
PALM-4U	+	+-	++
UWG	+	–	-
WRF	+	–	–

3.2. ENVI-met model

ENVI-met is designed for microscale CFD calculations of the thermal and environmental effects of urban design interventions (Bruse & Fleer, 1998). ENVI-met is widely used in urban-climate studies (Brozovsky et al., 2021). It is applied in various climate zones with 25% in Cfb climates (Tsoka et al., 2018).

ENVI-met is a prognostic, three-dimensional, grid-based microclimate model, designed to simulate complex surface-vegetation-air interactions in the urban environment. It consists of the following sub-models (Tsoka et al., 2018): a) The 1D boundary model, used for the initialisation of the simulation and for the definition of the boundary model conditions of the 3D atmospheric model. b) The 3D atmospheric model, in which air temperature and humidity, wind flow, turbulence, short-wave and long-wave radiation fluxes as well as pollutant dispersion and deposition are modelled. c) The soil model, in which the surface temperatures and distribution of the natural soil temperature and water balance are simulated. d) The vegetation model, including the simulation of transpiration rates, leaf temperatures of trees, and heat and vapour exchanges between plants and the atmosphere.

ENVI-met simulates the diurnal cycle of major climatic variables involving air and soil temperature and humidity, wind speed and direction, and radiative fluxes with a typical horizontal resolution from 0.5 to 5 m and a time step of 1 - 5 s (Bruse & Fleer, 1998; Bruse et al., 2023; Huttner, 2012; Simon, 2016). Different greening methods can be applied to walls and roofs, including the required vegetation parameters and modelling of the substrate layer (Bruse et al., 2023).

Although ENVI-met offers many advantages, several limitations have been identified. Tsoka et al. (2018) summarise the main shortcomings, including (a) simplified radiation flux calculations, (b) the use of the Yamada and Mellor E– turbulence model, (c) coarse grid generation, (d) limited representation of near-wall phenomena, (e) the inability to fully force wind speed and direction, and (f) the assumption of static cloud and wind conditions during simulations. Recent updates, however, have addressed several of these issues. ENVI-met v5 introduced a revised graphical interface, improved mean radiant temperature (MRT) calculations, and Python integration via ENVI-guide for automated workflows. Version 5.8 further enhanced radiation modelling for vegetation, refined turbulence representation around dense greenery, and fixed errors affecting green walls and roofs. These developments have reduced some of the earlier uncertainties, though it remains essential to note that not all

validation studies are based on the most recent model versions. More details about the structure and governing equations of ENVI-met can be found in Bruse and Fleer (1998), Bruse et al. (2023), Huttner (2012), Simon (2016).

3.3. ENVI-met validation

In this section, the use of ENVI-met for this specific study is validated. Reference studies are discussed and a prediction is made of the accuracy of the results of ENVI-met. Validation is performed for every green intervention, but trees, shrubs and grass are combined in green at surface level, as often these are combined in studies. Perceived temperature calculation by ENVI-met is also validated.

3.3.1. Validation for green at surface level

First, an overview study with 52 studies reported RMSE values for ENVI-met between 0.52 °C and 4.30 °C with a median of 1.51 °C, and R^2 values between 0.66 and 0.99 with a median of 0.92 (Tsoka et al., 2018). Another review study reported RMSE values between 0.73 °C and 1.61 °C and R^2 values between 0.69 and 0.96 (Balany et al., 2020). Furthermore a neighbourhood modelling study in Zurich reported an R^2 of 0.97 and RMSE of 1.02 °C for outdoor air temperature, although daytime temperatures were overestimated by up to 2 °C, which could impact energy demand estimations (Mosteiro-Romero et al., 2020). Overestimation of outdoor air temperature was also seen in Spain but ENVI-met maintained a strong Pearson correlation of 0.777, while relative humidity and MRT had even higher correlations of 0.960 and 0.870, respectively (Alves et al., 2022).

The validation study by Ouyang et al. (2022) shows promising results for modelling trees, with the R^2, d value, RMSE, and MBE visualised in Figure 3.1. Another tree-focused study found fairly good correlations between simulated and measured values for outdoor air temperature, with R^2 values of 0.79–0.81 and RMSE values of 0.9 °C for tree-shaded areas and 1.2 °C for unshaded areas (Morakinyo et al., 2018). For grass, Eingrüber et al. (2025) reported a Nash–Sutcliffe Efficiency (NSE) of 0.91 across different weather conditions, indicating strong accuracy.

Nevertheless, some studies reported weaker accuracy, especially in direct sunlight, with overestimated cooling effects of trees and grass. For example, Le and Chan (2023) found a reasonable RMSE of 0.9 °C and R^2 of 0.87 for air temperature, but MRT was strongly overestimated (RMSE of 8.1 °C and R^2 of 0.5). Furthermore in a complex urban green space such as a heterogeneous park, Yang et al. (2021) reported an RMSE of 1.89 °C for air temperature but R^2 values below 0.1 for multiple timesteps. While ENVI-met reproduced overall temperature levels in this study, it struggled to capture the spatial distribution, especially when grass was present.

The differences in air temperature relevant to this study are within a reasonable range, with most validation studies reporting RMSE values between 0.5 °C and 2 °C and R^2 values typically above 0.7. Based on this, an RMSE between 0.5 °C and 2 °C is expected for this study. However, performance varies by vegetation type and atmospheric parameter: while air temperature is generally well captured, RH often shows larger errors. This must be considered for coupling with the indoor climate. Grass or heterogeneous green spaces can lead to overestimated cooling effects and weaker correlations. ENVI-met is used for green surface levels, but the results should be interpreted with caution.

3.3.2. Validation for green roofs

The validation study by Ouyang et al. (2022) showed accurate results for green roofs modelled with ENVI-met. The R^2, d value, RMSE, and MBE are visualised in Figure 3.1. Another study in Beijing found that simulated and measured results were highly correlated, with R^2 and d values larger than 0.87 and 0.88 for all cases, respectively. Moreover, RMSE, MAE, and MBE were below 1.7 °C for all sensors (Feng et al., 2022). Another study showed similar graphs for ENVI-met and measurements but did not provide R^2, RMSE, or other statistical metrics to quantify the fit (Bakovic Ergün & Gocer, 2017).

Few validation studies for green roofs are available, but existing results indicated good accuracy between simulated and measured values. However, the limited number of studies highlights the importance of comparing the model outputs with measurement studies of similar green interventions, as done in chapter 6.

3.3.3. Validation for green walls

The validation study by Ouyang et al. (2022) showed promising results for green walls. The R^2, d value, RMSE, and MBE are visualised in Figure 3.1. Another study in Hong Kong compared simulated and measured data, with R^2 values of 0.66–0.70 for longwave radiation, 0.60–0.74 for surface temperature, 0.89 for air temperature, and 0.76 for relative humidity. The corresponding RMSE values were 0.5 °C for air temperature, 11.1% for relative humidity, 2.3 °C for the green wall surface temperature, 5.1 °C for the bare wall surface temperature, 40.7 W m^{-2}

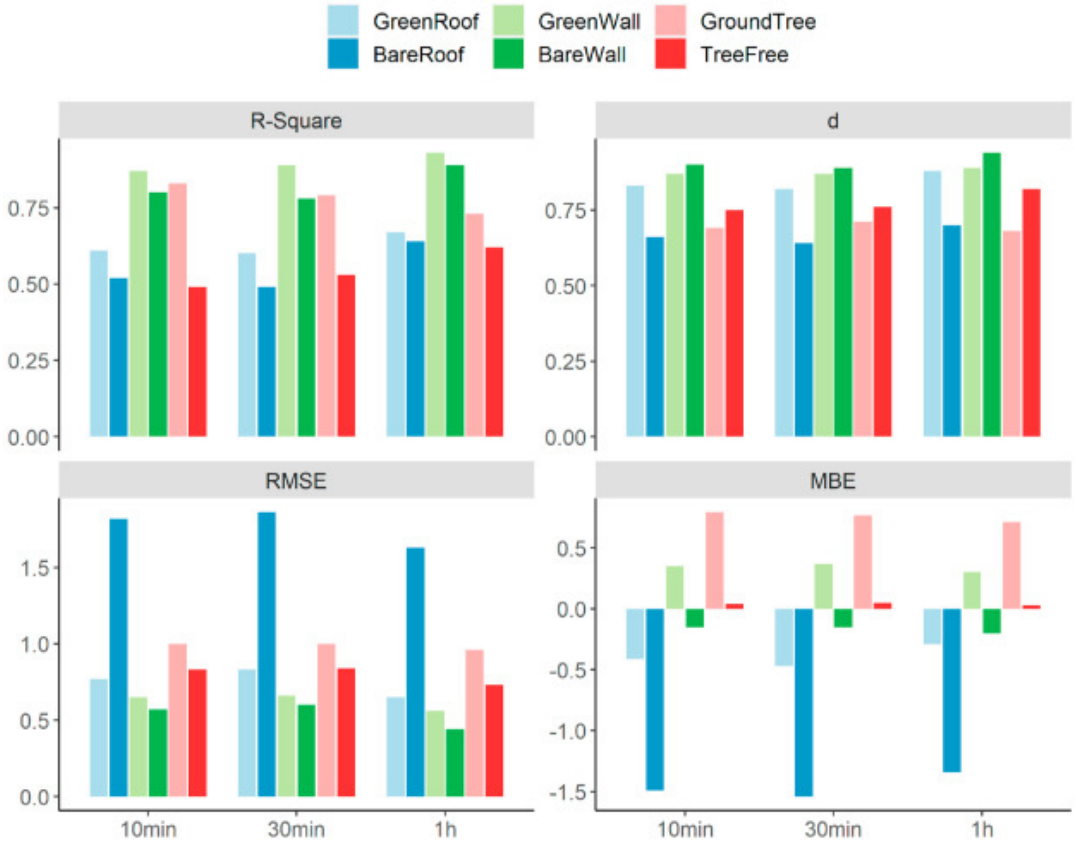

Figure 3.1: Results of validation study with green roof, green wall, and trees (Ouyang et al., 2022).

for the bare wall longwave radiation, and 42.0 W m^{-2} for the green wall longwave radiation (Morakinyo et al., 2019). Another validation study reported reasonable accuracy between measured and simulated air temperature, MRT, relative humidity, and wind speed, with average RMSE values of 0.76 °C, 2.86 °C, 4.26 %, and 0.37 m s^{-1}, respectively (Alsaad et al., 2022).

The limited validation studies showed that ENVI-met performs well for green walls, with reasonable accuracy across multiple microclimatic parameters. Nonetheless, the limited number of studies highlights the importance of comparing the results of this study with measurements, which is addressed in chapter 6.

3.3.4. Validation for perceived temperature

Several studies have evaluated the accuracy of ENVI-met in simulating mean radiant temperature (MRT) and the derived Physiological Equivalent Temperature (PET). Pantavou et al. (2022) found an index of agreement of 0.7 and an RMSE of 6.9 °C for PET, which corresponds to more than one class in the physiological stress scale, indicating limited accuracy in PET estimation. Multiple studies have highlighted that MRT, which strongly influences PET, is generally predicted less accurately than air temperature (Balany et al., 2020). For instance, Aleksandrowicz et al. (2023) reported RMSE values of 6.08 °C in shaded areas and 13.32 °C in full sun for MRT, while Le and Chan (2023) found an RMSE of 8.1 °C, and Alsaad et al. (2022) reported values ranging from 1.28 °C to 5.25 °C depending on the location. A tree-focused validation by Morakinyo et al. (2018) found R^2 values of 0.70–0.74 for MRT, with corresponding RMSEs of 2.1 °C under tree shade and 3.6 °C in unshaded conditions.

These results collectively show that PET values simulated with ENVI-met are expected to be less accurate than air temperature predictions, with potential deviations of up to around 10 °C. Nevertheless, ENVI-met provides useful insights for comparing scenarios, as long as the uncertainty in PET values is taken into account.

3.3.5. Overall validation for green interventions

Overall, the validation studies show that ENVI-met provides reasonable accuracy for simulating outdoor air temperature, surface temperature, and PET across different types of green interventions. Most studies report RMSE values for outdoor air temperature between 0.5 °C and 2 °C, with correlations typically above 0.7, indicating that

ENVI-met is generally reliable for this purpose. However, the model often overestimates cooling effects, especially in direct sunlight, and shows larger errors for relative humidity and mean radiant temperature, which directly affect PET. ENVI-met is more reliable for assessing relative differences between scenarios than for providing absolute values. For this study, ENVI-met is considered sufficiently accurate to capture relative differences between green interventions. However results need to be compared with measurement studies, which is addressed in chapter 6.

3.4. Building energy model selection

The selection of the BEM for this study is based on three main criteria: (i) use of the model in the Netherlands, (ii) available modelling detail and flexibility, and (iii) coupling possibilities with UCMs. The list of BEMs presented by Sezer et al. (2023) forms the starting point for the comparison. Vabi Elements Vabi (2025) is added as it is frequently used in the Netherlands for building energy modelling (personal communication, Sweco). The final models evaluated are:

- Vabi Elements
- IES-VE
- EnergyPlus
- IDA ICE
- DOE-2
- TRNSYS
- e_Quest
- umi
- CityBEM
- ESP-r
- DesignBuilder

The first selection criterion is whether a BEM is commonly used in the Netherlands. This is important because selecting a model that is already established in the Dutch context ensures that the developed methodology can be more easily applied in future projects and research in the Netherlands. Two experts in building energy modelling at Sweco were consulted to confirm which models are currently applied, and online sources were reviewed. Two BEMs that are widely applied in the Netherlands are Vabi Elements and IES-VE for specialised building energy modelling (personal communication, Sweco). Software packages such as Uniec 3/4 and BINK DGMR Software BV (2025), Uniec 3 (2025) are also common in the Netherlands, but since they focus on regulatory compliance (NTA 8800) rather than detailed dynamic modelling, they are excluded from further consideration in this study. Other international BEMs used in the Netherlands include EnergyPlus and DesignBuilder (Jalilzadeh et al., 2025; Kranen, 2021). DesignBuilder employs a simplified interface for EnergyPlus (Pasandi et al., 2024).

The second criterion concerns the flexibility and level of detail that a BEM can provide. Vabi Elements offers comprehensive modules for Dutch energy performance and indoor climate calculations, though its flexibility is relatively limited (Vabi, 2025). IES-VE provides extensive options for HVAC systems, comfort indices, and detailed building descriptions, making it suitable for in-depth simulations (IES-VE, 2025). EnergyPlus, IDA ICE, and TRNSYS are similarly flexible and versatile (Behrendt et al., 2021; Vadiee et al., 2019). In contrast, DOE-2 and eQuest are more restricted in dynamic modelling and design flexibility (Rallapalli, 2010). CityBEM focuses on neighbourhood-scale or aggregated modelling and therefore provides fewer detailed building-level options (Chen et al., 2017). ESP-r is also highly detailed (Bartak et al., 2003). umi integrates EnergyPlus within a Rhinoceros-based urban design environment (Reinhart et al., 2013).

The third criterion is the ability to couple with UCMs. Pasandi et al. (2024) identified 35 coupling studies in recent years, of which 14 used EnergyPlus, 6 used TRNSYS, and 3 used CityBEM, 1 used ESP-r, alongside other tools not considered in this study. Manapragada and Natanian (2025) summarised 42 coupling studies, with 24 using EnergyPlus, 10 using TRNSYS, 3 using IES-VE, and 2 using IDA ICE. In Vabi Elements, only EPW data can be modified. DOE-2, eQuest, and CityBEM are not mentioned in recent coupling studies and were therefore excluded. DesignBuilder inherits the coupling capabilities of EnergyPlus, and umi has EnergyPlus integrated within its model.

The qualitative assessment above is summarised in Table 3.2, where models are ranked using relative scores for their ability to couple with BEMs, represent vegetation, and provide detailed spatial outputs. Based on this analysis, EnergyPlus, TRNSYS and IES-VE appear to be the most suitable options for this study. IES-VE is ultimately selected, as it is often used in the Netherlands and experts from Sweco recommended IES-VE for this context.

Table 3.2: Evaluation of BEMs based on three criteria: (i) use in the Netherlands, (ii) modelling detail and flexibility, and (iii) coupling possibilities with UCMs.

Model	Use in the Netherlands	Detail / Flexibility	Coupling with UCMs
Vabi Elements	++	+-	–
IES-VE	++	++	+
EnergyPlus	+	++	++
IDA ICE	+-	++	+
DOE-2	-	-	–
TRNSYS	+	++	+
e_Quest	-	-	–
umi	-	++	++
CityBEM	-	-	–
ESP-r	-	++	+
DesignBuilder	+	++	+

3.5. IES-VE model

IES-VE is a BEM capable of modelling building energy usage in high detail (IES-VE, 2025). ApacheSim is the module within IES-VE used to model thermal performance. ApacheSim, the dynamic thermal simulation engine within IES-VE, calculates the internal temperature and cooling/heating loads of a building by resolving time-dependent energy balance equations. It calculates the effects of heat conduction, convection, air movement, solar radiation, and long-wave radiation, driven by weather data in EPW format (IES-VE, 2021a).

3.5.1. Room and building heat balance

ApacheSim uses a dynamic heat-balance model that computes the thermal response of a building zone based on the first law of thermodynamics. Further explanation is provided in section 2.2. The main formula used is:

$$\frac{dE_{\text{zone}}}{dt} = \sum Q_{\text{in}} - \sum Q_{\text{out}} \tag{3.1}$$

where:

- dE_{zone}: change in internal energy of the zone air [J]
- dt: time step (10 min) over which the energy balance is evaluated [s]
- Q_{in}: total incoming heat fluxes per zone, including solar gains, internal gains, and heating system input [W]
- Q_{out}: total outgoing heat fluxes per zone, such as convective, conductive, and ventilation losses [W]

This net energy change drives the zone air temperature. The main heat transfer terms contributing to the balance are as follows:

$$\frac{dE_{\text{zone}}}{dt} = Q_{\text{cond}} + Q_{\text{conv}} + Q_{\text{LW}} + Q_{\text{vent}} + Q_{\text{int}} + Q_{\text{SW}} + Q_{\text{HVAC}} \tag{3.2}$$

where:

- dE_{zone}: change in internal energy of the zone air [J]
- dt: time step (10 min) over which the energy balance is evaluated [s]
- Q_{cond}: Heat flux through building fabric (walls, roof, floor) [W]
- Q_{conv}: convective exchange with indoor surfaces [W]
- Q_{LW}: net longwave radiative exchange between surfaces [W]
- Q_{vent}: infiltration or mechanical ventilation exchange [W]

- Q_{int}: internal latent + sensible gains (occupants, lighting, equipment) [W]
- Q_{SW}: short-wave radiation from the sun transmitted through windows or absorbed by surfaces [W]
- Q_{HVAC}: Heating or cooling supplied by the building system [W]

ApacheSim solves this energy balance at each simulation time step to determine the zone air temperature and HVAC loads. The method uses a nodal network for surfaces and air nodes, typically assuming one mixed air node per zone (IES-VE, 2021a). Further details on each heat transfer coefficient and the IES-VE calculation process can be found in Appendix D.

3.6. IES-VE validation

The validation of IES-VE by other studies is essential to determine whether the model can accurately predict indoor temperature and energy performance. Several studies have evaluated the accuracy of IES-VE. Che-Ani and Raman (2019) found differences between measurements and simulation within an acceptable range, typically below 10–20%. IES-VE has also been validated against other simulation programs and measurements (Crawley et al., 2008). Furthermore, IES-VE complies with national and international standards, such as ASHRAE 140 (2001–2020), EU EN13791:2000, CIBSE TM33, and ISO 52000 (IES-VE, 2025). It is widely used for energy performance evaluation (personal communication, Sweco).

IES-VE cannot directly model green roofs or façades, coupling with ENVI-met is required. In IES-VE, green roofs and façades are represented as additional resistance layers added to the existing building. Trees, shrubs and grass are represented as structures. Validating IES-VE for individual green interventions is not possible, as no studies exist. Therefore, IES-VE is validated on its ability to model indoor air temperature and building energy usage.

With a temperature discrepancy of 11.03% and statistical metrics R^2 = 0.98, MBE = 0.8 °C, RMSE = 1.70 °C, IES-VE showed good agreement with observed data for cooling and indoor temperature forecasts in naturally ventilated buildings during the summer (Abdullahi et al., 2022). A comparative study with Ecotect and Green Building Studio for two academic buildings showed IES-VE was generally accurate for annual heating energy (within 15%). In this study IES-VE underestimated cooling energy and monthly trends, highlighting the importance of correct occupant behaviour inputs (Reeves et al., 2012). ApacheSim showed MBE below 1 °C in summer and RMSE below 1.5 °C across seasons (Yang & Becerik-Gerber, 2014).

The quality of input data, such as occupant behaviour, significantly affects the accuracy. IES-VE overestimated heat transfer coefficients by 27–54% when using calculated U-values and assumed infiltration rates. Errors reduced to 5–21% when using measured values (MBE 15%, RMSE 16%) (Ji et al., 2019). In another study, the model was calibrated to within 0.5% deviation from measured total energy consumption after adjusting key behavioural parameters, particularly heating set temperature (Ben & Steemers, 2014).

Therefore, the accurate implementation of behavioural parameters is essential for predicting indoor temperatures and energy usage. As not all behavioural parameters are known in this study, average parameters are chosen to represent a typical household. Consequently, the overall energy usage and indoor temperature may differ from those of actual households. However, because all scenarios use identical inputs except for the green interventions, the relative performance can be analysed and compared. The results are compared with a reference project in chapter 6.

4

Methodology

This chapter explains the modelling approach used to assess the impact of green interventions. ENVI-met version 5.8.0 is applied to simulate outdoor microclimate temperatures (ENVI-met, 2025). After defining the meteorological inputs, an appropriate grid and domain size are selected. The building typologies are then specified, and greening scenarios are introduced. The resulting ENVI-met outputs serve as input for the building energy model IES-VE version 2025 (IES-VE, 2025). In this section, the methodology for both models and the coupling between them are described.

4.1. ENVI-met

First, the meteorological inputs are stated. Then, a grid and area sensitivity check is carried out to identify the most suitable grid and domain characteristics for this study. Building typologies and greening interventions used in this study are described in more detail.

4.1.1. Inputs

The input parameters for ENVI-met are outlined in this subsection. A more detailed explanation of the ENVI-met inputs is provided in Appendix B. All input data were obtained from the Cabauw meteorological station, covering the period from 23 to 28 August (Knap, 2019; KNMI, 2019). Cabauw is used as it is the only station in the Netherlands with BSRN radiation data (KNMI, n.d.-a). The simulation runs from 23 August 06:00 until 28 August 00:00 (UTC +1). The temperature input is visualised in Figure 4.1.

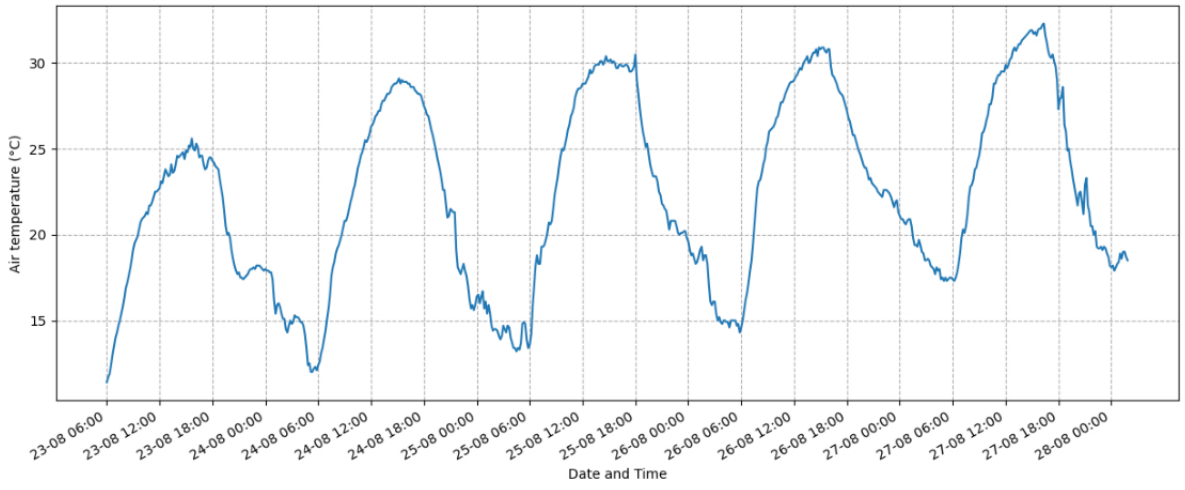

Figure 4.1: Air temperature data from 23–28 August 2019 at 2 m from the Cabauw meteorological station in UTC +1 (KNMI, 2019)

Meteorological input

The following meteorological inputs are used from the Cabauw station:

- LW downward radiation at surface [W m^{-2}] (Knap, 2019)

- SW direct radiation at surface [W m^{-2}] (Knap, 2019)
- SW diffuse radiation at surface [W m^{-2}] (Knap, 2019)
- Wind speed [m s^{-1}] and direction [°] at 10 m (KNMI, 2019)
- Air temperature [°C] at 2 m (KNMI, 2019)
- Relative humidity [%] at 2 m (KNMI, 2019)
- Precipitation [mm] (KNMI, 2019)
- Forced radiation function for direct, diffuse, and longwave radiation is used in ENVI-met (Ouyang et al., 2022).

4.1.2. Grid resolution and area size

A reference case is used to assess the sensitivity of grid resolution and area size. This reference case uses the same reference building as the low-rise scenario. The reference case in ENVI-met can be seen in Figure 4.2a. A typical Dutch low-rise building is used; further information can be found in Appendix I. Additionally, five trees and a road surface are included to evaluate their impact. The primary aim of this reference case is to examine how variations in grid resolution and area size influence the model. Following the sensitivity analysis, the appropriate grid resolution and area size are determined. Increasing resolution or area size has a large impact on run-time; therefore, in this section an option with a maximum of two days' run-time is chosen.

4.1.3. Grid sensitivity

The reference case is applied for a grid sensitivity check. The reference case is simulated for 24 hours with different grid sizes: small (1x1x1 m), medium (2x2x1 m), and large (3x3x1 m). The vertical (z) cell size is kept at 1 m, since extracting the temperature at 1.5 m height is not possible with coarser vertical resolutions. The reference case and the grid cells used are shown in Figure 4.2. In this study, the grid cells within 6 m of the building are analysed, as they are the most relevant for coupling to the indoor temperature. In Figure 4.3, the results of the grid sensitivity are visualised. Detailed maps of the ENVI-met outputs for each grid size are provided in Appendix F. The 1 m resolution is in this study used as the reference, as there are no validation measurements available. Other studies comparing ENVI-met with measurements indicate that an RMSE of 0.5–2 °C for air temperature can be expected in this study, explained in section 3.3.

Visually, the 3 m resolution displays a clear loss of detail, while the 2 m resolution closely matches the 1 m resolution. This is confirmed by statistical analysis. In Table 4.1, the statistics within 6 m of the building for different grid sizes are stated. Statistically, the 2 m resolution yields an RMSE of 0.13 °C compared to the 1 m resolution, while the 3 m resolution yields 0.23 °C. Although the 1 m resolution would be preferred, its run-time exceeds two days and is therefore not feasible in this study.

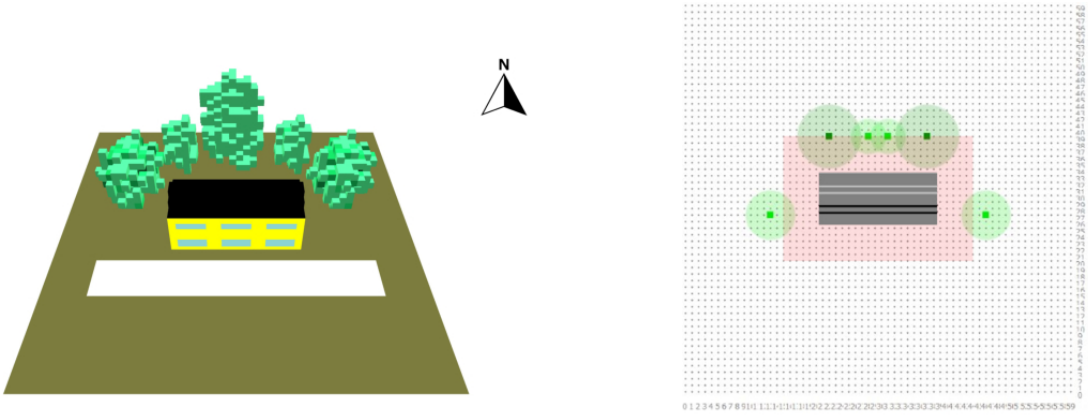

(a) Reference case in ENVI-met Spaces.

(b) Grid cells within 6 m of the building are used to compare resolution 1, 2 and 3 m.

Figure 4.2: Overview reference case and grid cells used in ENVI-met for grid and area sensitivity

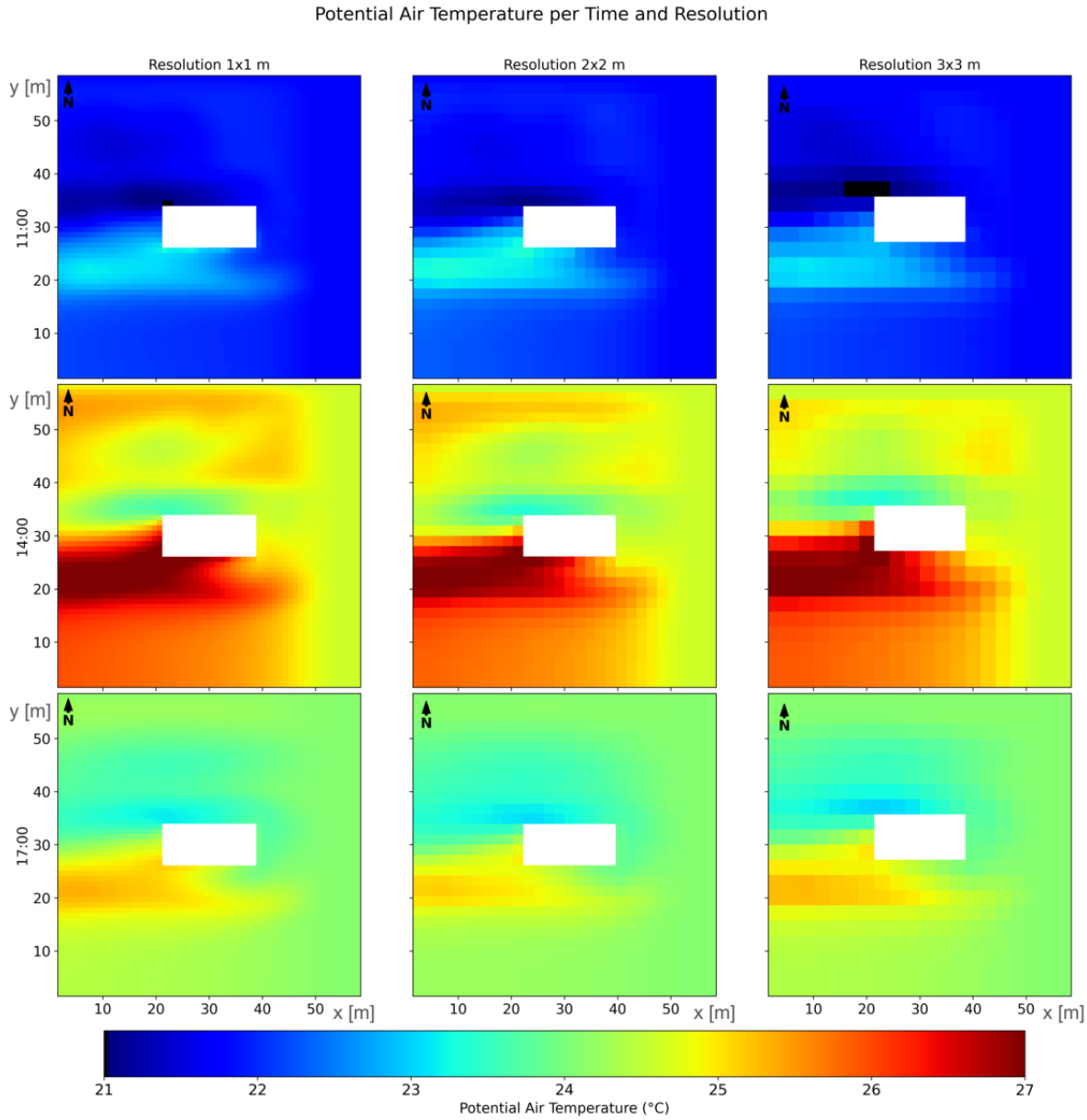

Figure 4.3: Potential air temperature for 23-08-2019 at 11:00, 14:00 and 17:00 at resolution of 1, 2, and 3 m

4.1.4. Area size

The simulated domain size strongly influences the microclimate results. In this part, three scenarios are created with different area sizes. The small area size (60×60 m) consists of the isolated row of houses with cells around it to limit boundary effects. The second area size (100×100 m) provides a larger area around the building. Domain size has a large effect on computational time, and therefore the optimal size needs to be chosen (ENVI-met, n.d.). For example, increasing the domain size from 60×60 m to 100×100 m increases the number of cells by a factor of 2.78, but the number of relationships changes by N^2, meaning the number of relationships increases by a factor of 7.7. In Appendix F, the output of the runs is presented. Both domains have 24 vertical cells. Another option was a 180×180 m domain with nine repetitions of the building typology, which would be more realistic, as buildings in urban areas are typically surrounded by other buildings. However, this domain size is not feasible due to the required calculation time. As these nine buildings particularly influence the wind speed, the wind speed is lowered accordingly. For a stable run, a wind speed of 1.5 m s^{-1} is chosen (ENVI-met Support Center, 2022). Because

Table 4.1: Potential air temperature statistics within 6 meters of the building, per time and grid resolution. The 2 m resolution shows an RMSE with the 1 m resolution over all statistics of 0.13 °C. The 3 m resolution has an RMSE of 0.23 °C.

Time (hh:mm)	Day (dd.mm)	Resolution (m)	Mean (°C)	Min (°C)	Max (°C)	Q25–Q75 (°C)
11:00	23.08	1x1 m	22.07	21.02	23.27	21.58–22.65
11:00	23.08	2x2 m	22.12	21.05	23.36	21.61–22.77
11:00	23.08	3x3 m	21.96	20.96	23.02	21.44–22.46
14:00	23.08	1x1 m	25.30	23.56	27.52	24.44–26.39
14:00	23.08	2x2 m	25.08	23.37	27.22	24.25–26.18
14:00	23.08	3x3 m	25.08	23.38	27.01	24.03–26.11
17:00	23.08	1x1 m	24.11	23.16	25.21	23.58–24.66
17:00	23.08	2x2 m	23.98	23.08	25.00	23.49–24.48
17:00	23.08	3x3 m	24.01	23.03	25.13	23.50–24.54

only a single building was modelled instead of the full urban environment, the radiative exchange within the urban canopy layer is not fully represented. In reality, multiple buildings would increase the internal reflection of shortwave radiation, trap longwave radiation, and create additional shading patterns. This simplification likely leads to an overestimation of reflected shortwave radiation, an overestimation of outgoing longwave radiation fluxes, and an overestimation of sky view factors, thereby affecting the thermal environment around the building. In chapter 6, the impact of these modelling choices on the results is discussed.

The simulations show that the temperature does not fully stabilise within the domain. ENVI-met calculates the temperature in every grid cell using the specified meteorological inputs and surface characteristics. The input temperature is only forced at the boundary where wind enters the domain, which results in a temperature increase across the area.

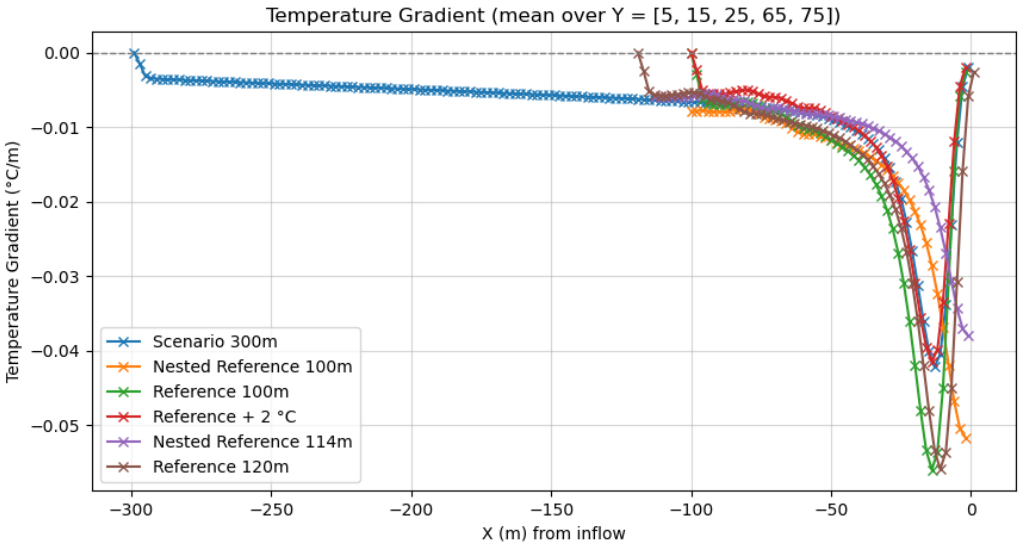

Figure 4.4: Air temperature gradient for different reference runs. The wind source is at the input boundary, which is at 0 m.

To assess the extent of this effect, multiple domain sizes were tested and visualised in Figure 4.4: 60×60 m, 80×80 m, 100×100 m, 300×80 m, and 122×80 m. In all cases, a clear temperature gradient emerged—from the inflow boundary to the outflow boundary. However, this gradient consistently diminished further from the inflow boundary. In all runs, the gradient reduced to an acceptable level (< 0.01 °C) approximately 75 m from the input boundary. This distance was therefore selected as the minimum spacing between the house model and the inflow boundary. As a result, the 122×80 m domain is used in this study. The final characteristics of the main area for low-rise are presented in Table 4.2. Three building typologies (low-, mid-, and high-rise) are applied in this study, and the dimensions of each building typology and domain are adjusted accordingly.

Table 4.2: Grid characteristics of the final domain used in the ENVI-met simulation.

Property	Low-rise	Mid-rise	High-rise
Grid dimensions	61 (x) × 40 (y) × 24 (z) cells	69 (x) × 48 (y) × 29 (z) cells	69 (x) × 48 (y) × 39 (z) cells
Physical domain size	122 m (x) × 80 m (y) × 39.96 m (z)	138 m (x) × 96 m (y) × 44.96 m (z)	138 m (x) × 96 m (y) × 54.96 m (z)
Horizontal resolution	dx = 2 m, dy = 2 m	dx = 2 m, dy = 2 m	dx = 2 m, dy = 2 m
Vertical resolution	dz = 1 m (with 20% telescoping from 15 m, and 5-fold split in first cell)	dz = 1 m (with 20% telescoping from 20 m, and 5-fold split in first cell)	dz = 1 m (with 20% telescoping from 30 m, and 5-fold split in first cell)
Building dimensions	18 m (x) × 8 m (y) × 6–8 m (z)	18 m (x) × 8 m (y) × 15 m (z)	18 m (x) × 8 m (y) × 24 m (z)
Runtime	21–24 hours	30-36 hours	40-48 hours

4.1.5. Building typologies

Three building typologies in formation are used in this study (Daniel et al., 2023). The buildings used as reference cases for low-, mid-, and high-rise are visualised in Figure 4.5. The low-rise scenario is analysed with 13 greening scenarios, the mid-rise with three, and the high-rise with one. The low-rise building is closely replicated from blueprints of a typical 1970s Dutch house; further information on this house is provided in Appendix I. The mid- and high-rise buildings are simplified in this study. The exact dimensions of each building typology are presented in Table 4.2. For mid- and high-rise cases, the domain is adjusted according to the height of the building. Sufficient space is required between the building and the edges of the modelling area to ensure stable calculations in ENVI-met.

Figure 4.5: Reference buildings for low-rise (left), mid-rise, and high-rise (right) typologies used in this study. Mid- and high-rise buildings are used as examples, a more simplified building is used in this study.

4.1.6. Green interventions

Input parameters in ENVI-met for every green intervention are stated.

Green roof

In this study, both extensive and intensive green roofs are considered. Only 70% of each roof surface is covered with a green roof system, as technical installations and roof edges typically remain uncovered (Personal communication, Sweco). For the low-rise scenario, the roof is tilted at 34.8°, making only an extensive green roof feasible. For the mid-rise scenario, both extensive and intensive green roofs are used to compare their effects. For the high-rise, no green roof is included, as the results from the mid-rise case are considered sufficient.

Extensive systems are lightweight, require little maintenance, and can be installed on slopes up to 45° with appropriate anti-slip measures. However, water retention and plant survival can be more challenging due to runoff and drought risk (Groenblauwe Netwerken, n.d. Nationale Dakenplan, 2021; Sedumspecialist, n.d.). Vegetation typically consists of sedum (succulents), mosses, or herbs. In this study, a sedum roof is applied.

Intensive green roofs, by contrast, are generally limited to slopes of up to 4° and require significantly more structural support and maintenance (Groenblauwe Netwerken, n.d. Nationale Dakenplan, 2021; Sedumspecialist, n.d.). Mixed plants are applied with an average height of 40 cm, and the substrate height is set to 25 cm. The exact ENVI-met inputs for each greening intervention are listed in Appendix B.

The composition of both extensive and intensive green roofs is provided in Table 4.3. Furthermore, all input values for the green roofs in ENVI-met are shown. These values were verified with a specialist from Rooftop Revolution.

Table 4.3: Composition and ENVI-met input parameters for extensive and intensive green roofs (Gomes et al., 2019; Groenblauwe Netwerken, n.d. Nationale Dakenplan, 2021; Sedumspecialist, n.d.). Furthermore parameters are stated for the green wall (Ottelé et al., 2011; Pérez et al., 2022; Perini et al., 2011).

Parameter	Extensive green roof	Intensive green roof	Green wall
Vegetation layer	Sedum, height = 5 cm	Mixed, height = 40 cm	Hedera Helix, thickness = 20 cm
Substrate	Soil, height = 5 cm	Soil, height = 25 cm	-
Drainage & protection	HDPE and air, height = 5 cm	HDPE and air, height = 5 cm	-
LAI (m^2 m^{-2})	1.00	3.00	3.00
Leaf Angle Distribution (0-1)	0.30	0.30	0.30
Thickness (m)	0.15	0.80	0.20
Albedo	0.25	0.25	0.20
Emissivity	0.96	0.96	0.97
Transmittance	0.05	0.05	0.30

Green roofs are tested in two scenarios:

- coverage of extensive green roof
- coverage of intensive green roof

Green wall

Several types of green walls are possible. In this study, a *Hedera helix* (ivy) is used as a direct climbing plant on the façade. The green wall covers 100% of the façades (excluding windows). The glazing percentage for the

low-rise case is 26.8% on the north façade and 29.5% on the south façade. For the mid- and high-rise cases, a standard glazing percentage of 33.3% is applied to both façades. Although this represents maximum coverage, in practice the percentage would likely be lower. Input parameters are shown in Table 4.3.

Green walls are tested in three scenarios:

- Green coverage on the north façade
- Green coverage on the south façade
- Green coverage on both north and south façades

Green at surface level

To assess the impact of vegetation around buildings, scenarios are developed using three categories of vegetation:

- Low vegetation: Grass, height ≤ 0.5 m
- Medium vegetation: Shrubs, height 0.5–2 m
- High vegetation: Trees, height > 2 m

For low vegetation, the standard ENVI-met grass type *grass 25 cm average dense* is used. For medium vegetation, the standard ENVI-met hedge type *Hedge dense, 1 m* is applied. Input parameters are listed in Table 4.4. For high vegetation, a tree species was selected that had to meet several criteria to ensure suitability for this study (Hirons & Sjöman, 2019; Noome et al., 2023). The criteria were:

- contribute to heat stress mitigation,
- have high drought resistance, as droughts may intensify in both frequency and duration (KNMI, 2023),
- be native to the region,
- have low allergenic potential,
- tolerate paved environments,
- and be implementable within ENVI-met.

Based on these criteria, the field maple (*Acer campestre*) was selected as the most suitable species (Bomentabel, 2024; Spijker et al., 2024). This choice was further validated through consultation with a specialist from Boomkwekerij Ebben.

For the ENVI-met simulations, the standard field maple *Field Maple (young)* is used. This model is scaled to represent a 10-year-old tree, with a height of 5.59 m and a canopy width of 2.99 × 3.55 m. To explore the impact of larger trees, an additional scenario includes a medium-aged tree, *Field Maple (middle)*. This tree represents a 20–30-year-old specimen and is scaled to 11.08 m in height, with a canopy width of 6.30 × 6.90 m. This study focuses primarily on younger trees, as the aim is to evaluate short-term effects in the near future. Moreover, large trees are often difficult to accommodate in gardens or close to houses. Input parameters are provided in Table 4.4. Additional details for each greening intervention are presented in Appendix B.

Table 4.4: Composition and ENVI-met input parameters for grass, shrubs, and two field maple trees (Bomentabel, 2024; Boomkwekerij Ebben, n.d. Spijker et al., 2024).

Parameter	Grass	Shrubs	Field maple 6 m	Field maple 11 m
Height (m)	0.25	1.0	5.59	11.08
Thickness (m)	-	-	2.99–3.55 canopy width	6.30–6.90 canopy width
Albedo	0.20	0.20	0.18	0.18
Emissivity	0.97	0.97	0.96	0.96
Transmittance	0.30	0.30	0.30	0.30

Vegetation is added within the 10 m in front of the north and south façades, representing the area where a garden could be located. Different scenarios are developed to model the effect of each vegetation type:

- 50% grass,
- 50% shrubs,
- Three trees (6 m height) north of the building at 3 m distance, and three trees south of the building at 9 m distance,
- Three trees (6 m height) north of the building at 9 m distance, and three trees south of the building at 3 m distance,
- Three trees (11 m height) north of the building at 9 m distance, and three trees south of the building at 5 m distance,
- Combination of 11 m height trees with 50% shrubs and 50% grass.

Finally, an integrated scenario is created with maximum greening: 11 m height trees with 50% shrubs and 50% grass combined with 70% coverage of extensive green roof and green coverage on both north and south façades.

4.1.7. Low-rise building

All inputs are discussed, so the scenarios can be selected for every building typology, starting with the low-rise. For low-rise, all scenarios are tested except for the intensive green roof. To evaluate the effect of building height, some scenarios are also tested on mid- and high-rise cases.

In the Netherlands, low-rise buildings typically consist of two to four storeys, often including a pitched roof or rooftop extension. These structures include single-family homes, townhouses, and semi-detached villas, typically characterised by ground-level access and private gardens (TU Delft OpenCourseWare, 2016).

A representative example of low-rise housing is found at The Green Village near TU Delft. An image of these buildings is shown in Figure 4.5. Further specific information about the building is provided in Appendix I. Blueprints of the houses are used to model them as accurately as possible. The houses are replicated in this modelling study, with the orientation adjusted to south-facing. The modelled row consists of three houses, each with a width of 6.164 m. Since ENVI-met can only model rectangular blocks, a schematic representation of the houses is created with a width of 6 m for each house. Low-rise buildings often have roof angles exceeding the threshold for intensive green roofs. The building at The Green Village has a roof angle of 34.8 °. Therefore, the intensive green roof scenario is not included. The glazing percentage for the low-rise case is 26.8% on the north façade and 29.5% on the south façade. The exact parameters used in ENVI-met for walls, roofs, and glazing are listed in Appendix B. Of all greening interventions described in subsection 4.1.6, only the intensive green roof is excluded. Exact grid characteristics for every low-rise scenario are stated in Table 4.2. All low-rise scenarios in ENVI-met are visualised in Figure 4.6.

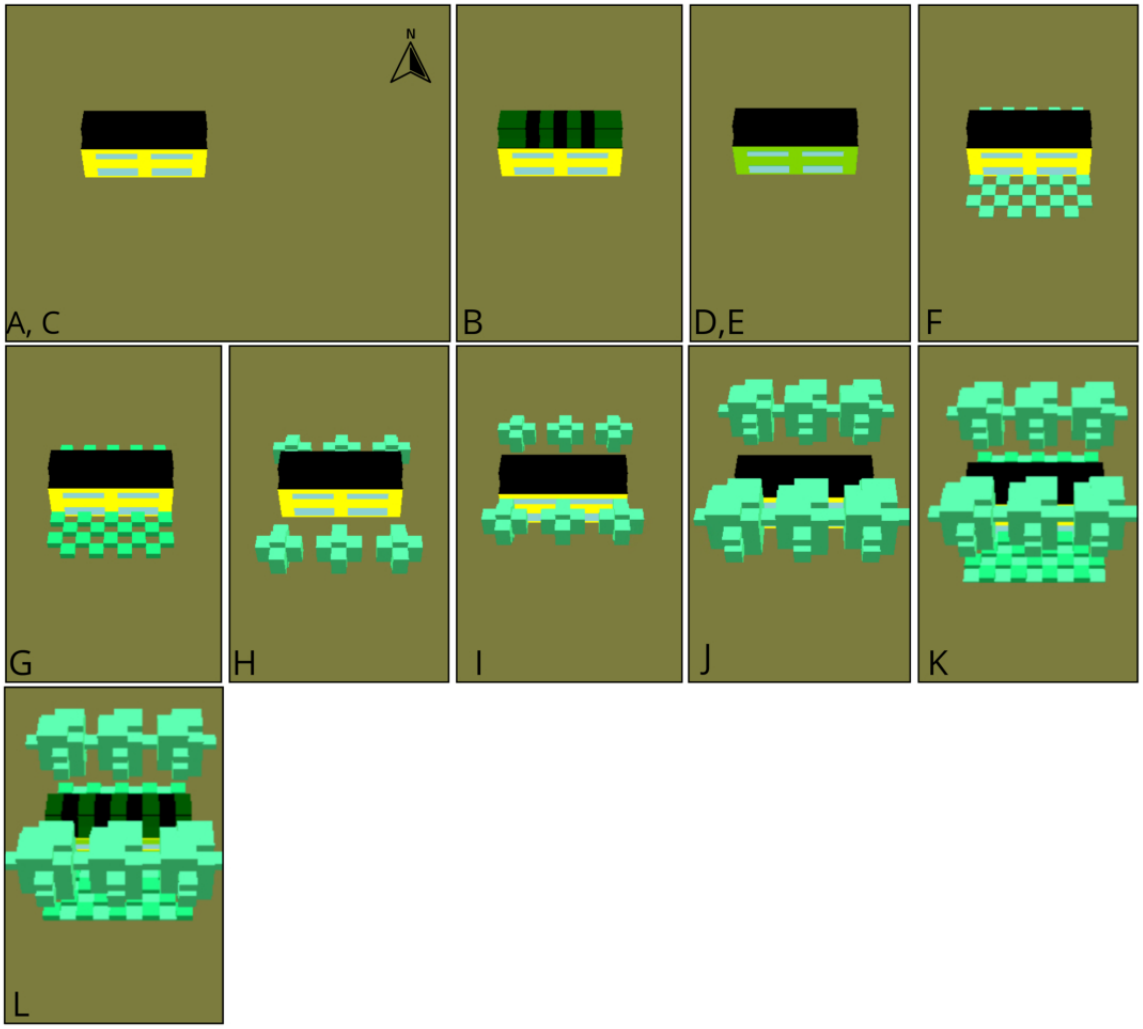

Scenario	Code	Description
A	LOW-REF	Reference scenario (no greening)
B	LOW-GR-EXT	70% coverage of extensive green roof
C	LOW-GW-N	Green coverage on north façade
D	LOW-GW-S	Green coverage on south façade
E	LOW-GW-S-N	Green coverage on both façades
F	LOW-GRASS	50% grass
G	LOW-SHRUBS	50% shrubs
H	LOW-TREE-6m-N3S9	Three trees (6 m height): 3 m north and 9 m south of the building
I	LOW-TREE-6m-N9S3	Three trees (6 m height): 9 m north and 3 m south of the building
J	LOW-TREE-11m-N9S5	Three trees (11 m height): 9 m north and 5 m south of the building
K	LOW-TREE-11m-N9S5+SHRUB+GRASS	Trees + 50% shrubs + 50% grass
L	LOW-INTEGRATED	Integrated: trees (11 m) + grass/shrubs + façades + roof greening

Figure 4.6: All scenarios used for the low-rise building typology visualised in ENVI-met with descriptions. From now on, the scenario codes are used throughout the analysis.

4.1.8. Mid-rise building

Following the first simulation round for the low-rise, an evaluation is made of the effect of green interventions for taller buildings. Mid-rise buildings range from three to six storeys and are common in Dutch cities. This category includes apartment buildings with portico entrances, low-rise flats, and stacked housing units, sometimes with external galleries or maisonettes (TU Delft OpenCourseWare, 2016). Greening options that had an indoor effect < 0.25 °C in the low-rise analysis are excluded from the mid-rise calculations. This means that green walls are not modelled for mid-rise. Furthermore, the scenarios with 50% grass and 50% shrubs are excluded. Integrated scenarios are tested in the low-rise simulations to explore whether an optimal amount or configuration of greenery exists. These scenarios are not repeated for mid-rise. The mid-rise scenarios are used to assess how effects change with building height. Therefore, only the scenario with code LOW-TREE-11m-N9S5 is used. In addition, mid-rise is used to compare the impact of extensive and intensive green roofs across all floors. A coverage of 100% is applied, although 70% is more realistic (Personal communication, Sweco). For comparison, 70% coverage introduced local variation in cells, complicating the analysis.

No exact building is replicated for mid-rise. Parameters of average mid-rise buildings are used in this study. A building with five storeys is modelled, making it 15 m in height. The building consists of three units in total, with dimensions of 18 m (x) and 8 m (y). The grid characteristics are stated in Table 4.2. Meteorological inputs are identical to those for the low-rise. A glazing percentage of 33.3% is used for the south and north façades, which falls within the expected range of 20–45% (RVO, 2017; Shaik et al., 2021). The exact parameters used in ENVI-met for walls, roofs, and glazing are listed in Appendix B.

Of all greening interventions described in subsection 4.1.6, three are tested for mid-rise to assess their effect on taller buildings. The mid-rise scenarios are visualised in Figure 4.7.

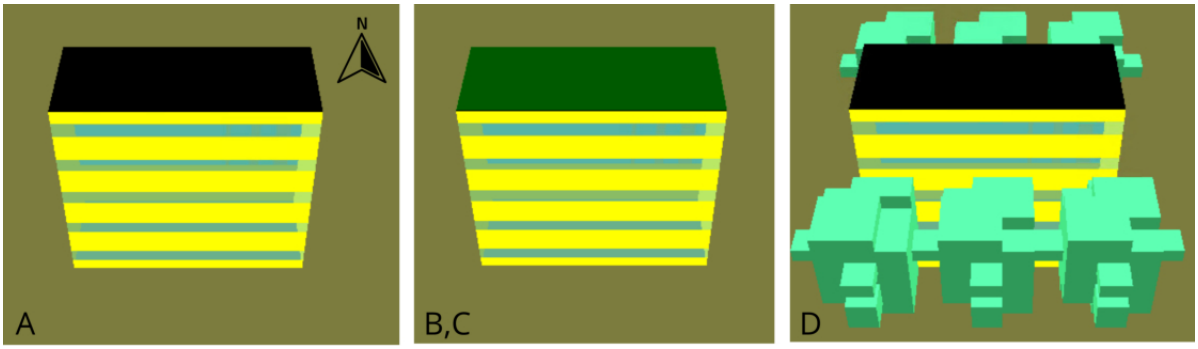

Scenario	Code	Description
A	MID-REF	Reference scenario (no greening)
B	MID-GR-EXT	100% coverage of extensive green roof
C	MID-GR-INT	100% coverage of intensive green roof
D	MID-TREE-11m-N9S5	Three trees (11 m height): 9 m north and 5 m south of the building

Figure 4.7: All scenarios used for the mid-rise building typology visualised in ENVI-met with descriptions. From now on, the scenario codes are used throughout the analysis.

4.1.9. High-rise building

After the low- and mid-rise simulations, an evaluation is made of the scenarios. High-rise buildings are those exceeding five storeys, requiring elevators and additional emergency exits. They include tall apartment towers, connected high-rise buildings, and large-scale residential flats, with modern skyscrapers reaching up to 150 m in height (TU Delft OpenCourseWare, 2016). A high-rise building is used to examine at what height the cooling effect of trees diminishes. Therefore, the scenario described in subsection 4.1.6 with 11 m tall trees is tested.

No exact building is replicated for high-rise. Parameters of average high-rise buildings are used in this study. A building with eight storeys is modelled, making it 24 m in height. Due to licensing constraints, IES-VE limited the number of storeys to eight. For every storey, a gallery is modelled on both the north and south façades. The building consists of one flat with total dimensions of 18 m (x) and 8 m (y). The grid characteristics are listed in Table 4.2. Meteorological inputs are the same as those used for the low-rise. A glazing percentage of 33.3% is

applied for the south and north façades, which is within the expected range of 20–45% (RVO, 2017; Shaik et al., 2021). The exact parameters used in ENVI-met for walls, roofs, and glazing are stated in Appendix B.

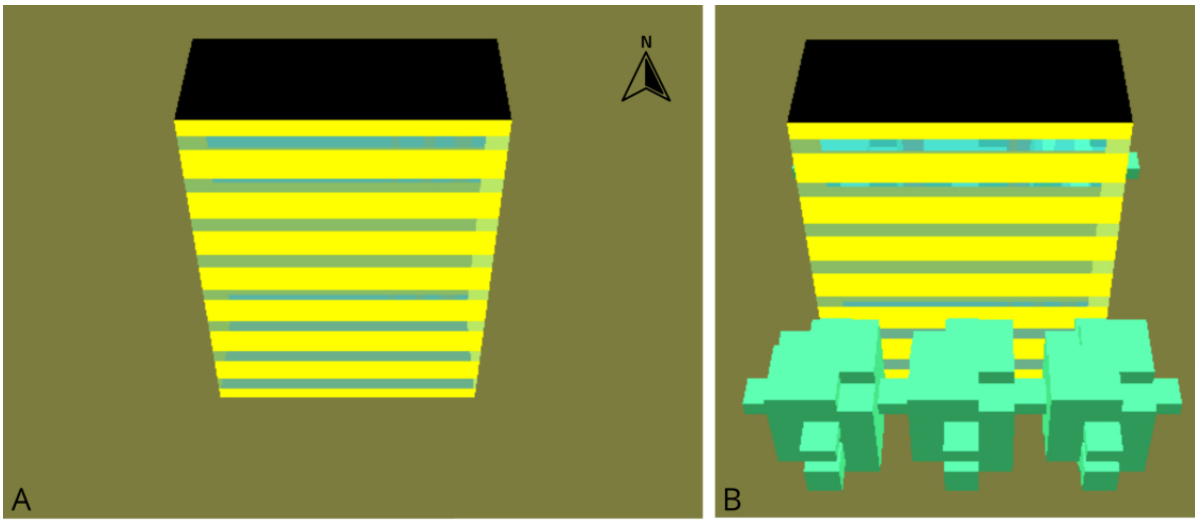

Scenario	Code	Description
A	HIGH-REF	Reference scenario (no greening)
B	HIGH-TREE-11m-N9S5	Three trees (11 m height): 9 m north and 5 m south of the building

Figure 4.8: All scenarios used for the high-rise building typology visualised in ENVI-met with descriptions. From now on, the scenario codes are used throughout the analysis.

4.1.10. ENVI-met outputs

After the modelling phase in ENVI-met, the results are visualised and used to evaluate Hypothesis 1: *green interventions reduce local outdoor air temperature and PET*. A 10 m area around both the north and south façades (hereafter *Area 1*) of the building is analysed to assess the local effects near the building. This area corresponds to the same zone where the green interventions are implemented, allowing for the evaluation of the direct impact of greening within private gardens. Additionally, a 20 m area around all façades (hereafter *Area 2*) is used to examine the broader effects of the interventions. A visual representation of these analysed areas is provided in Figure 4.9. Both outdoor air temperature [°C] and PET [°C] are used as performance indicators. To quantify the effects, three types of averages are calculated:

- *all*: daily average over the 5-day heatwave,
- *day*: average during daytime hours (07:00–20:00), when latent heat fluxes from vegetation are strongest,
- *max*: maximum 1-hour reduction, typically occurring between 12:00–14:00 depending on the scenario.

In addition, diurnal outdoor air temperature is plotted for Areas 1 and 2 for each low-rise scenario to assess the hourly variation in cooling performance of the green interventions.

ENVI-met provides Python tools for post-processing within the LEONARDO 5.8.0 environment. The *Compare Locations* and *Compare Scenarios* scripts were modified to export results in .csv format, enabling automated processing (Appendix E). These .csv files were subsequently analysed in Python. The advantage of this workflow is that multiple scenarios can be processed simultaneously, whereas the ENVI-met interface allows comparison of only two scenarios at once.

Outputs for air temperature, relative humidity, and wind speed from the cells directly adjacent to the building walls and roof are used as input for IES-VE. These cells are also visualised in Figure 4.9. The outputs are exported as .csv files using the Building Performance Simulation (BPS) module in ENVI-met, where results are grouped per façade orientation (north, south, east, west, and roof). An overall average across all façades is also provided.

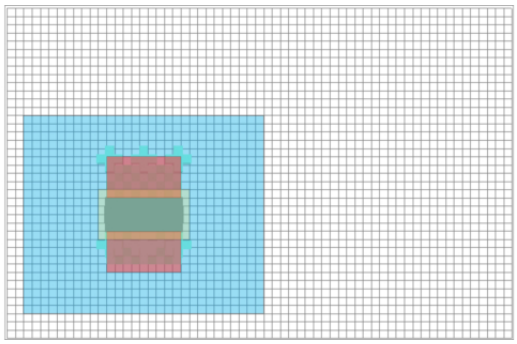

Figure 4.9: Area 1 (red): temperature calculated within 10 m of the greening interventions, representing the area where the green interventions are introduced. Area 2 (blue): temperature calculated within 20 m, representing the wider effect around the buildings of the green interventions. The yellow cells adjacent to the building indicate the cells used for coupling with IES-VE. The scenario shown as an example combines low-, medium-, and high-vegetation types for the low-rise building typology.

4.2. Coupling ENVI-met with IES-VE

To assess the effect of the green interventions on the thermal performance of buildings, a one-way coupling method is applied between ENVI-met (UCM) and IES-VE (BEM). Coupling UCM-BEM is widely adopted in the literature to incorporate microclimatic feedback into building energy simulations (Santamouris et al., 2018; Sezer et al., 2023; Tsoka et al., 2021; Yang et al., 2012). Only one-way coupling is reported for ENVI-met at the start of this study, therefore one-way is used (Pasandi et al., 2024). However, a recent study successfully implemented a two-way coupling between ENVI-met and EnergyPlus (Pasandi et al., 2025). Coupling procedures between ENVI-met and EnergyPlus are most commonly used (Manapragada & Natanian, 2025; Morakinyo et al., 2016; Pastore et al., 2017; Santamouris et al., 2018; Sezer et al., 2023; Yang et al., 2012).

Two coupling studies with IES-VE exist, both converting air temperature, relative humidity, and wind speed from ENVI-met to IES-VE (Shareef, 2021; Shareef & Altan, 2022). These studies do not address the effect of greenery and do not adjust dew point temperature or outside resistance.

In this study, an external coupling is implemented in Python to convert data from ENVI-met to the weather file of IES-VE. Dew point temperature is also calculated from ENVI-met output; the calculation is shown in Appendix C. The wind speed, air temperature and surface temperature averaged over each wall is used to calculate the outside resistance of every wall, roof, and window in IES-VE. Outside resistance represents the combined convective and radiative heat loss. In both models similar materials and material properties are used for every building part. Finally, a coupling is also made in the geometries.

4.2.1. Weather file

For each vegetation scenario (baseline and green interventions), ENVI-met is run at a spatial resolution of 2 m and provides hourly output for the simulation period. The following parameters are extracted for all cells adjacent to the building:

- Air temperature ($\mathtt{T}_a$)
- Relative humidity ($\mathtt{RH}$)
- Wind speed ($\mathtt{v}_s$)

These parameters were selected because they directly influence convective and moisture exchanges at the building envelope. Although ENVI-met also outputs variables such as shortwave and longwave radiation fluxes and surface temperatures, these were not imported since IES-VE cannot overwrite radiation per grid cell and therefore uses its own radiation balance model. In subsection 4.2.3, it is further explained how shortwave radiation is kept constant between both models. Wind direction, while simulated in ENVI-met, was also not transferred, as it is highly influenced by the surrounding walls and local turbulence. Since only a single prevailing wind direction can be defined in IES-VE rather than separate values per façade, a constant wind direction was applied. The resulting windward and leeward sides associated with this direction affect the outside resistance of each wall, as described in subsection 4.2.2, thereby influencing the convective heat transfer of the building through the outside resistance. The extracted parameters overwrite the corresponding hourly values in a baseline `.epw` weather file used by IES-VE. This modified weather file ensures that the IES-VE simulation reflects the localised effects of greenery interventions on microclimate. Air temperature and relative humidity also serve as input for calculating the dew point temperature ($\mathtt{T}_{dew}$), which is likewise overwritten in the EPW. See Appendix C for the formulas used to calculate dew point temperature.

As IES-VE requires an EPW input file, the results from ENVI-met were inserted into an existing EPW file. A complete EPW is required for IES-VE, but only the period 23–28 August was used in the modelling. The Typical Meteorological Year (TMY) file for Cabauw was initially used (Climate.OneBuilding, n.d.-a). Meteorological data and radiation were aligned with the inputs for ENVI-met (Knap, 2019; KNMI, 2019). Cloud cover data were extracted from KNMI hourly observations at De Bilt (KNMI, 2025). Thus, all data for 23–28 August originated from measured or modelled sources. For a schematic representation of the origin of each parameter for IES-VE, see Figure 4.10.

All data were converted to hourly values using averaging and resampling in Python to match EPW format requirements. All parameters used in the EPW are discussed in Appendix C. Wind direction follows ENVI-met and is set to 85°. Ground albedo has the same value as in ENVI-met, 0.2.

While building energy models typically simulate annual performance, microclimate simulations are often restricted to peak conditions due to computational constraints. In this study, inputs are provided for an entire year, but IES-VE selects the period 23–28 August 2019 to simulate indoor heat and energy usage. Only the heatwave period is modelled and analysed.

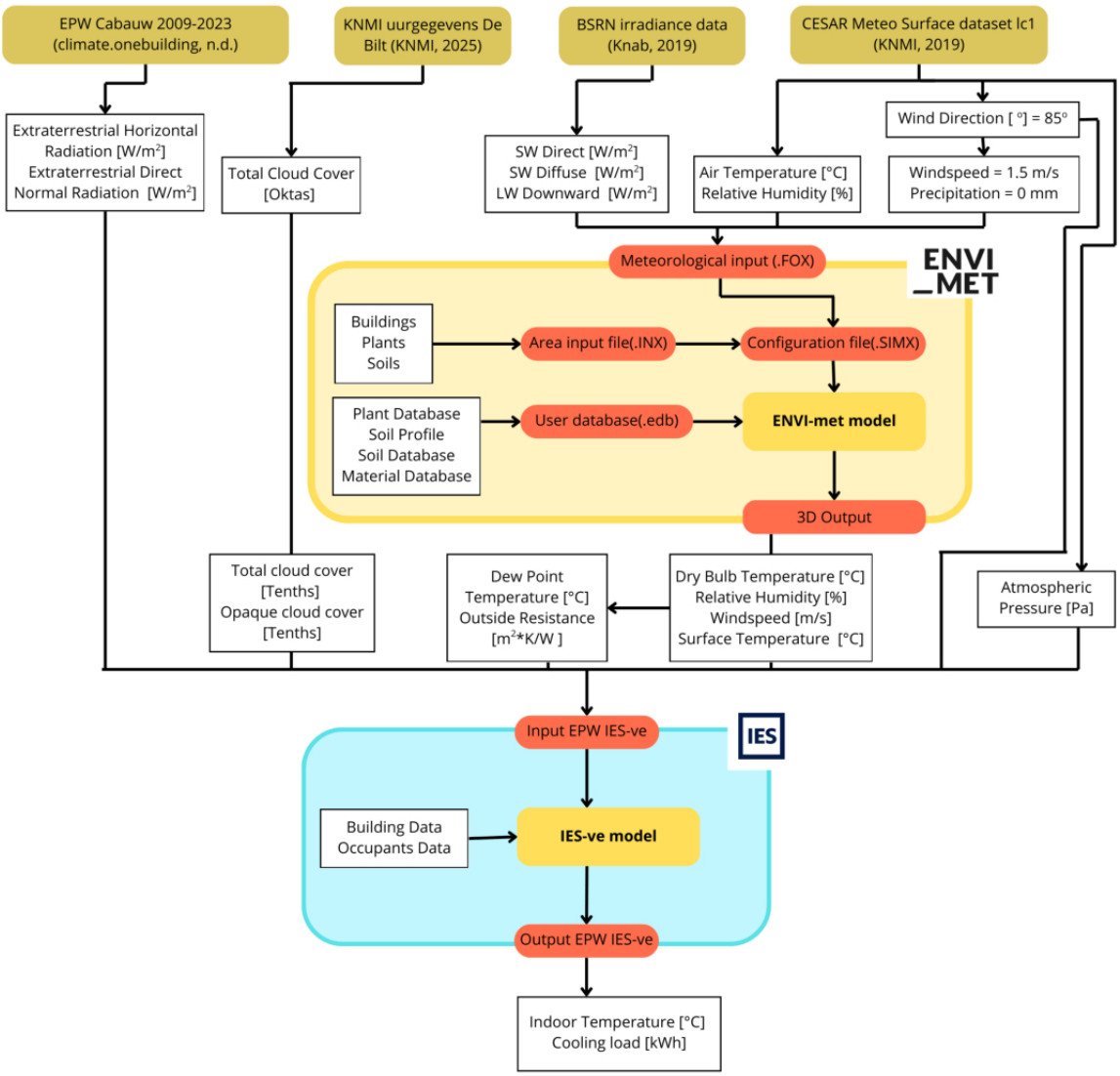

Figure 4.10: Flow diagram of meteorological input parameters for IES-VE

4.2.2. Outside resistance

In Gobakis and Kolokotsa (2017) an approach is used to calculate convective heat transfer heat coefficients from the UCM as input for the BEM. A similar approach is applied in this study for the outside resistance input in IES-VE. Outside resistance can be calculated from both convective and radiative heat transfer coefficients (ASHRAE, 2020; IES-VE, 2021b).

The wind speed (v_s) for each façade is obtained from the ENVI-met output files, measured 1 m from the façade. The convective heat transfer coefficient is then calculated using the correlation given in Equation 4.1. Since all wind speeds in the scenarios are relatively similar, no major differences in h_e and the resulting resistance are expected. However, this approach remains relevant because differences in wind speed between windward and leeward walls influence the external resistance coefficient of these walls.

IES-VE provides approximations of this resistance based on surface emissivity (high vs. low) and wind conditions (severe, neutral, or sheltered). In this study, however, wind conditions are explicitly modelled in ENVI-met, and the resulting microclimate outputs are used to calculate the resistance. The outside resistance is therefore based on the combined effect of convective and radiative heat loss (ASHRAE, 2020; IES-VE, 2021b).

Both the radiative heat transfer coefficient (h_r) and the convective heat transfer coefficient (h_c) are calculated explicitly. They are combined into the total external heat transfer coefficient h_e.

The convective heat transfer coefficient can be correlated either with wind speed at 10 m, at a fixed distance above the roof, or with the local surface wind speed. Since ENVI-met provides detailed microclimatic wind conditions close to the building, the wind speed at 1 m from the façade was selected. Defraeye et al. (2011) reviewed correlations between wind speed and h_c, and the empirical correlation derived from experimental data by Sharples (1984) is used here, as it applies to both windward and leeward façades:

$$h_c = 1.7\, v_s + 5.1 \tag{4.1}$$

where v_s is the wind speed measured 1 m from the façade in ENVI-met [m s^{-1}] and h_c is the approximation of the convective heat transfer coefficient in [W m^{-2} K^{-1}].

The radiative heat transfer is governed by the Stefan–Boltzmann law. This law is converted to a formula for the effective radiative heat transfer coefficient h_r (International Organization for Standardization, 2007):

$$h_r = 4\, \varepsilon\, \sigma\, T_m^3 \tag{4.2}$$

where h_r is the radiative heat transfer [W m^{-2} K^{-1}] ε is the surface emissivity [-], σ is the Stefan–Boltzmann constant ($\sigma = 5.67 \times 10^{-8}$ W m^{-2} K^{-4}), and T_m [K] is the mean temperature defined as:

$$T_m = \left(\frac{T_a + T_s}{2}\right) + 273.15 \tag{4.3}$$

where T_a is the outdoor air temperature [°C] in front of the wall and T_s is the surface temperature of the wall [°C].

Surface emissivity is a measure of the emissive efficiency of a surface. It equals 1 for an ideal black body, while most construction materials typically have values around 0.9 depending on material and surface finish. For example, in the low-rise scenario, an emissivity of 0.9 is used for walls and 0.837 for glazing (Oke et al., 2017).

Mean façade surface temperatures were approximated for the low-, mid-, and high-rise reference scenarios, ranging from 22.6 °C (north) to 28 °C (south). As this parameter has only a marginal effect on h_e, temperatures for each scenario were averaged every three hours. A misestimation of 1 °C in surface temperature would lead to an error of only about 0.2% in h_e and a maximum error of 0.05% in the total U-value of a wall.

Finally, the total external heat transfer coefficient h_e and external resistance (R_e) are calculated as:

$$h_e = h_c + h_r \tag{4.4}$$

$$R_e = \frac{1}{h_e} \tag{4.5}$$

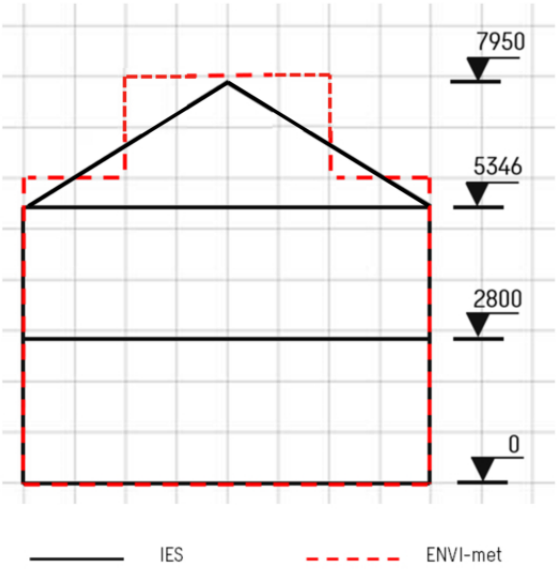

Figure 4.11: Comparison of geometry between IES-VE and ENVI-met

Where h_c, h_r and h_e are the convective, radiative and total external heat transfer coefficients respectively in [W m^{-2} K^{-1}] and (R_e) is the external resistance in [m^2 K^1 W^{-1}].

These resistance values are then input for every external wall, window, and roof in IES-VE. By using the wind speed, air, and surface temperatures from ENVI-met, every scenario has microclimate-adapted external resistance. In practice, the differences in external resistance resulting from this method are very small. In Appendix C, the resistance values are presented for every wall.

4.2.3. Geometry

Both simulation models (ENVI-met and IES-VE) share corresponding building geometries and surfaces. The ENVI-met model discretises the building into uniform block-shaped grid cells, while IES-VE retains a higher-resolution representation of surfaces and orientations. The geometries are aligned as accurately as possible by converting the geometries from blueprints to ENVI-met, see Figure 4.11.

The height and width of each tree are coupled from ENVI-met to IES-VE. For grass and shrubs, a shading structure is created with height, albedo, emissivity, and transmission values identical to those used in ENVI-met.

4.3. IES-VE

After the coupling of parameters from ENVI-met, the other inputs in IES-VE are required. In this section, the inputs and methodology for IES-VE are discussed.

4.3.1. Inputs

Meteorological inputs for IES-VE follow from the EPW file generated in the coupling procedure. Then the building is modelled in IES-VE. First, each room is modelled in the ModelIT environment of IES-VE. An example for the low-rise is shown in Figure 4.12. The interior of the building is represented as four equally sized rooms. Each building therefore has four rooms per level and one full-sized attic. This approach allows differences between north- and south-facing rooms to be captured. Windows and doors are modelled according to the blueprints. Since IES-VE requires a frame percentage within each window, windows are modelled as a combination of window and frame. The percentage of frame per window or door is then specified. Doors are modelled as windows with a different frame percentage, again following the blueprints. Exact glazing percentages are shown in Appendix C.

In Apache, parameters can be defined for every wall, window, door, floor, and roof. Walls are constructed by layers with specific thicknesses. Conductivity, density, specific heat capacity, and vapour resistivity must be defined per layer. On the outside, emissivity, solar absorptance, and the coupled outside resistance are required. For the

inside, emissivity, solar absorptance, and resistance must also be defined. Indoor parameters are kept constant with emissivity 0.9, solar absorptance 0.7, and resistance 0.13 m^2 K W^{-1}.

Doors and windows are defined as glazing structures. Parameters for glass are required, such as pane thickness, cavity thickness, and conductivity of the glass. Outdoor resistance follows from the coupling procedure, and emissivity for the selected glass is 0.837 in IES-VE. A frame percentage is then chosen, with absorptance specified for the frame. Frame resistance is calculated using the thickness (54 mm in all scenarios) and the conductivity of softwood (0.13 W $m^{-1}K^{-1}$) (Klinger et al., 2025; Suleiman et al., 1999). A resistance value of 0.42 m^2 K W^{-1} is obtained, which is applied to all door and window frames. Exact U-values per wall, roof, window, door, and floor are provided per building typology in Appendix C.

Finally, the model is run with the ApacheSim module. The simulation is conducted from 23 August to 27 August with a timestep of 10 minutes. Outputs include indoor temperature, and indoor heat gains and losses. In the following subsections, the inputs per greening type and building typology are explained in more detail.

Greening parameters

For the green roof, an additional layer is modelled. This layer represents the extra insulation provided by soil, drainage, and protection layers. The effect of plants is neglected for the U-value but is included in the outside resistance. The modelled air temperature, surface temperature, and wind speed from ENVI-met are used to calculate the outdoor resistance, with the green roof influencing these parameters in ENVI-met.

The extensive green roof consists of a sedum layer of 5 cm, a soil layer of 5 cm, and a 5 cm protection and drainage layer. The intensive green roof includes a plant layer of 20 cm, a soil layer of 25 cm, and a 5 cm protection and drainage layer. Soil layers are modelled in IES-VE as insulation with thermal conductivity 0.5 W m^{-1} K^{-1} (Bellazzi et al., 2020; Ochsner, 2019; Oke et al., 2017). This value may vary between 0.05 and 5 W m^{-1} K^{-1} depending on soil type and moisture content, with strong influence on results. The 5 cm drainage/protection layer is divided into 1 cm plastic and 4 cm cavity. The plastic layer has a conductivity of 0.32 W $m^{-1}K^{-1}$ and a resistance of 0.0313 m^2 K W^{-1}. The cavity has a resistance of 0.18 m^2 K W^{-1}. More information is given in Table C.7. The U-value for a conventional roof is 0.7130 W m^{-2} K^{-1}; in this study, it is reduced to 0.5840 W m^{-2} K^{-1} for the extensive green roof and to 0.4734 W m^{-2} K^{-1} for the intensive green roof. Research comparing U-values of conventional and green roofs shows reductions of similar magnitude (Aw et al., 2024; Mohapatra et al., 2021).

For green walls, no additional insulation layer is modelled as *Hedera helix* grows directly on the wall. The modelled air temperature, surface temperature, and wind speed from ENVI-met are used to calculate the outdoor resistance.

Trees are modelled as shading structures to replicate the shading simulated in ENVI-met. In IES-VE, trees have a transmittance of 0. As a result, the cooling potential of trees is likely overestimated, since in reality tree canopies transmit part of the solar radiation. Reported shortwave transmittance values for tree canopies typically range between 10–30%, depending on species, leaf density, and season (Heisler, 1986). The implications of this are further discussed in chapter 6. Ground parameters are adjusted for the low- and medium-vegetation scenarios in IES-VE. Outdoor resistance is calculated using ENVI-met outputs. For grass and shrubs, a shading structure is defined with height, albedo, emissivity, and transmission identical to those in ENVI-met. All scenarios are visualised in Figure 4.16.

Ventilation and infiltration

Ventilation and infiltration are kept constant per room. An average window opening is assumed for every room. Ventilation and infiltration are identical across all rooms and building typologies. Ventilation is calculated in Appendix C. Final ventilation is 0.020 m^3 s^{-1} per room, which is equivalent to 20 l s^{-1}. No difference is made between upstairs and downstairs rooms. Total ventilation for the house is 160 l s^{-1}. The attic does not contain windows, so no natural ventilation is modelled.

The infiltration rate is assumed to be 0.4 air changes per hour (ACH), consistent with values from literature (Henderson & Harley, 2022; Sailor, 2011).

Internal gains

A household of four persons (two adults and two children) is assumed. Standard values from IES-VE are used for a person. Four persons per house correspond to an average of 0.5 person per room. In reality, occupancy would differ per room, but this introduces an additional variable and would complicate analysis. Each person emits 90 W sensible and 60 W latent heat (IES-VE, 2025).

Internal heat gains from household equipment are also assumed uniform across all rooms. Average internal equipment gains are estimated at 2.5 W m^{-2} (Mata & Sasic Kalagasidis, 2009).

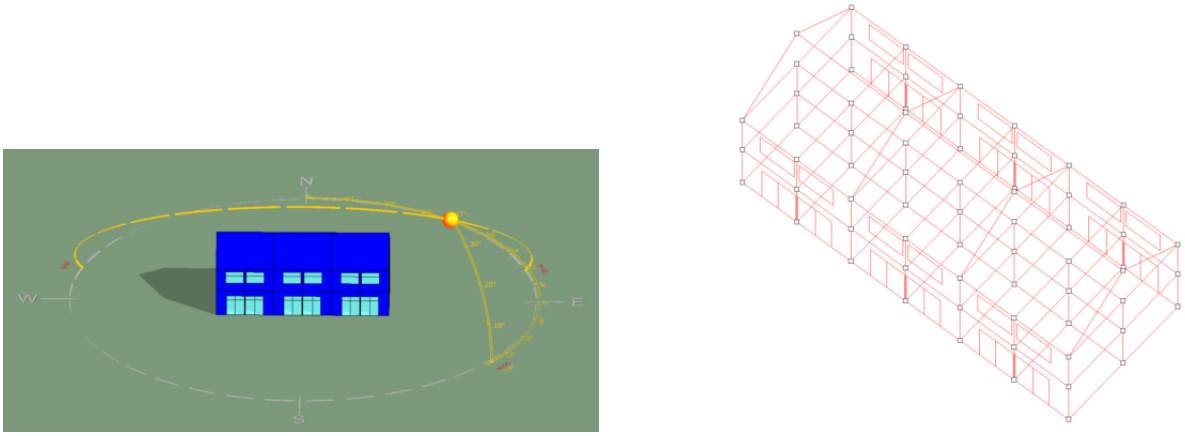

(a) IES-VE low-rise building at 11:00, showing solar altitude

(b) IES-VE low-rise showing all rooms

Figure 4.12: IES-VE low-rise visualisation

4.3.2. Low-rise building

The building's south and north walls are 6.1 m in length, and the other walls (west/east) are 7.3 m. The height of the first floor is 2.8 m and the second floor 2.546 m. The attic height is 2.604 m. A visual representation of the low-rise building in IES-VE is given in Figure 4.12. For a per-floor representation with room structure and codes used in the results, see Figure 4.13. Only the middle building is used for analysis. All scenarios are visualised in Figure 4.16.

The materials used for the low-rise are taken directly from the building blueprints. Exact U-values and inputs per wall, roof, window, door, and floor are provided in Appendix C.

4.3.3. Mid-rise building

The building's south and north walls are 6 m in length, and the west/east walls 8.0 m, consistent with ENVI-met. Three buildings are placed adjacent to each other. Floor height is 3.0 m, giving a total building height of 15.0 m. A glazing percentage of 33.3% is applied for every storey. Equal glazing percentages are used across storeys to ensure a fair comparison. Due to the room limit of 50 in the IES-VE licence used for this study, only the middle building is analysed. The analysed building contains four rooms per floor, whereas the adjacent buildings have three rooms per floor. Ideally, the adjacent buildings would be divided into four rooms, similar to the central building. However, the student version of IES-VE is limited to a maximum of 50 rooms; therefore, this simplified structure was adopted. A visual representation of the mid-rise building modelled in IES-VE with room structure and codes is given in Figure 4.14. All scenarios are visualised in Figure 4.16. Exact U-values and inputs per wall, roof, window, door, and floor are provided in Appendix C.

4.3.4. High-rise building

The building's south and north walls are 6 m in length, and the west/east walls 8 m. All floors are 3 m in height, giving a total of 8 floors. A glazing percentage of 33.3% is applied for every storey. Due to the room limit of 50 in the IES-VE licence used for this study, only the middle building is analysed. The analysed building contains four rooms per floor, whereas the adjacent buildings have one room per floor. Ideally, the adjacent buildings would be divided into four rooms, similar to the central building. However, the student version of IES-VE is limited to a maximum of 50 rooms; therefore, this simplified structure was adopted. A visual representation of the high-rise building in IES-VE with room structure and codes is given in Figure 4.15. All scenarios are visualised in Figure 4.16.

The materials used for the high-rise are directly taken from the blueprints of the building. Exact U-values and inputs per wall, roof, window, door, and floor are provided in Appendix C

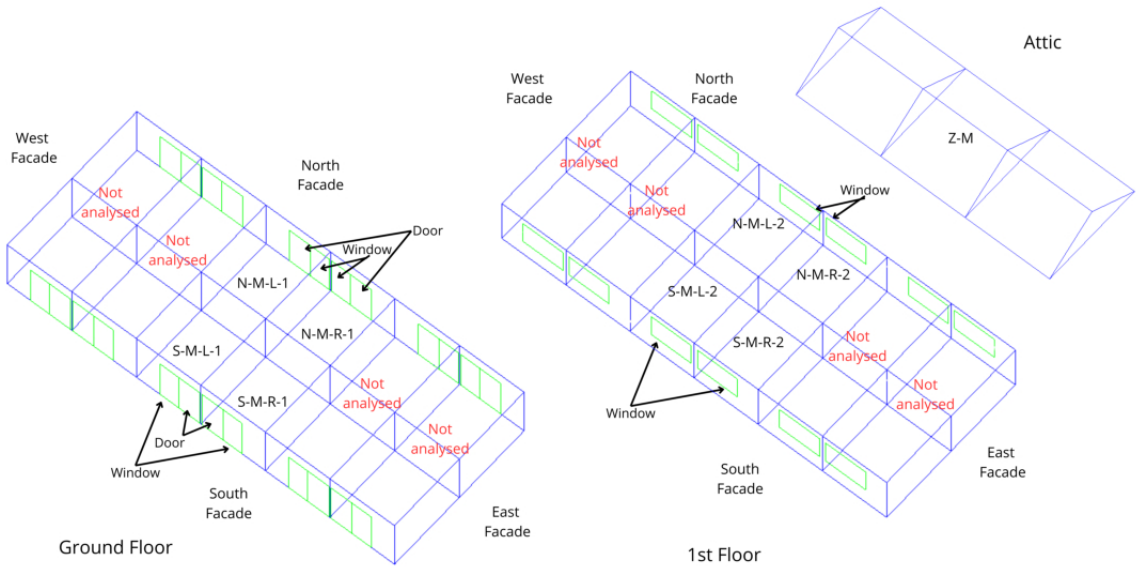

Figure 4.13: All floors for the low-rise building with code for every room. All buildings are modelled, but only the middle building is analysed in the results section.

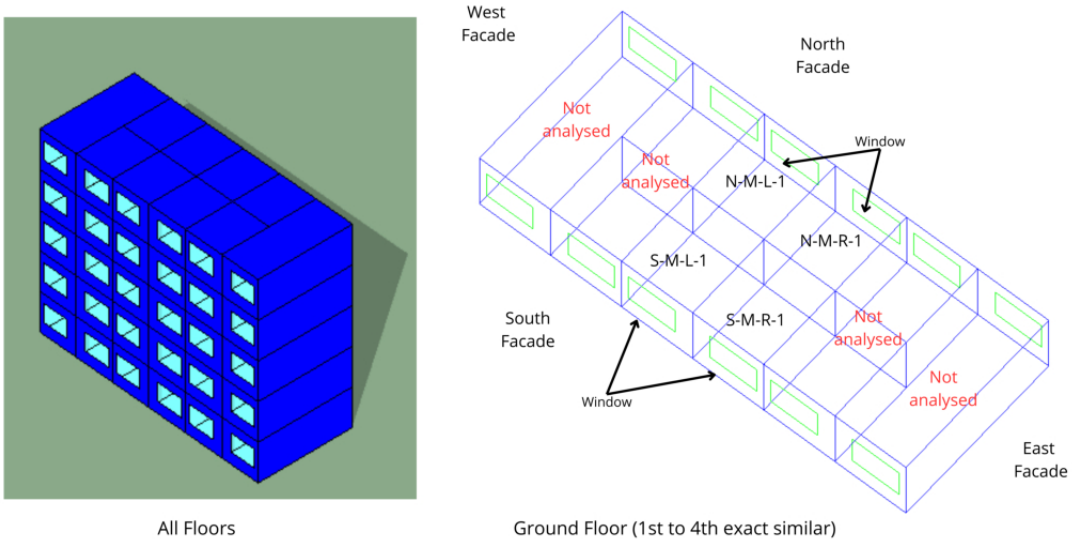

Figure 4.14: Left: visualisation of the mid-rise building used in this study. Right: all buildings are modelled, but only the middle building is analysed. Every floor is similar; room coding is shown for the ground floor, with the floor above coded as 2, etc.

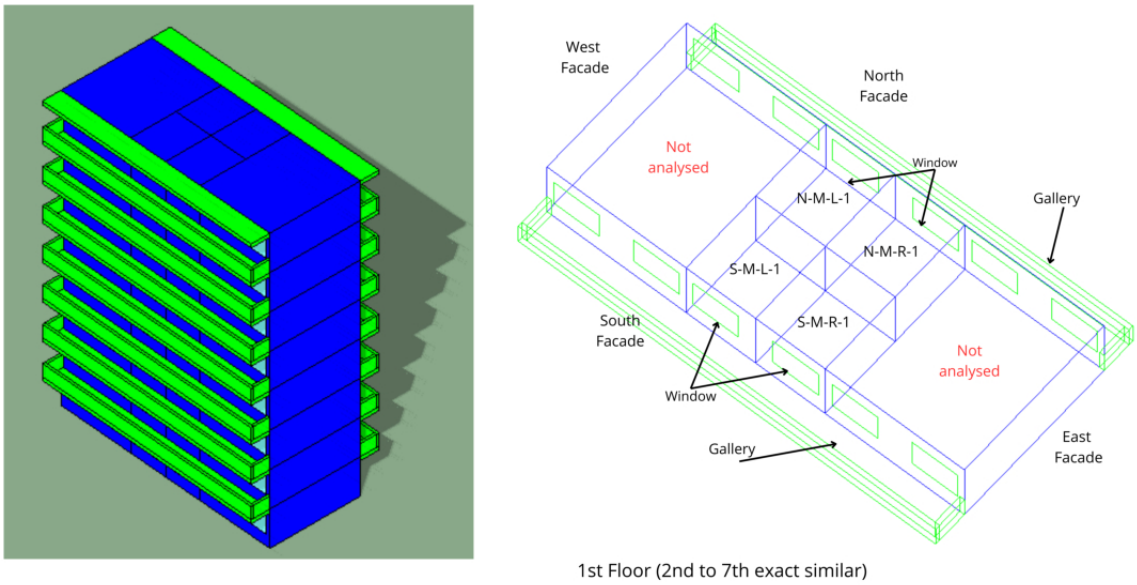

Figure 4.15: Left: visualisation of the high-rise building used in this study. Right: every floor is similar, except for the gallery (visible on the left). Room coding is shown for the first floor.

4.3.5. Outputs IES-VE

Every scenario is run twice in IES-VE. The first run gives indoor air temperature output for every room. This is needed for hypothesis 2: Green interventions maintain indoor temperatures within the comfort range. Furthermore the differences in indoor air temperature between building typologies are assessed. An overview is made of gains which influence indoor temperature, and the lag is calculated between indoor and outdoor temperature peaks.

In the second run, the cooling load is calculated to maintain the building temperature below the threshold value of 25 °C. The amount of kWh is summed for the entire heatwave and serves as output. it is used to see what effect green has on building cooling load. This is needed for Hypothesis 3: Green interventions (partly) reduce the need for mechanical cooling by limiting indoor overheating.

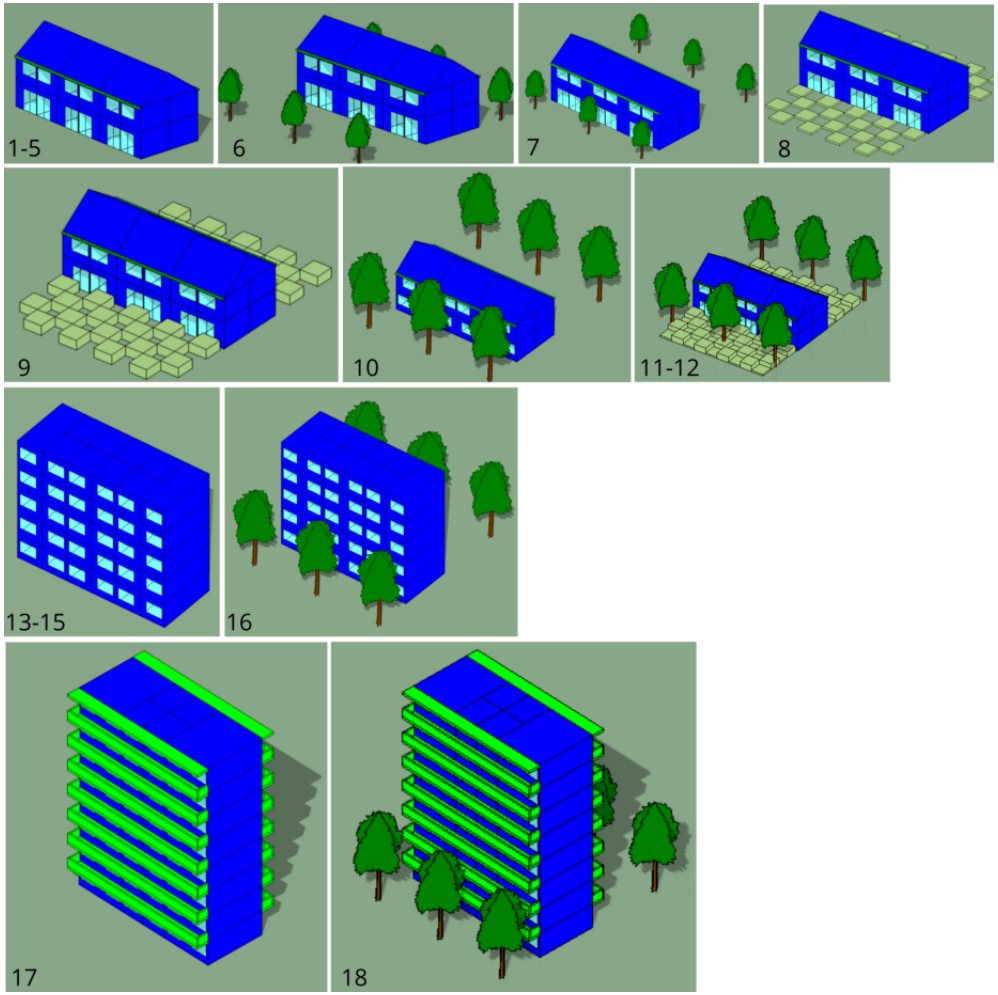

No.	Code	Description
1	LOW-REF	Reference scenario (no greening)
2	LOW-GR-EXT	Extensive green roof
3	LOW-GW-N	Green wall north façade
4	LOW-GW-S	Green wall south façade
5	LOW-GW-S-N	Green wall both façades
6	LOW-TREE-6m-N3S9	Trees (6 m): 3 m north, 9 m south
7	LOW-TREE-6m-N9S3	Trees (6 m): 9 m north, 3 m south
8	LOW-GRASS	50% grass
9	LOW-SHRUBS	50% shrubs
10	LOW-TREE-11m-N9S5	Trees (11 m): 9 m north, 5 m south
11	LOW-TREE-11m-N9S5 + SHRUB + GRASS	Trees (11 m): 9 m north, 5 m south + 50% shrubs + 50% grass
12	LOW-INTEGRATED	Integrated: trees + grass/shrubs + façades + roof greening
13	MID-REF	Reference scenario
14	MID-GR-EXT	Extensive green roof
15	MID-GR-INT	Intensive green roof
16	MID-TREE-11m-N9S5	Trees (11 m): 9 m north, 5 m south
17	HIGH-REF	Reference scenario
18	HIGH-TREE-11m-N9S5	Trees (11 m): 9 m north, 5 m south

Figure 4.16: All scenarios used in IES-VE for low- (1-12), mid- (13-16), and high-rise (17-18) typologies.

5

Results

This chapter presents the results of the scenario analysis performed in ENVI-met and IES-VE. The findings are structured around the three main hypotheses formulated in the introduction, addressing the effects of green interventions on (1) outdoor thermal comfort, (2) indoor temperature, and (3) building cooling demand. All simulations are analysed for the 23–27 August 2019 heatwave, with results expressed in UTC +1 and taken at 1.5 m height. An overview of all greening scenarios is provided in Table 5.1.

5.1. Impact of greening on outdoor thermal comfort

Hypothesis: Green interventions reduce local outdoor air temperature and PET.

The results for Area 1 and Area 2 are summarised in Table 5.1, showing values for all timesteps, daily averages, and maximum hourly reductions. The corresponding measurement areas are illustrated in Figure 4.9.

5.1.1. Outdoor air temperature

Green interventions affect air temperature through shading and evapotranspiration, and by altering wind flows and surface albedo. Vegetation cools the environment through evapotranspiration, which is driven by solar radiation. Part of the incoming energy is used as latent heat, converting water into vapour. In addition, vegetation provides shade, which reduces radiation at the surface. Green interventions also influence wind speed and direction, affecting mixing in the urban canopy layer. Finally, vegetation alters albedo, changing the local energy balance (Bowler et al., 2010; Oke et al., 2017; Shashua-Bar et al., 2009).

Low vegetation and façade greening

The cooling effects of low vegetation and wall and roof greening are generally small in this study (<0.5 °C).

- **Grass:** 50% coverage reduces local air temperature only marginally (max 0.05 °C) in Area 1.
- **Shrubs:** 50% coverage reduces local air temperature more than grass but still small (max 0.44 °C) in Area 1.
- **Green walls:** Minimal impact at pedestrian level (max 0.26 °C) in Area 1, as cooling remains concentrated on the façade surface and in a narrow downwind wake.
- **Green roofs:** Negligible impact at pedestrian level (max 0.02 °C) in Area 1; cooling occurs 0.5 m above the roof (max 2.41 °C) and within its downwind wake at 1.5 m (max 0.63 °C).

Trees

Scenarios with trees produce the highest degree of cooling. Shading and evapotranspiration from 11 m-high trees result in a daily average air temperature reduction of 0.32 °C and a maximum area-averaged reduction of 0.72 °C in Area 1, with a localised peak of 2.78 °C (see Table 5.1). The strongest cooling occurs directly beneath the tree canopy. Trees cool the environment not only with evaporation but also by shading. Furthermore trees affect the wind pattern and albedo.

Trees are the most effective green intervention, and combinations of trees, shrubs, and grass further amplify cooling. Adding green walls and roofs to such integrated scenarios can enhance performance, as discussed in chapter 6. The diurnal effect of each green intervention compared with the reference scenario for Areas 1 and 2 is visualised in Figure 5.2.

5.1.2. PET results

In addition to air temperature, PET is an important indicator of outdoor thermal comfort. A detailed explanation of PET is provided in Appendix A.

Low vegetation and façade greening

The PET effects of low vegetation and building greening are generally small.

- **Grass:** 50% coverage results in a daily average PET reduction of 0.05 °C in Area 1.
- **Shrubs:** 50% coverage results in daily average PET reduction of 0.53 °C in Area 1, mainly due to higher evapotranspiration.
- **Green walls:** Combining north and south wall greening reduces daily average PET by 0.53 °C in Area 1. Localised maxima of up to 3.68 °C occur on downwind section of the wall.
- **Green roofs:** Negligible PET reduction at 1.5 m (maximum 0.02 °C); reductions occur only at roof level.

The limited PET reductions are primarily due to minor air temperature changes and the absence of shading effects for these green interventions.

Trees

Trees provide the largest PET reductions. The 6 m trees already reduce daily PET in Area 1 by 0.88–1.11 °C, while the 11 m trees reduce PET by an average of 1.62 °C in Area 1. The maximum area-averaged PET reduction reaches 2.81 °C, with localised PET reductions of up to 11.51 °C directly under tree canopies (Table 5.1). PET benefits from both reduced air temperature and, more importantly, shading that decreases short-wave radiation. ENVI-met shows short-wave radiation reductions of up to 550 W m^{-2} under trees, which strongly lower PET. The small reduction in wind speed has a negligible warming effect on PET.

Integrated scenarios combining 11 m trees, shrubs, and grass yield the greatest PET benefits, with maximum localised reductions of up to 13.45 °C. These outcomes are compared with findings from reference studies in chapter 6.

5.1.3. Diurnal variation of temperature reduction

Vegetation cools the air primarily through evapotranspiration driven by solar radiation. Around midday, cooling peaks due to maximum radiation and higher air temperatures, which raise the saturation vapour pressure and vapour pressure deficit (VPD), enhancing evapotranspiration and latent heat flux (Bowler et al., 2010; Oke et al., 2017; Shashua-Bar et al., 2009). At night, when solar input is lost, vegetation has limited cooling effects.

This study found a maximum air temperature and PET reduction between 13:00 and 15:00 h. In Table 5.1, the reductions in temperature and PET are presented. The reference diurnal variation is shown in Figure 5.1, where peak temperatures occur around 14:00 h. The diurnal effect during the heatwave compared with the reference is visualised in Figure 5.2 for air temperature and PET. Peak temperature reductions are reached on 24 August at 14:00 h. At night, the cooling effect is almost zero, with some scenarios even showing a slight increase in nighttime temperature. For example, the scenario with 11 m trees (LOW-TREE-11m-N9S5) shows a nighttime temperature increase of 0.1 °C in Area 1.

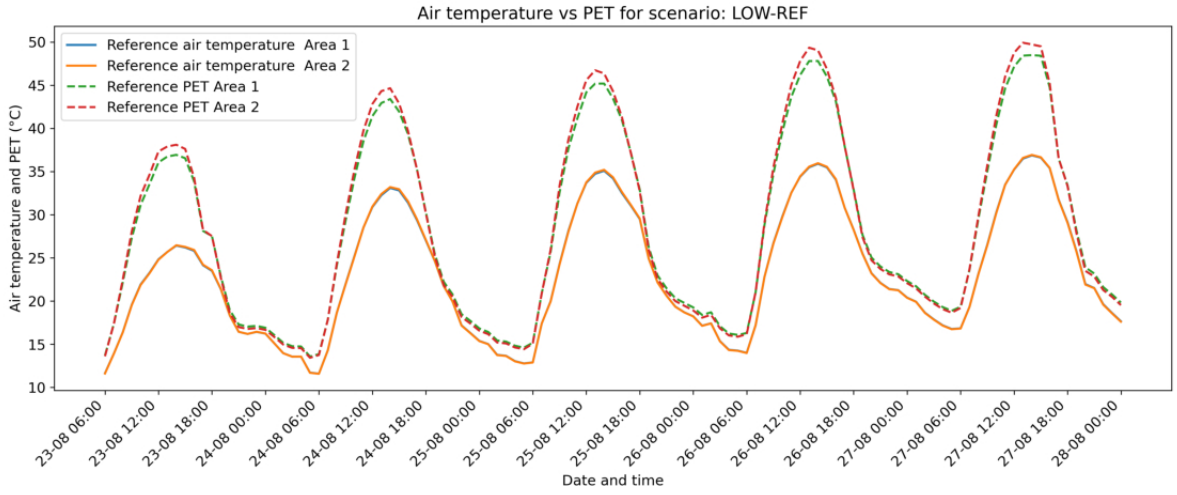

Figure 5.1: Average outdoor air temperature and PET at 1.5 m for Area 1, and Area 2 for scenario: LOW-REF.

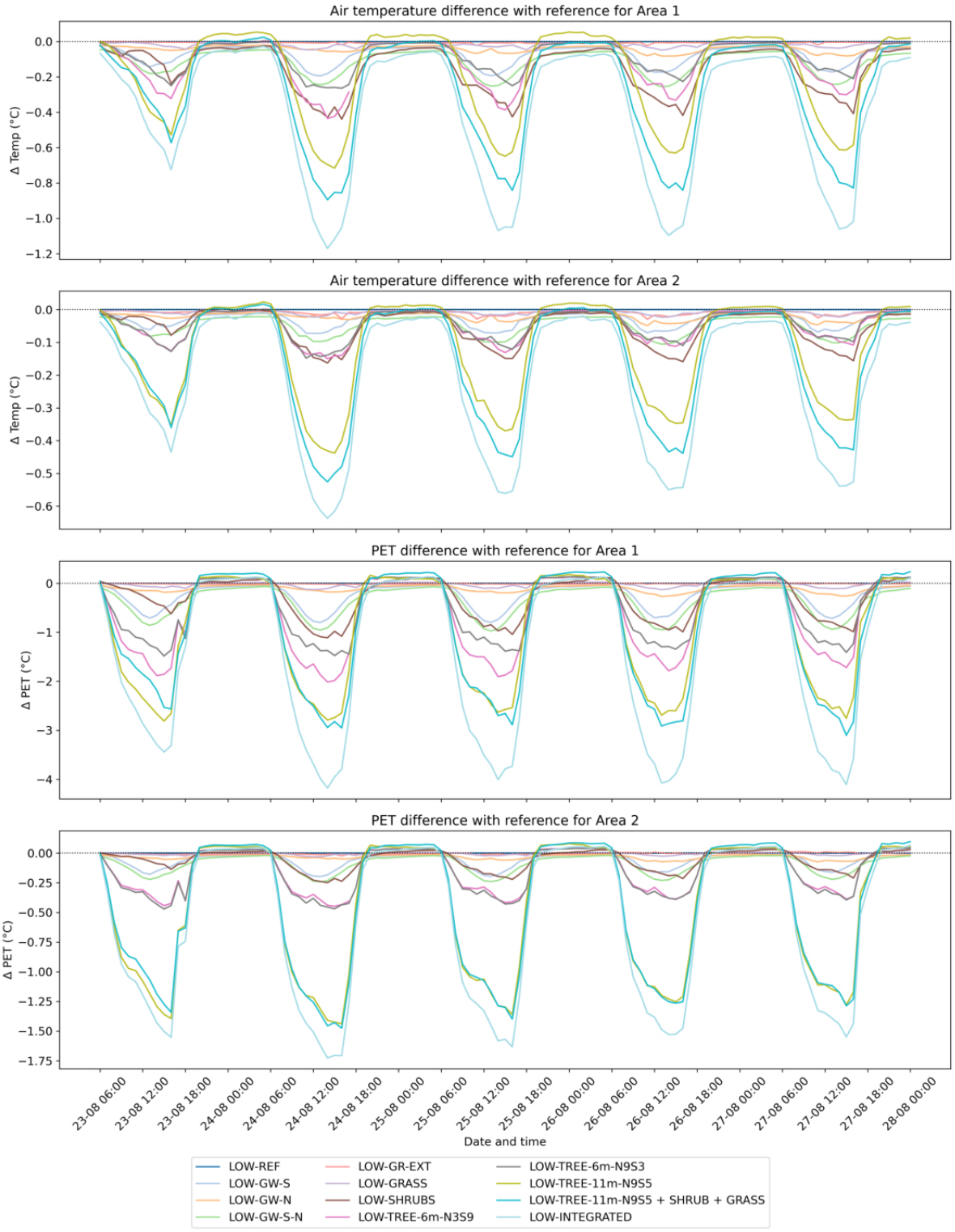

Figure 5.2: Average outdoor air temperature and PET at 1.5 m height for Area 1 and Area 2 for all scenarios. The combination of all greening measures produces the largest reduction in air temperature and PET.

Scenario	Avg ΔT Area 1 (°C)			Avg ΔT Area 2 (°C)			Avg ΔPET Area 1 (°C)			Avg ΔPET Area 2 (°C)			Max ΔT (°C)	Max ΔPET (°C)	Avg Indoor ΔT (°C)		Total energy usage HVAC (kWh)
	All	Day	Max	All	Day	Max	All	Day	Max	All	Day	Max			ΔT_{Avg}	ΔT_{Max}	
LOW-REF (absolute values)	23.15	27.38	36.87	23.15	27.39	36.93	28.21	34.66	48.49	28.46	35.24	49.92	-	-	25.56	34.51	114.3
LOW-GR-EXT	-0.01	-0.01	-0.02	-0.01	-0.01	-0.03	-0.01	-0.01	-0.02	-0.00	-0.00	-0.02	-0.29	-0.31	-0.44	-0.22	106.4
LOW-GW-S	-0.08	-0.10	-0.19	-0.03	-0.04	-0.07	-0.26	-0.38	-0.80	-0.06	-0.09	-0.20	-1.59	-3.68	-0.06	-0.08	112.1
LOW-GW-N	-0.04	-0.05	-0.08	-0.02	-0.03	-0.05	-0.11	-0.15	-0.27	-0.03	-0.04	-0.07	-0.80	-1.47	-0.04	-0.08	112.8
LOW-GW-S-N	-0.12	-0.15	-0.26	-0.05	-0.06	-0.10	-0.36	-0.53	-0.97	-0.09	-0.13	-0.24	-1.57	-3.68	-0.12	-0.19	110.1
LOW-GRASS	-0.02	-0.02	-0.05	-0.01	-0.01	-0.02	-0.03	-0.05	-0.13	-0.00	-0.01	-0.03	-0.36	-0.19	-0.00	-0.00	114.2
LOW-SHRUBS	-0.16	-0.22	-0.44	-0.05	-0.08	-0.16	-0.29	-0.53	-1.11	-0.06	-0.11	-0.25	-1.58	-2.07	-0.15	-0.18	108.0
LOW-TREE-6m-N3S9	-0.12	-0.19	-0.44	-0.05	-0.07	-0.15	-0.64	-1.11	-2.01	-0.14	-0.25	-0.45	-0.97	-6.09	-0.06	-0.04	112.6
LOW-TREE-6m-N9S3	-0.09	-0.13	-0.26	-0.05	-0.07	-0.15	-0.49	-0.88	-1.45	-0.15	-0.27	-0.47	-1.32	-7.85	-0.18	-0.29	105.9
LOW-TREE-11m-N9S5	-0.18	-0.32	-0.72	-0.12	-0.21	-0.44	-0.95	-1.62	-2.81	-0.48	-0.81	-1.44	-2.78	-11.51	-0.62	-0.95	87.3
LOW-TREE-11m-N9S5+SHRUBS+GRASS	-0.28	-0.45	-0.90	-0.16	-0.26	-0.53	-0.96	-1.69	-3.10	-0.47	-0.81	-1.48	-2.74	-10.42	-0.66	-0.95	85.9
LOW-INTEGRATED	-0.40	-0.60	-1.17	-0.21	-0.33	-0.64	-1.41	-2.36	-4.18	-0.58	-0.98	-1.73	-3.92	-13.45	-1.12	-1.20	77.9
MID-REF (absolute values)	23.01	27.18	36.02	23.09	27.38	36.65	27.68	33.86	47.09	28.33	35.14	49.31	-	-	24.96	35.18	247.8
MID-TREE-11m-N9S5	-0.17	-0.30	-0.66	-0.11	-0.20	-0.42	-0.92	-1.60	-2.75	-0.44	-0.77	-1.42	-2.64	-11.45	-0.26	-0.27	220.8
MID-GR-EXT	-0.01	-0.01	-0.02	-0.00	-0.01	-0.03	-0.01	-0.01	-0.02	-0.00	-0.00	-0.01	-0.44	-0.32	-0.16	-0.18	232.6
MID-GR-INT	-0.01	-0.01	-0.02	-0.00	-0.01	-0.02	-0.01	-0.01	-0.02	-0.01	-0.01	-0.01	-0.63	-0.46	-0.30	-0.28	221.4
HIGH-REF (absolute values)	22.99	26.98	35.72	23.05	27.17	36.39	27.59	33.52	46.72	28.15	34.62	48.66	-	-	22.74	28.18	112.5
HIGH-TREE-11m-N9S5	-0.16	-0.29	-0.64	-0.10	-0.17	-0.38	-0.90	-1.55	-2.72	-0.38	-0.66	-1.40	-2.68	-11.37	-0.05	-0.03	107.1

Table 5.1: Scenario comparison for low-rise, mid-rise, and high-rise building greening strategies. *All* means average over the whole heatwave, *Day* only account for hours (7-20) and *Max* accounts only for the maximum hour. Max ΔT (°C) and Max ΔPET (°C) are the cells with the maximum differences which can be found over the entire heatwave at one location. Average and indoor temperature over all rooms ΔT_{Avg} is calculated and the differences with the reference is stated. Furthermore indoor maximum temperature reduction for 1 room is calculated ΔT_{Max} (always S-M-R-2 or S-M-L-2). Finally the total HVAC energy usage for keeping the middle building in the comfortable range ($T_{in} < 25$°C) , is calculated.

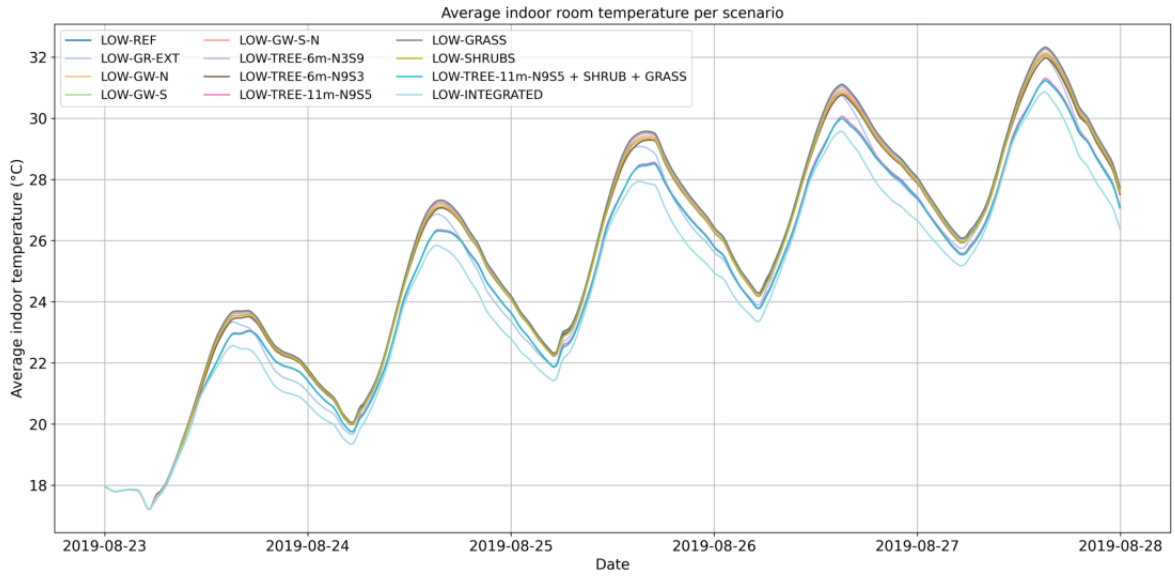

Figure 5.3: Diurnal variation of the average indoor room temperature for all low-rise scenario.

5.2. Potential of greening to reduce indoor air temperature

Hypothesis: Green interventions maintain indoor temperatures within the comfort range.

Green interventions have a cooling effect on outdoor temperatures, which also influence the indoor environment through ventilation, convection, and conduction. Façade greening lowers external wall temperatures, thereby reducing heat conduction through walls. Green roofs reduce roof surface temperatures and heat transfer, while trees provide shade, decreasing incoming solar radiation and lowering façade temperatures. In this study, an air temperature below 25 °C is used as the upper limit of the comfort range.

The results of the greening scenarios for indoor temperature are presented in Table 5.1. The average and maximum indoor temperature reductions remain below 1.2 °C for all scenarios. The effect of green walls, in particular, is minimal (below 0.20 °C). The extensive green roof achieves an average reduction of 0.44 °C, primarily due to the increased insulation provided by the soil layer. The 11 m high trees provide shading, reducing incoming solar radiation and thus indoor temperatures with 0.62 °C. Scenario LOW-INTEGRATED shows the largest average reduction of 1.12 °C, with average indoor maximum temperature reduction of 1.46 °C and the highest temperature measured in all rooms is reduced by 1.20 °C. For every scenario the highest temperature is measured in room S-M-R-2 or S-M-L-2.

In Figure 5.3, the scenarios are plotted over the course of the heatwave. The threshold for thermal comfort is set at 25 °C. This limit is exceeded for four consecutive days in all scenarios. Hence, for the heatwave used in this study, green interventions alone are not sufficient to maintain indoor temperatures below 25 °C in low-rise buildings.

5.2.1. Differences across building typologies

Three building typologies are modelled in this study. Differences in indoor temperature are expected because higher floors are not shaded by trees, and the geometrical forms of mid- and high-rise buildings differ significantly.

The shading effect of trees is less effective in mid- and high-rise buildings, as only a small part of their façade area receives shade. For the 11 m tree scenario (LOW-TREE-11m-N9S5), the average indoor temperature decrease is 0.62 °C in the low-rise, 0.26 °C in the mid-rise, and only 0.05 °C in the high-rise typology. Therefore, the effect of trees in mid- and high-rise buildings is limited to the lower floors.

Mid-rise scenarios are used to assess the effects of 11 m trees and both extensive and intensive green roofs on every floor. In Table 5.2, the reduction relative to the reference scenario is shown for each floor. The 11 m trees reduce the average indoor temperature by 0.71 °C on the first floor and 0.35 °C on the second floor, whereas only minor effects are visible on the higher floors. Green roofs primarily affect the top floors of buildings. In the mid-rise scenario with an intensive green roof (MID-GR-INT), the average reduction on the fifth floor is 0.78 °C, compared

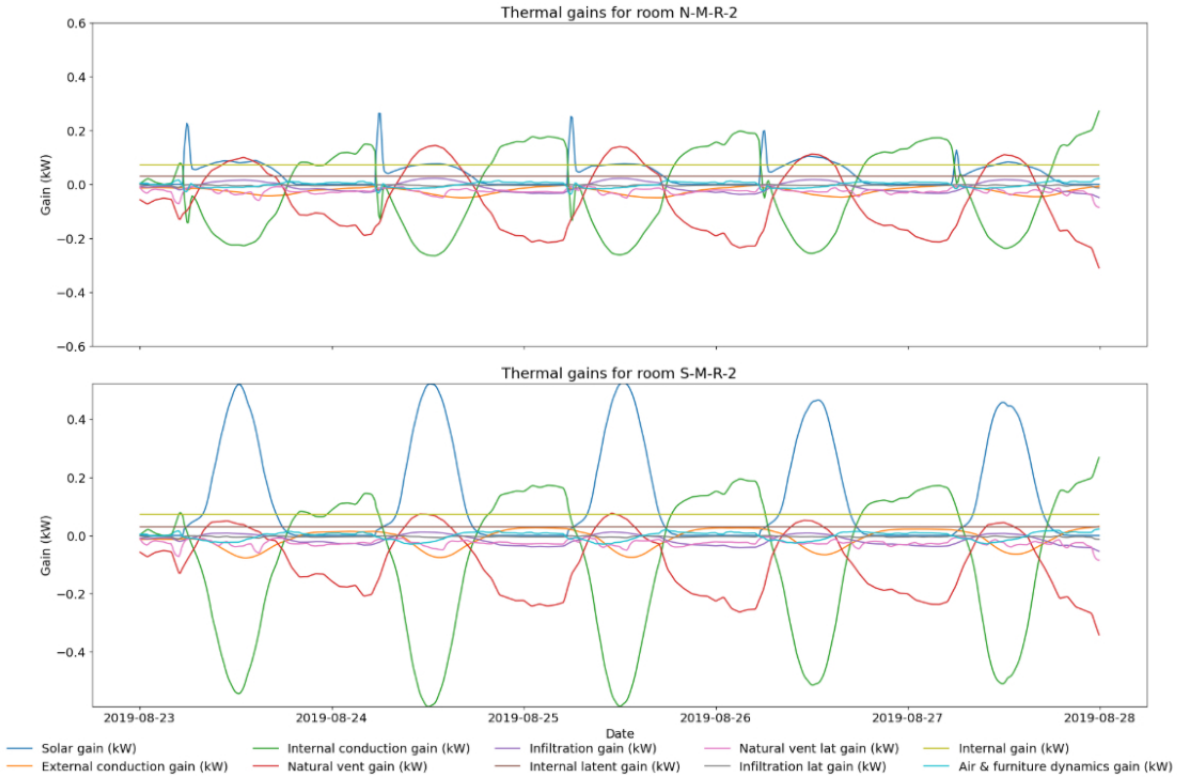

Figure 5.4: Thermal gains per room for scenario: LOW-REF

to an overall reduction of only 0.30 °C across all floors.

Table 5.2: Reduction in average indoor temperature per floor compared to the reference scenario

Floor	MID-GR-EXT	MID-GR-INT	MID-TREE-11m-N9S5
1	-0.11 °C	-0.14 °C	-0.71 °C
2	-0.11 °C	-0.15 °C	-0.35 °C
3	-0.12 °C	-0.17 °C	-0.12 °C
4	-0.15 °C	-0.27 °C	-0.07 °C
5	-0.32 °C	-0.78 °C	-0.05 °C

5.2.2. Indoor heat gains

The reference low-rise building is dominated by solar gains, particularly in the south-facing rooms, as shown in Figure 5.4. North-facing rooms experienced a smaller peak in the morning when the sun rises. Heat gains in the south-facing rooms are transported through internal conduction to the north-facing rooms and stored in building materials.

Because the modelled trees can only partially reduce solar radiation, additional simulations are conducted in which green interventions are combined with sunshades. These additional scenarios are discussed in detail in Appendix G.

5.2.3. Lag between outdoor and indoor temperature

Indoor temperature peaks typically lag behind outdoor peaks, with one study reporting an average delay of 260 minutes (Steeneveld & Peerlings, 2025).

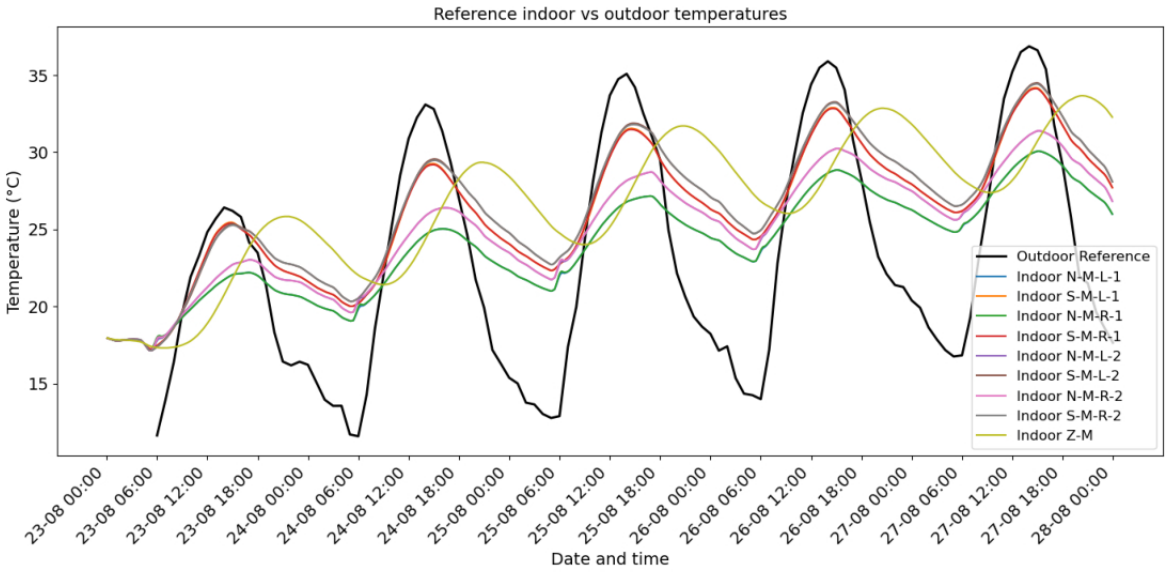

Figure 5.5: Indoor air temperature per room compared to outdoor temperatures. Differences between rooms can be seen. The Attic shows the largest lag between indoor and outdoor temperature.

In this study, the lag is calculated by comparing indoor and outdoor temperature peaks. Indoor temperature per room from scenario LOW-REF compared with outdoor temperatures is shown in Figure 5.5. Because ENVI-met outputs data on an hourly basis, the lag estimation is approximate. The times at which peak temperatures are reached in each room of scenario LOW-REF are visualised in Table 5.3. The average lag over all rooms is 119 minutes. The maximum outdoor temperature is reached at 14:00. The south-facing rooms reach their maxima within one hour after the outdoor peak, whereas the north-facing rooms show a lag of approximately two hours. The attic (Z-M) reaches its maximum much later, with a lag of 397 minutes. As this room has no windows and no natural ventilation, this longer delay is expected

Without natural ventilation and no change in infiltration (0.4 ACH), the lag increases to 171 minutes. For scenario LOW-INTEGRATED, the lag is 133 minutes, whereas the reference low-rise with sunshades has a lag of 145 minutes. The scenarios MID-REF and HIGH-REF show lags of 58 and 119 minutes, respectively.

Table 5.3: Time when maximum temperature is reached for each room and the lag relative to the outdoor environment. The left and right rooms were combined because they exhibited similar patterns. The average lag for the reference low-rise scenario is 119 minutes.

Date	N-M-L/R-1	N-M-L/R-2	S-M-L/R-1	S-M-L/R-2	Z-M	Avg. All rooms	Outdoor
2019-08-23	16:55	17:05	14:45	15:05	21:15	16:45	14:00
2019-08-24	16:00	16:15	14:55	15:05	20:35	16:00	14:00
2019-08-25	16:45	16:55	14:30	14:45	20:35	16:15	14:00
2019-08-26	15:05	15:05	14:30	14:45	20:25	15:05	14:00
2019-08-27	15:05	15:05	14:45	14:55	20:15	15:05	14:00
Average lag	+118 min	+125 min	+41 min	+55 min	+397 min	+119 min	0 min

5.3. Potential of greening to replace or reduce cooling demand

Hypothesis: Green interventions partly reduce the need for mechanical cooling by limiting indoor overheating.

Green interventions reduced indoor temperatures and consequently lower the building's cooling load. In this study, the cooling load is calculated to maintain the indoor temperature below the threshold of 25 °C. The total cooling energy demand in [kWh] is calculated for the entire heatwave. Figure 5.6 visualises the HVAC cooling effect for two rooms (south- and north-facing rooms on the second floor). The HVAC system in this study has unlimited cooling capacity.

Green interventions reduced cooling demand by up to 30%, but do not keep indoor temperatures below 25 °C.

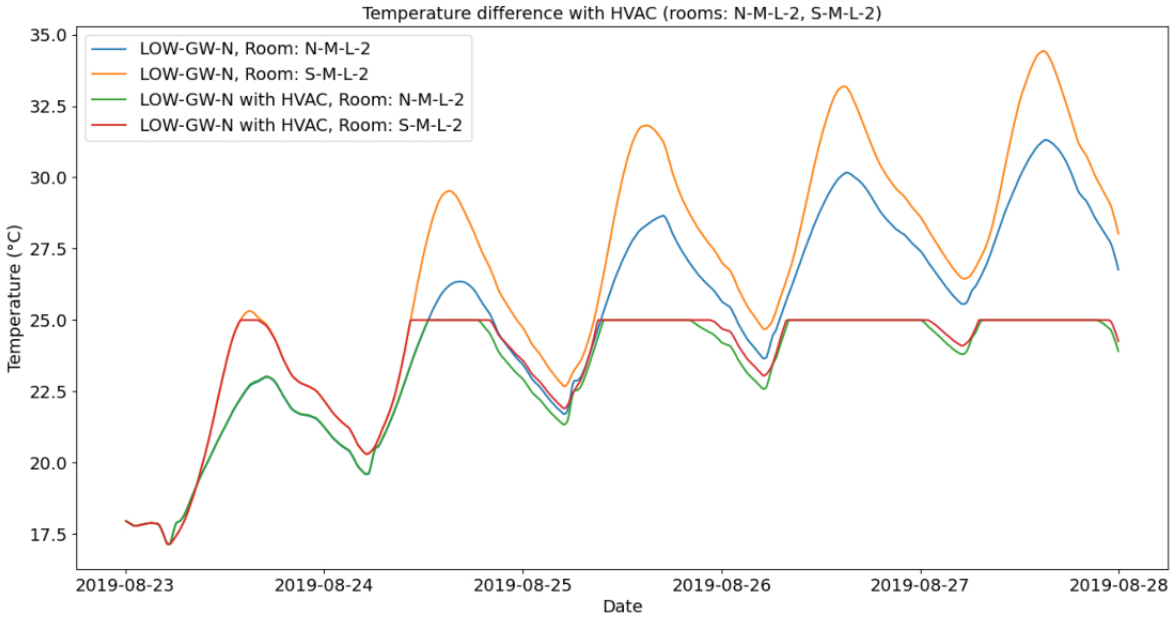

Figure 5.6: Example of HVAC cooling effect on scenario: LOW-GW-N

It should be noted that constant ventilation is applied during the day. The main driver of indoor temperature is solar radiation through glazing. When this radiation is blocked by a tree, a reduction in indoor temperature and cooling energy usage is observed. In particular, the 11 m trees shade both façades effectively, whereas 6 m trees mainly shade the ground floor. The integrated scenario achieved the largest reduction of 30% in total cooling demand. This reduction increased to 53% when green interventions are combined with shading structures such as sunshades, as shown in Appendix G.

6

Discussion

This chapter first discusses the methodology used in this study to couple the UCM with the BEM, followed by a reflection on the model inputs. Subsequently, the effects of green interventions on outdoor and indoor temperatures and energy usage are evaluated.

6.1. Methodology

This section first discusses the methodology used in this study to select a UCM and a BEM. Subsequently, the coupling approach between ENVI-met and IES-VE is discussed. The limitations of both models are discussed followed by a reflection on the model inputs and their influence on the results.

6.1.1. Model selection

The selection of the UCM was based on several criteria, which identified ENVI-met as the most suitable model with reasonable accuracy. While other models offer interesting coupling options, ENVI-met remains the most appropriate when the focus lies on green interventions. A drawback of ENVI-met is its runtime: each simulation required 24 hours to complete, which restricted the number of scenarios that could be tested. For computational reasons, the spatial domain had to remain relatively small.

For the BEM, two aspects encountered during the coupling reduced the flexibility of IES-VE in a coupled UCM–BEM setup: (i) the limited possibility of overwriting wall boundary conditions, and (ii) the lack of direct representation of vegetation within the model itself. In IES-VE, wall temperatures cannot be defined per wall section, and vegetation can only be represented indirectly by adding material layers. Therefore, in this study, the coupling was limited to the modified EPW inputs and the adjustment of external resistance values. Ideally, surface temperatures from ENVI-met would be imposed directly on each wall, allowing the BEM to resolve conductive heat transfer, internal gains, and ventilation.

Other BEMs offer greater flexibility. For instance, TRNSYS has been coupled with ENVI-met meteorological outputs in previous studies (Li, Zheng, Bedra, et al., 2021; Palme et al., 2017), where even surface temperatures of vegetation were applied directly (Perini et al., 2017). Further options include the use of shadow masks, modified weather files, or linking hourly urban surface data to building walls (Salvati et al., 2020). This demonstrates that TRNSYS provides more options for defining wall boundary conditions than IES-VE.

EnergyPlus also enables advanced coupling. Several studies have successfully coupled ENVI-met outputs, including temperature, humidity, and wind fields (Sezer et al., 2023; Yang & Becerik-Gerber, 2014). One-way couplings via modified EPW files, similar to the present study, have also been validated in the context of vegetation effects (Morakinyo et al., 2016; Morakinyo et al., 2017). Additionally, EnergyPlus includes built-in objects for green roofs and walls, such as the *Material:RoofVegetation* material (Pastore et al., 2017), which allows a more direct representation of vegetation than is possible in IES-VE.

Another important factor in model selection is the number of validation studies. ENVI-met has been widely validated for various vegetation types. Most studies have validated trees in ENVI-met with satisfactory results. Grass tends to be overestimated, and for shrubs only a limited number of validation studies are available. Green roofs and walls have also been validated to a certain extent, although the number of studies directly comparing ENVI-met outputs with measurements is limited.

For IES-VE, validation studies with green infrastructure are absent, and validation is restricted to indoor climate

and energy use. EnergyPlus and TRNSYS, on the other hand, include more work on vegetation and urban greening (Berardi, 2016; Morakinyo et al., 2016; Perini et al., 2017; Sailor et al., 2012). Both have embedded functions to represent green walls, and TRNSYS has already been applied in combination with ENVI-met (Djedjig et al., 2012; Djedjig et al., 2016). In summary, although IES-VE offered a novel approach for coupling in this study, TRNSYS and EnergyPlus can provide additional functionalities for representing vegetation and therefore may be advantageous for future work.

6.1.2. Coupling approach

The coupling approach between ENVI-met and IES-VE is visualised in Figure 4.10.

Coupling UCMs and BEMs is widely used in the literature (Santamouris et al., 2018; Sezer et al., 2023; Tsoka et al., 2021; Yang et al., 2012). The coupling approach between ENVI-met and IES-VE employed in this study uses outputs for air temperature, relative humidity, and wind speed. This provides a more realistic coupling than using data from a weather station as input for IES-VE.

The geometry was coupled as accurately as possible; however, differences between the models remained. The buildings in ENVI-met were represented as block forms, whereas those in IES-VE included angled surfaces. The effects of these simplifications are expected to be minor.

In this study, a one-way coupling was applied. Comparative analyses between one-way and two-way coupling approaches show that two-way coupling provides higher accuracy in predicting cooling load and thermal demand. Two-way coupling accounts for feedback from indoor to outdoor environments. Currently, no two-way coupling is available for ENVI-met (Pasandi et al., 2024). However, a recent study successfully implemented a two-way coupling between ENVI-met and EnergyPlus (Pasandi et al., 2025). Future research could explore this approach to assess its applicability for modelling the effects of green interventions.

In the one-way coupling implemented in this study, the influence of indoor conditions on the surrounding microclimate is not captured. In reality, indoor environments affect outdoor conditions through heating, ventilation, and air conditioning (HVAC) exhaust, which release anthropogenic heat into the atmosphere. The absence of this feedback likely leads to a slight underestimation of outdoor temperatures near the building. In practice, this additional heat is dispersed and mixed into the UBL. Previous urban climate studies have reported similar contributions from building ventilation and HVAC exhaust, with anthropogenic heat effects of approximately 1 °C during the day and up to 1.5 °C at night under heatwave conditions (Molnár et al., 2020; Sailor, 2011).

In this study, a fixed wind direction of 85° was prescribed in the EPW file used by IES-VE. Ideally, wind direction would vary per wall in accordance with ENVI-met output, as this has a substantial influence on wall-level convective heat transfer and infiltration. However, the EPW format requires a single directional input, which makes wall-specific implementation impossible. Consequently, IES-VE consistently treated the eastern and western walls as windward and leeward, respectively, throughout the simulation period. This simplification may lead to discrepancies compared with reality, where wind direction varies over time and across scenarios. Although the average wind direction from ENVI-met could have been used, this option was not applied in this study. The choice was made to implement windward and leeward sides in the outside resistance. Using wind-direction output from ENVI-met could be interesting for future research.

The outside resistance was calculated based on wind conditions and emissivities instead of using the preset IES-VE values. This approach improved model realism, although the resulting differences between scenarios were almost negligible. For example, for the north wall, the outside resistance values ranged between 0.0843 $m^2\,K^1\,W^{-1}$ and 0.0869 $m^2\,K^1\,W^{-1}$, which translated to a difference of only 0.6892 $W^1\,m^{-2}\,K^{-1}$ to 0.6904 $W^1\,m^{-2}\,K^{-1}$ in the wall U-value. As solar gain in buildings dominates over conduction gain (see Figure 5.4), this parameter had only a minimal effect on indoor temperature. Therefore, the outdoor resistance strategy was not essential in this study. The results will be compared with validation studies in section 6.2 to determine whether this approach resulted in accurate results.

The formula from Sharples (1984) used in this study was originally tested on a 78 m-high slab-type building. The buildings used here had different dimensions, which affected the exact convective heat exchange. The surface temperature approximation, based on a 3-hourly average, also introduced a small uncertainty.

The most important limitation of the coupling procedure is the absence of validation against measurements. Therefore, the exact accuracy of the model remains uncertain. In section 6.2 the results are evaluated against reference studies on green interventions to evaluate the extent to which they appear reasonable.

6.1.3. Model limitations

In this subsection, the implications of the known model limitations of both ENVI-met and IES-VE are discussed, with specific reference to their effect on the outcomes of this study.

ENVI-met

The main limitations of ENVI-met have already been introduced in section 3.2. The implications of the results are presented in this section. ENVI-met shows challenges in calculating radiation fluxes and representing differences in urban geometry. Consequently, contrasts in microclimatic conditions between low-rise and high-rise settings may be underestimated (Sharmin et al., 2017; Tsoka et al., 2018). Another limitation is that the mean radiant temperature (T_{mrt}) is often overestimated. Ouyang et al. (2022) demonstrated that recent updates in ENVI-met improved accuracy when applying full forcing, the IVS radiation scheme, and the ACRT module. In this study, full forcing and the IVS option are used which reduce but not solve the deviations. For example, Alsaad et al. (2022) reported RMSE values between 1.28 and 5.25 K, even under these improved settings.

Grid resolution affects shadow simulation, as local shading by individual urban elements is differentiated by the grid size, resulting in significant deviations in the modelled T_{mrt} and PET compared to field data (Acero & Herranz-Pascual, 2015; Sharmin et al., 2017). Consequently, PET results, especially those regarding localised maxima and reductions, should be interpreted with caution. The spatial resolution of 2 m in this study further restricts its ability to capture small-scale processes such as near-wall effects (Acero & Arrizabalaga, 2018). This implies that cell-level analyses should be interpreted with caution.

Simplifications in the ENVI-met vegetation module have also been highlighted in previous studies (Tsoka et al., 2018). Trees are represented as parametrised volumes rather than explicit crowns with branches and leaves. In warm-humid climates, Liu et al. (2018) showed that ENVI-met tends to overestimate leaf surface temperature and underestimate latent heat flux, particularly around midday. Consequently, the cooling effects of vegetation may have been underestimated or spatially overgeneralised in this study.

Overall, these limitations imply that the magnitude and spatial heterogeneity of cooling from green interventions are subject to uncertainty. In particular, the restricted grid resolution prevents detailed turbulence patterns near walls from being captured, while simplified vegetation parametrisation may reduce the accuracy of evapotranspiration cooling. The spatial maximum reductions visualised in chapter 5 are therefore very prone to errors. The averaged values for Area 1 and 2 have a lower uncertainty as multiple grid cells are used. The results will be compared with measurement studies to validate the results in section 6.2.

IES-VE

IES-VE (ApacheSim) assumes well-mixed air within rooms, uses a single radiant node, and does not resolve stratification or complex airflow (CIBSE, 2006; IES-VE, 2021a). External convective heat transfer relies on empirical correlations, whereas reflected shortwave radiation between buildings is neglected, which can affect the wall-level heat balance. Moreover, weather inputs are restricted to EPW files, which limit the temporal resolution to one hour.

In addition, vegetation in the IES-VE is represented in a highly simplified manner. Trees were not modelled as individual 3D canopy structures but only indirectly as opaque shading objects. Therefore, tree shading was overestimated by 10-30%. Two rooms (S-M-R-1 and S-M-L-1) are almost fully shaded by the trees. Both rooms show a reduction of 10 kWh over the entire heatwave compared with the reference scenario (LOW-REF). The reduction is overestimated by 10-30% ,therefore overestimated by 1-3 kWh per room. Two other rooms (S-M-R-2 and S-M-L-2) are partly shaded with a reduction of 2.2 kWh, this has a effect of 0.22-0.66 kWh per room. A total overestimation of 2.44-7.32 kWh (2-8%) is expected. Furthermore IES-VE calculates solar gain using the SunCast module. Small variations in tree placement or crown geometry do not always alter the simulated solar gain. This reduces the sensitivity of the model to tree placement and canopy geometry. Small changes of 0.5 m in tree position therefore can not be assessed.

Green walls could not be represented in IES-VE and were therefore only represented in terms of albedo, emissivity, and outside resistance. Therefore, the green wall had no additional insulating effect. The soil contribution from green roofs was visualised in the calculation. The effect of green space was neglected. Therefore, the effect of trees was slightly overestimated, and the effect of walls and roofs was underestimated. These uncertainties do not affect the ranking of interventions, although absolute values may differ.

Overall, the combined limitations of ENVI-met and IES-VE imply that results should be interpreted with caution. As two models are used, the errors of both models must be considered when analysing the indoor effects.

6.1.4. Model inputs

Weather inputs were obtained from the Cabauw meteorological station. To reflect urban conditions, wind speeds were reduced to 1.5 $m\ s^{-1}$ for all hours, preventing large variations that could mask the effects of vegetation. This wind speed is reasonable for an urban environment (Droste et al., 2020). The temperature and relative humidity inputs were derived from Cabauw, as it is the only Dutch station providing detailed BSRN radiation data (WRMC, 2022). Cloud cover data were obtained from De Bilt to complete the EPW file for IES-VE. A small sensitivity test showed that changes in cloud cover had no impact, as IES-VE only uses the radiation values stored in the EPW.

A key limitation is that the simulated nighttime temperatures during the heatwave remained relatively low. The daily minimum temperatures in ENVI-met were compared with measurements from four KNMI stations: Schiphol, De Bilt, Rotterdam, and Cabauw. ENVI-met consistently produced slightly cooler minima than Cabauw and notably lower values than Schiphol or Rotterdam, both of which are located in more urbanised areas. Therefore, the UHI effect was probably not well captured in the model. An explanation for this limitation is that the soil was modelled as natural soil rather than concrete or other high-heat-capacity materials.In addition, the relatively small modelled area limited the accumulation of heat, and anthropogenic heat was not represented. Anthropogenic heat is also not captured in the model. Consequently, the cooling load at night was underestimated. However, most cooling occurred during the daytime. A small underestimation for every scenario is expected for cooling load.

Another constraint relates to the model resolution and domain size. A resolution of 2 m yielded results comparable to a 1 m resolution (RMSE = 0.13 °C) but kept runtimes feasible. More critical was the limited domain size: buildings were modelled in isolation, resulting in higher wind speeds compared with dense urban areas. To compensate, wind speeds were reduced in the boundary conditions. However, the absence of surrounding buildings limited the representation of SW radiation trapping, thermal mass effect and LW radiation exchange. A configuration with nine buildings would have better reproduced urban conditions but was not computationally feasible. This would also have enhanced the UHI effect in the model.

The simplified urban form also led to minor limitations in the results. For example, in the early morning, the northern rooms showed a small temperature peak (up to 0.4 °C at 06:00), caused by the absence of shading from adjacent buildings. Such peaks would not occur in dense urban settings.

Finally, simplified building constructions were used in IES-VE. For the low-rise building exact wall materials and properties are copied. For mid and high-rise more general approach is used. Walls and glazing were copied from the low-rise building if reasonable. Therefore for mid and high-rise the exact U-values could differ from a real case. As mid and high-rise are not used for an absolute temperature evaluation but only relative between scenario's the impact of these assumptions on the results is expected to be minor.

6.2. Simulation outputs

This section uses a similar structure as the results section. The three hypotheses are stated with a discussion of the simulation results.

6.2.1. Impact of green interventions on outdoor thermal comfort

Hypothesis: Green interventions reduce local outdoor air temperature and PET.

The results confirmed that vegetation reduced both air temperature and PET, but the magnitude of these effects remained modest in Areas 1 and 2. Among all interventions, trees provided the largest reductions in air temperature and PET, whereas low vegetation and wall or roof greening showed only minor effects.

Low vegetation, wall, and roof greening

Low vegetation primarily provides evapotranspirative cooling, but its effect is spatially limited and generally modest. Green walls, roofs, grass, and shrubs produced only small daily average reductions in air temperature (< 0.25 °C) and PET (< 1.11 °C) in Area 1, and even smaller effects in Area 2 (< 0.1 °C and < 0.25 °C, respectively).

The overall reduction in outdoor temperature and PET from the grass was minimal. This is consistent with earlier studies (Balany et al., 2020; Irmak et al., 2017; Ng et al., 2012), although Shashua-Bar et al. (2009) reported slightly higher maximum air temperature reductions (~0.5 °C) and Knight et al. (2021) found an average daily reduction of -1.14 °C to -0.39 °C. Other studies found stronger PET reductions of up to 4 °C (Lobaccaro & Acero, 2015).

For shrubs, limited cooling effects are also expected (Balany et al., 2020). Sun et al. (2012) reported reductions of ~0.4 °C for shrubs of 1 m height. Given the lower shrub coverage in this study, the observed reduction of 0.16 °C is consistent with expectations.

Green walls showed only a small effect in Area 1, which is plausible because the results were averaged over a relatively large area. The maximum spatial reductions in air temperature and PET were consistent with case studies (Spanjar et al., 2023).

Green roofs had negligible effects on pedestrian height. The maximum reduction in air temperature was 0.03 °C, much lower than the reported ranges of 0.10–1.70 °C at street level, with a median of 0.30 °C (Tsoka et al., 2018). Similarly, Solcerova et al. (2022) found a reduction of 0.3 °C when 27% of roofs were greened. In this study, 70% of the roof surface was greened, but because the modelled domain contained only a small proportion of built-up area (1.5%), a much lower effect was found. A localised maximum reduction of 0.63 °C at 1.5 m height occurred west of the building, caused by the 85° wind direction. The area of this reduction is not situated in Area 1 and is only a small portion of Area 2. Future research should model larger urban extents with multiple green roofs to see the effect at larger scale.

Overall, the limited cooling of these green interventions was mostly explained by the small greening fraction in the domain. A larger coverage at the neighbourhood or city scale would likely result in stronger impacts. These findings emphasise that while small-scale green interventions have small local benefits, substantial urban cooling requires larger amounts of green infrastructure.

Trees

Trees mitigate urban heat through multiple mechanisms:

1. **Shading:** reduces solar radiation on surfaces, lowering both surface and air temperatures (Akbari et al., 2001). In ENVI-met, shortwave radiation reductions of up to 550 W m^{-2} were observed under the canopy, corresponding with surface temperature decreases of up to 12 °C.
2. **Evapotranspiration:** increases latent heat flux, reducing sensible heat flux and thereby lowering air temperature (Bowler et al., 2010). Latent heat fluxes near the 11m trees reached up to 150 W m^{-2}.
3. **Wind alteration:** slight increases in wind speed were modelled at 1.5 m (<0.1 m s^{-1}), while decreases of up to 0.5 m s^{-1} occurred in the canopy and wake, altering microclimate and wall convection.
4. **Albedo:** trees have an albedo of 0.18 compared to 0.20 for soil, reducing reflected shortwave radiation by up to 20 W m^{-2}. This has a minor impact on air temperature.

In this study, average air temperature reductions of 0.09–0.18 °C and peak reductions of 0.26–0.72 °C were found within 10 m of the wall (Area 1), with maximum localised reductions of up to 2.78 °C. These values are consistent with earlier field and modelling studies reporting street-level reductions of 0.2–2.27 °C, with medians around 1 °C (Balany et al., 2020). Other reviews reported peak reductions between 0.2 and 5 °C (Tsoka et al., 2018) and median values of 1.5 °C (Santamouris et al., 2017). The relatively modest results of this study can be explained by the limited greening fraction in the domain and the small (6 m) and medium (11 m) tree size. When spatial averages are taken over larger areas, the localised cooling directly under canopies is diluted, lowering the overall values.

While the average air temperature reductions are modest, the effect of trees on PET is much stronger. Localised PET reductions above 10 °C were observed directly under the canopy, with area-averaged PET reductions of up to 0.95 °C. These reductions were driven mainly by shading, which lowered SW radiation exposure at the pedestrian level. Similar results have been reported by Akbari et al. (2001) and a review by Balany et al. (2020), but on the lower side. The specific field maple used by van der Velde et al. (2023) reduced local PET between 21.6 and 23.4 °C. The shading in ENVI-met for this tree could be underestimated, contributing to this difference, but it is very difficult to compare cases.

Taken together, these results indicate that while most greening types provide only small reductions in air temperature and PET, strategically placed trees can substantially improve outdoor thermal comfort. This suggests that interventions such as isolated wall greening or grass lawns alone are insufficient and that trees combined with other vegetation are optimal for air temperature and PET reduction.

Diurnal variation of temperature reduction

Peak temperature reductions in this study occurred between 13:00 and 15:00, which is consistent with previous findings (Bowler et al., 2010; Shashua-Bar et al., 2009). A systematic review by Knight et al. (2021) also

reported that most studies found the strongest air temperature reductions during the daytime, when shading and evapotranspiration are most effective. In contrast, a meta-analysis by Santamouris and Osmond (2020) showed that the largest cooling can also occur at night. This is mainly because (a) increased tree cover reduces daytime heat storage in the ground and impervious surfaces, limiting the release of sensible heat during the night, and (b) trees themselves release less sensible heat than built surfaces.

During the daytime, evapotranspiration is the primary cooling mechanism; however, in some cases, it is insufficient to counterbalance the sensible heat fluxes from the surrounding impervious surfaces and advective warming. At night, additional effects appear: dense canopies can trap longwave radiation and thereby reduce cooling, sometimes even leading to local nighttime warming.

The differences between this study and the meta-analysis by Santamouris and Osmond (2020) can be explained by the modelling setup. The ENVI-met domain used here contained natural soil rather than impervious pavement, meaning less daytime heat was stored and therefore less night-time cooling was released. Moreover, the combination of trees and building geometry in this setup blocks a substantial fraction of the outgoing longwave radiation, further limiting nocturnal cooling compared to the treeless scenario. These mechanisms help explain why cooling in our results peaked during the day rather than at night.

6.2.2. Potential of green interventions to reduce indoor air temperature

Hypothesis: Green interventions maintain indoor temperatures within the comfort range.

The maximum total indoor temperature reduction in this study was 1.20 °C, measured in room S-M-R-2. Grass and shrubs had almost no effect on indoor temperature, which is expected as they only reduce outdoor temperatures marginally.

The effect of green walls on indoor temperature was below 0.20 °C. As no green wall option was available in IES-VE, the additional insulation provided by the green wall was not captured in the model. Only the outside resistance, albedo, emissivity, and outdoor air temperature could be adjusted. Therefore, the results are slightly underestimated, but even then a very small indoor effect is expected. No or marginal indoor effects have also been reported in the literature (Hoelscher et al., 2016; Ottelé & Perini, 2017). A study by Tilley (2012) found reductions of up to 4 °C in indoor temperatures. Such large indoor reductions are not expected with only *Hedera helix* as a wall-climbing plant. Furthermore, indoor temperature is primarily influenced by solar infiltration through windows, while conduction through the outer walls plays a much smaller role, thereby reducing the impact of green walls. Overall, a reduction below 0.5 °C is expected for green walls.

The effect of the green roof was generally consistent with findings in the literature. For the low-rise building, the average reduction achieved by the extensive green roof was 0.44 °C. In the mid-rise building, the average reductions were 0.16 and 0.30 °C, while on the top floor the reductions were 0.28 and 0.78 °C for the extensive and intensive cases, respectively. These values fall within the range of 0.5–1.0 °C reported by Parizotto and Lamberts (2011), who studied an extensive green roof with a substantially thicker soil layer of 14 cm and an additional 18 cm gravel drainage layer, and are also comparable to the value of 0.6 °C reported by Langewen et al. (2022), who investigated a roof with a 6 cm substrate layer combined with additional insulation. The outcomes in this study represent the average air temperature of the room, whereas the measurement studies used specific sensor heights of 1.5 m (Parizotto & Lamberts, 2011) and 0.10 m below the roof (Langewen et al., 2022). As the additional soil layer decreases the U-value, the extra insulation of the green roof has a smaller effect than for green walls. Nevertheless, a small underestimation may still be present in the model. Overall, the effects observed in this study can be considered reasonable; however, to draw firm conclusions, the methodology should be applied to case studies with in-situ measurements.

In this study, trees had an average indoor temperature decrease of up to 0.7 °C and a maximum temperature decrease of up to 1.0 °C. This is consistent with the 0.6 °C found in literature (Guzman, 2023). Another study showed results between 0.0-2.0 °C (Morakinyo & Lam, 2016). As IES-VE models trees with zero transmission, the amount of solar radiation reduced is probably overestimated by the model by 10-30% A small sensitivity test is conducted by increasing solar gain by 30% for the LOW-TREE-11m-N9S5 scenario, resulting in a indoor temperature increase of max 0.2 °C.

Overall, cooling benefits from green walls were slightly underestimated, green roofs were consistent with the literature, and trees were overestimated in the model but consistent with the literature.

Differences across building typologies

The effect of 11 m high trees is most pronounced on the lower floors of the mid-rise building. For green roofs, the top floor shows the largest reduction owing to decreased conduction through the roof.

The intensive green roof achieved a larger reduction on the top floor, as higher plants and thicker soil layers enhanced both insulation and evapotranspiration. The reductions for the top floor are consistent with the literature (Langewen et al., 2022; Parizotto & Lamberts, 2011).

In the EPW file, only one input temperature can be defined based on the ENVI-met output, which represents the average over all walls. Consequently, in the green roof scenario, the lowest floors were also slightly cooled due to the lowered average outdoor air temperature. In practice, this is unlikely, as the cooling effect is diluted by mixing and is affected by the wind speed and direction. Therefore, this approach is less suitable for comparing different floors, as for green roofs the lower floors are slightly overestimated, whereas the top floor is underestimated.

Indoor heat gains

Indoor heat gains were primarily driven by solar radiation in south-facing rooms. In north-facing rooms, a temperature peak occurred in the morning when the rising sun entered through the window. In a real urban environment, this peak would likely not occur, as shading from adjacent buildings typically blocks sunlight at this low solar angle. During the day, ventilation introduces air that is warmer than the indoor environment, resulting in positive heat gains, whereas at night, ventilation acts as a cooling mechanism. Future research should investigate scenarios with night-time ventilation only, as this would reduce the overall cooling load of the building. Internal conduction gains represent heat transfer through interior walls, partly towards adjacent rooms and partly stored within the building mass.

In this study, reducing solar gains during the day proved to be the most effective strategy for lowering energy demand. Therefore, in Appendix G, the scenarios LOW-REF, LOW-TREE-11m-N9S5, and LOW-INTEGRATED include the addition of sunshades to assess the combined impact of greening and solar shading. Average indoor temperature reductions from solar shading ranged between 0.6 °C and 1.05 °C. The main advantage of shading structures over trees is their optimal positioning to block direct solar radiation entering through the windows. Trees, on the other hand, must be positioned very close to the wall to effectively obstruct radiation between 12:00 and 14:00 hours.

Lag between outdoor and indoor temperature

Steeneveld and Peerlings (2025) analysed a unique indoor temperature dataset collected by citizen weather stations in seven residences (with building ages ranging from 2 to 27 years). They found an average lag of approximately 260 min between indoor and outdoor temperatures over the diurnal cycle, based on cross-correlation analysis. In comparison, the Harlem Heat Project in Manhattan, New York, using the same method, reported a shorter delay of around 180 min (Vant-Hull et al., 2018).

In the present study, a smaller lag was observed for the reference scenario (119 min). Several factors may explain this difference. First, the model setup assumes relatively high natural ventilation rates during the day, which enhance indoor–outdoor heat exchange and reduce the building's thermal buffering capacity. Second, in this study, only daily peak temperatures were compared, whereas Steeneveld and Peerlings (2025) used a full cross-correlation of hourly indoor and outdoor time series. Moreover, ENVI-met provides outdoor air temperature data at hourly intervals, which may obscure the precise timing of the true outdoor temperature peak.

When natural ventilation was set to zero—representing closed windows and only infiltration—the lag increased to 171 min, confirming that ventilation strongly reduces the indoor–outdoor delay. Introducing ventilation from the afternoon onwards can therefore be an effective strategy to reduce evening and night-time overheating, as a longer lag means more heat is retained during the night. Future research could further investigate this relationship using cross-correlation and higher-resolution outdoor data (e.g., from nearby KNMI stations) to better capture the timing between outdoor and indoor temperatures.

6.2.3. Potential of green interventions to replace or reduce mechanical cooling

Hypothesis: Green interventions partly reduce the need for mechanical cooling by limiting indoor overheating.

The green interventions in this study reduce the cooling demand by up to 30%. In particular, scenarios with trees limit incoming solar radiation, thereby lowering the indoor temperature rise. Similar to the indoor temperature results, the effect of trees may be slightly overestimated because no transmission of radiation through the canopy

was modeled. Based on a small sensitivity analysis in IES-VE, the effect on the cooling load is expected to be within 2.44–7.32 kWh. Considering this, trees remain the best-performing individual green intervention in this study.

In the mid-rise scenario, the effect of trees is also visible, but only a reduction of 11% is achieved as the 3rd–5th floors are hardly affected by tree shading. Intensive green roofs achieve a larger reduction (11%) in cooling load than extensive roofs (7%), which conforms to expectations. The strongest effect was observed on the top floor, where the improved insulation reduces conduction through the roof.

Other studies found that a continuous tree canopy can achieve up to 54% reduction in building energy usage for the first floor, with the highest reductions for closely planted trees with high foliage density (Tsoka et al., 2018). In this study, trees were planted 9 m apart rather than in a continuous canopy. With this planting pattern, reductions of 12–18% for the first floor and 9–10% for the third floor are expected, which is consistent with the 11% reduction found for the mid-rise case. The reference building in Tsoka et al. (2018) used a cooling set-point of 26 °C, while in this study 25 °C was applied. For the low-rise building, a stronger effect of 24% was found as the centrally placed tree blocks a large share of solar radiation. Overall, the results are promising, though future work should confirm whether the method applied here can reliably predict cooling energy usage.

The stronger effect of intensive compared to extensive green roofs is explained by their higher LAI, thicker soil layer, and greater foliage height (Mihalakakou et al., 2023). The magnitude of the reductions in this study falls within the range of values reviewed by Mihalakakou et al. (2023), although on the lower side. For the mid-rise building, the reduction in cooling load of the top floor is 16% for the extensive roof and 28% for the intensive roof. Direct comparison between studies is difficult because buildings often differ in cooling strategies. However, since the reductions are consistent with observed indoor air temperature decreases in case studies, the results can be considered reasonably accurate. While they can be used to compare scenarios within this study, firm conclusions about the absolute magnitude of cooling load reductions should be avoided.

6.2.4. Overall effectiveness of green interventions

Among all green interventions, trees appear to be the most effective. Trees provide substantial shading capacity that reduces the amount of radiation reaching pedestrian height. In addition, trees shade the building walls, lowering its surface temperature and decreasing the solar radiation entering the building through windows. Tree placement is crucial: to achieve the maximum indoor temperature reduction, trees should be positioned to block direct solar radiation through windows, particularly between 11:00 and 15:00 hours. Green walls make only a small contribution to outdoor and indoor temperature reduction. Green roofs show limited effects at the surface level, and their influence decreases with increasing building height. However, green roofs have a stronger impact on indoor temperatures than wall greening, as the substrate layer provides additional insulation. Grass and shrubs have only minor cooling effects.

While this study focuses on the local effects of relatively small amounts of greenery, literature shows that implementing green infrastructure at larger scales results in more pronounced cooling. The impact of green interventions becomes particularly interesting when applied at the district or city scale. Large-scale urban greening is expected to produce temperature reductions of 0.3–2.7 °C at the city level (Licón-Portillo et al., 2024). Meta-analyses indicate that urban parks are, on average, 0.94 °C cooler than their surroundings (Bowler et al., 2010), with cooling extending up to 1.25 km and averaging 0.55 °C (Knight et al., 2021). Tree cover reduces local air temperature by approximately 0.09 °C for every 1% increase in canopy cover, which is about four times more effective than grass (Smith et al., 2023). Increasing tree cover generally results in mean temperature reductions of 1.3–1.4 °C, ranging between 1.0 and 2.3 °C (Manso et al., 2021). Beyond thermal effects, greening can also reduce building energy consumption: every 10% increase in vegetation cover lowers air-conditioning demand by 5.5% at 22–28.9 °C and by 2.4% at 28.9–37 °C (Luo et al., 2022).

6.3. Relevance

This research is relevant from scientific, practical, and societal perspectives and has several implications.

From a scientific perspective, this study applied a coupling approach between a UCM and a BEM by implementing a one-way coupling between ENVI-met and IES-VE. While most coupling studies have focused on EnergyPlus, applications involving IES-VE remain rare. This study demonstrates that coupling with IES-VE is feasible and can be used to estimate both outdoor and indoor effects of greening. However, when evaluating green interventions, both the coupling strategy and the IES-VE model introduce uncertainties. In particular, the cooling effect of trees

tends to be overestimated, whereas the influence of green walls is underestimated. These findings contribute to a better understanding of the capabilities and limitations of using IES-VE for urban climate studies.

From a practical perspective, the results give clear and useful insights for municipalities, urban planners, and property owners. The findings show that green interventions (especially trees) can reduce outdoor heat stress, with PET reductions of several degrees. Furthermore reductions in indoor temperature and energy usage are found. For municipalities, this study offers a solid basis for investing in urban greening to reduce air temperature and PET, particularly in dense city areas where heat stress is highest. Earlier research shows that large-scale greening can reduce city averaged temperatures by 0.3–2.7 °C, and this study confirms that smaller, local applications can also make a measurable difference (Licón-Portillo et al., 2024). Trees stand out as the most effective option, but their placement is key: when they are positioned to block direct sunlight from entering windows, they provide the greatest indoor cooling benefit during heatwaves. Deciduous species are most suitable, since they block sunlight in summer but still allow solar gains in winter.

For property owners and real-estate managers, this study showed how practical greening strategies can reduce cooling energy use and improve indoor comfort. This study is based on common Dutch building typologies, meaning that the proposed measures are relevant for many residential buildings. The results indicate that green interventions can help lower indoor temperatures, reduce cooling loads, and lower energy costs. Combining vegetation with shading structures and natural ventilation makes these effects even stronger. Such an integrated approach can significantly reduce the need for mechanical cooling while improving both comfort and energy performance. Green roofs can be a good option for improving comfort on the upper floors of buildings.

In a broader societal sense, this research supports the goals of climate adaptation and the energy transition. By showing that vegetation can simultaneously mitigate urban overheating and reduce building energy demand, it highlights the practical value of nature-based solutions. Beyond temperature regulation, greenery also improves air quality, enhances stormwater retention, supports biodiversity, and creates more attractive urban spaces that promote well-being (Manso et al., 2021). Compared to purely technical shading structures, nature-based solutions offer multifunctional co-benefits, emphasising the importance of integrating green interventions into urban planning and building management.

7

Conclusion

This thesis investigated the extent to which green interventions (green roofs, walls, trees, shrubs, and grass) can reduce outdoor heat stress and indoor overheating in the Netherlands. This study used a one-way coupling between ENVI-met for the outdoor microclimate and IES-VE for indoor simulations. This was followed by an evaluation of the effects of different greening scenarios during the 23–27 August 2019 heatwave for three building typologies: low-, mid-, and high-rise.

The results show that green interventions are effective in mitigating outdoor and indoor heat stress, although cooling effects remain modest for most measures other than trees. Trees proved to be the most influential intervention for both outdoor thermal comfort and indoor cooling. When combined with other green interventions such as green roofs and walls, trees yielded the greatest reductions in outdoor air temperature, PET, and indoor temperature. In Area 1 (<10 m from the north and south walls), the maximum outdoor air temperature decreased by 1.17 °C, while the largest local reduction reached 3.92 °C. PET was reduced by up to 13.45 °C. Indoors, temperature reductions of up to 1.20 °C and cooling load savings of up to 32% were achieved.

These reductions are at the lower end of the ranges reported in the literature for similar types of interventions. This can largely be explained by the limited amount of greenery used in this study, as only Area 1 was vegetated to focus on local effects. Even so, the findings show that green interventions help to improve outdoor thermal comfort, lower indoor temperatures, and reduce cooling energy demand during heatwaves. However, vegetation alone did not keep indoor conditions within a comfortable range. The greatest improvements are achieved when green interventions are combined with shading elements and ventilation strategies, possibly supported by mechanical cooling.

This research also showed that coupling ENVI-met and IES-VE is a possible way to estimate how green interventions influence both the outdoor and indoor environment. Still, validation against field measurements is needed to confirm the accuracy of this method. The main limitations of this study are the lack of measurement data for validation, the relatively small greening area, the simplified way vegetation was represented in IES-VE, and the uncertainties that come with both models.

Overall, this study demonstrates that green interventions can make a meaningful contribution to reducing urban heat stress and indoor overheating in typical Dutch building typologies. By giving priority to trees and combining them with other green interventions, municipalities and urban designers can improve outdoor comfort, lower energy demand, and make cities more resilient to future heatwaves.

8

Recommendation

Future research should focus on improving the coupling between microclimate and building models. In particular, applying a two-way coupling approach would be valuable, as this allows feedback between indoor and outdoor conditions. One recent study demonstrated a two-way coupling between ENVI-met and EnergyPlus, showing strong agreement with measured cooling energy data (R^2 = 0.9). Compared with conventional one-way or EPW-based methods, this approach captured surface temperature dynamics, diurnal cooling load patterns, and peak demand behaviour much more accurately (Pasandi et al., 2025). Future research could explore this approach further and include the effect of vegetation and shading in such a two-way framework.

Field measurements are also essential to strengthen the method used in this study. For this study a validation with an on-site case was not possible. Measuring the effects of the green interventions in a case study would help to evaluate how reliable the model outcomes are. These measurements could also support calibration of the coupling between ENVI-met and IES-VE or other building models.

After validation of the coupling, a wider range of building typologies should be tested. This study focused on three generic Dutch building types, but future work could include other typologies, such as apartment blocks, schools, or offices, as well as more urbanised environments. Different layouts, orientations, and materials could all influence the effectiveness of green interventions. Applying the same method in other cities or climates would also help to test how transferable the results are.

In this study, the cooling load was calculated based on maintaining indoor temperatures below a threshold of 25 °C, which primarily affects HVAC operation during daytime hours. However, heat stress indoors is often experienced most severely at night, when prolonged exposure to high temperatures compromises sleep quality and health. Moreover, many occupants are not at home during the daytime, reducing the relevance of a purely day-focused comfort criterion. Future research should therefore evaluate additional comfort thresholds that specifically address nighttime exposure and sleeping conditions. A nighttime comfort temperature of around 22 °C for dwellings with children could be adopted (GGD Twente, n.d.). This threshold also seems reasonable for dwellings with elderly occupants (Baniassadi et al., 2024; van Loenhout et al., 2016). For dwellings with non-vulnerable occupants a higher comfortable overnight temperature may be acceptable.

From a policy and design perspective, it is recommended that municipalities prioritise tree planting near buildings where shading can directly lower solar gains through windows. Combining vegetation with architectural shading elements and natural ventilation gives the strongest reductions in cooling load. In dense urban areas where space is limited, vertical greenery and green roofs can still provide meaningful local cooling. Designers and planners should consider both the location and type of vegetation.

Suggestions for practical implementation

Based on this research and literature, the following advice is recommended for municipalities, urban planners, and property owners:

- **Prioritise trees over other green interventions.** Trees provide a stronger reduction in both outdoor and indoor temperatures than green roofs, green walls, shrubs, or grass.
- **Prioritise façade shading with trees.** Plant trees close enough to south-facing façades— and where possible also, west- and east-facing façades — to block direct solar radiation entering windows between 11:00 and 15:00 during summer.

- **Select and maintain future-proof trees.** The changing climate needs to be taken into account when selecting tree species (Hirons & Sjöman, 2019; Noome et al., 2023). Choose drought-resistant, high-LAI deciduous species with suitable root structures. Deciduous species allow solar gains in winter while providing essential shade in summer. Therefore deciduous trees are well suited for optimising building energy usage.
- **Match the greening type to building height.** Trees are most effective for low-rise buildings. For mid- and high-rise buildings, combine trees with green roofs and façade shading structures.
- **Adopt green roofs to improve top floor comfort** Install extensive roofs where structural capacity is limited; apply intensive roofs when additional load and maintenance are feasible, especially to improve comfort on top floors.
- **Integrate greening into neighbourhood heat plans.** Implement greening first in heat-stress hotspots and densely built areas. Increasing vegetation fraction at district scale strengthens neighbourhood-wide cooling (Bowler et al., 2010; Knight et al., 2021; Licón-Portillo et al., 2024).
- **Combine vegetation with architectural shading and ventilation.** External shading devices and controlled (night-time) ventilation complement vegetation and further reduce indoor heat and cooling demand.
- **Optimise operation of shading devices.** Ensure blinds or automated shading systems are activated during hours of high solar radiation (11:00-15:00) to minimise indoor heat gains.
- **Apply simple operational strategies for heat resilience.** Encourage closing windows during peak heat, afternoon pre-cooling, and night ventilation during heatwaves to maintain comfortable temperatures indoors.

Bibliography

Abdullahi, M., Ojobo, H., Sani, M., Naibi, A., & Aliero, M. (2022). Validating integrated environmental solutions software for air temperature of a typical malaysian recessed wall façade office building. *Journal of Civil Engineering and Environmental Sciences*, *8*(1), 031–040. https://doi.org/10.17352/2455-488X.000048

Acero, J., & Arrizabalaga, J. (2018). Evaluating the performance of envi-met model in diurnal cycles for different meteorological conditions. *Theoretical and Applied Climatology*, *131*, 455–469. https://doi.org/10.1007/s00704-016-1971-y

Acero, J. A., & Herranz-Pascual, K. (2015). A comparison of thermal comfort conditions in four urban spaces by means of measurements and modelling techniques. *Building and Environment*, *93*, 245–257. https://doi.org/10.1016/j.buildenv.2015.06.028

Akbari, H., Pomerantz, M., & Taha, H. (2001). Cool surfaces and shade trees to reduce energy use and improve air quality in urban areas. *Solar Energy*, *70*(3), 295–310. https://doi.org/10.1016/S0038-092X(00)00089-X

Alamdari, F., & Hammond, G. (1983). Improved data correlations for buoyancy-driven convection in rooms. *Building Services Engineering Research and Technology*, *4*(3), 106–112.

Aleksandrowicz, O., Saroglou, T., & Pearlmutter, D. (2023). Evaluation of summer mean radiant temperature simulation in envi-met in a hot mediterranean climate. *Building and Environment*, *245*, 110881. https://doi.org/10.1016/j.buildenv.2023.110881

Allegrini, J., Dorer, V., & Carmeliet, J. (2012). Influence of the urban microclimate in street canyons on the energy demand for space cooling and heating of buildings [Cool Roofs, Cool Pavements, Cool Cities, and Cool World]. *Energy and Buildings*, *55*, 823–832. https://doi.org/https://doi.org/10.1016/j.enbuild.2012.10.013

Allegrini, J., Orehounig, K., Mavromatidis, G., Ruesch, F., Dorer, V., & Evins, R. (2015). A review of modelling approaches and tools for the simulation of district-scale energy systems. *Renewable and Sustainable Energy Reviews*, *52*, 1391–1404. https://doi.org/10.1016/j.rser.2015.07.123

Alsaad, H., Hartmann, M., Hilbel, R., & Voelker, C. (2022). The potential of facade greening in mitigating the effects of heatwaves in central european cities. *Building and Environment*, *216*, 109021. https://doi.org/10.1016/j.buildenv.2022.109021

Alves, F. M., Gonçalves, A., & del Caz-Enjuto, M. R. (2022). The use of envi-met for the assessment of nature-based solutions' potential benefits in industrial parks—a case study of argales industrial park (valladolid, spain). *Infrastructures*, *7*(6). https://doi.org/10.3390/infrastructures7060085

Armson, D., Stringer, P., & Ennos, A. (2012). The effect of tree shade and grass on surface and globe temperatures in an urban area. *Urban Forestry Urban Greening*, *11*(3), 245–255. https://doi.org/10.1016/j.ufug.2012.05.002

Arnfield, A. J. (2003). Two decades of urban climate research: A review of turbulence, exchanges of energy and water, and the urban heat island. *International Journal of Climatology*, *23*(1), 1–26. https://doi.org/10.1002/joc.859

Arveson, P. (2017). *A low-cost method for measuring solar irradiance using a lux meter* (tech. rep. No. TR-16) (March 29, 2017). Solar Household Energy, Inc.

ASHRAE. (2020). *Standard method of test for the evaluation of building energy analysis computer programs* (tech. rep.) (PDF addendum to Standard 140–2017, galley version). American Society of Heating, Refrigerating and Air-Conditioning Engineers.

Aw, S. B., Leng, P. C., Ling, G. H. T., Wong, K. Y., Mohamed Anuar, M. R., Mohd Rokhibi, I. W., Ng, C. H., Law, N. H. K., & Goh, S. Y. Z. (2024). Strategic integration of a vegetative component on a metal roof base: An evaluation of its impacts on thermal and acoustic performance in the tropics. *Buildings*, *14*(4). https://doi.org/10.3390/buildings14040915

Bakovic Ergün, M., & Gocer, O. (2017). Envi met modeling of green roof effects on microclimate and outdoor thermal comfort. *The 12th Conference on Sustainable Development of Energy, Water and Environment System*.

Balany, F., Ng, A. W., Muttil, N., Muthukumaran, S., & Wong, M. S. (2020). Green infrastructure as an urban heat island mitigation strategy—a review. *Water*, *12*(12), 3577. https://doi.org/10.3390/w12123577

Baniassadi, A., Yu, W., Travison, T., Lipsitz, L., & Manor, B. (2024). Nighttime ambient temperature and sleep in older adults. *Innovation in Aging*, *8*, 191–191. https://doi.org/10.1093/geroni/igae098.0618

Bartak, M., Drkal, F., Hensen, J., Lain, M., Matuska, T., Schwarzer, J., & Sourek, B. (2003). Esp-r: Integrated simulation tool for design of buildings and systems. *Proc. Int. Workshop Integrated Building Simulation, 23 - 26 September, Gliwice*, 108–116.

Behrendt, B. M., Raimondo, D., Zhang, Y., Schwarz, S., Christensen, J. E., & Olesen, B. W. (2021). A system for the comparison of tools for the simulation of water-based radiant heating and cooling systems. *Proceedings of Building Simulation 2011: 12th Conference of International Building Performance Simulation Association, Sydney, 14-16 November.*

Bellazzi, A., Barozzi, B., Pollastro, M., & Meroni, I. (2020). Thermal resistance of growing media for green roofs: To what extent does the absence of specific reference values potentially affect the global thermal resistance of the green roof? an experimental example. *Journal of Building Engineering*, *28*, 101076. https://doi.org/10.1016/j.jobe.2019.101076

Ben, H., & Steemers, K. (2014). Energy retrofit and occupant behaviour in protected housing: A case study of the brunswick centre in london. *Energy and Buildings*, *80*, 120–130. https://doi.org/10.1016/j.enbuild.2014.05.019

Berardi, U. (2016). The outdoor microclimate benefits and energy saving resulting from green roofs retrofits. *Energy and Buildings*, *121*, 217–229. https://doi.org/10.1016/j.enbuild.2016.03.021

Berardi, U., GhaffarianHoseini, A., & GhaffarianHoseini, A. (2014). State-of-the-art analysis of the environmental benefits of green roofs. *Applied Energy*, *115*, 411–428. https://doi.org/10.1016/j.apenergy.2013.10.047

Blocken, B. (2014). 50 years of computational wind engineering: Past, present and future. *Journal of Wind Engineering and Industrial Aerodynamics*, *129*, 69–102. https://doi.org/10.1016/j.jweia.2014.03.008

Boers, R., van Weele, M., van Meijgaard, E., Savenije, M., Siebesma, A. P., Bosveld, F., & Stammes, P. (2015). Observations and projections of visibility and aerosol optical thickness (1956–2100) in the netherlands: Impacts of time-varying aerosol composition and hygroscopicity. *Environmental Research Letters*, *10*(1), 015003. https://doi.org/10.1088/1748-9326/10/1/015003

Bomentabel. (2024). *Bomentabel.nl – Nuttige bomen met positieve effecten op ons ecosysteem*. https://bomentabel.nl/

Boomkwekerij Ebben. (n.d.). *Tree ebb* [Accessed: 2025-06-05]. https://www.ebben.nl/nl/treeebb/accampes-acer-campestre/#?search%5B0%5D=Acer%20campestre

Bosveld, F. C. (2020). *The cabauw in-situ observational program 2000 - present: Instruments, calibrations and set-up* (Technical report No. TR-384). KNMI. De Bilt.

Bowler, D. E., Buyung-Ali, L., Knight, T. M., & Pullin, A. S. (2010). Urban greening to cool towns and cities: A systematic review of the empirical evidence. *Landscape and Urban Planning*, *97*(3), 147–155. https://doi.org/10.1016/j.landurbplan.2010.05.006

Brousse, O., Simpson, C., Zonato, A., Martilli, A., Taylor, J., Davies, M., & Heaviside, C. (2024). Cool roofs could be most effective at reducing outdoor urban temperatures in london (united kingdom) compared with other roof top and vegetation interventions: A mesoscale urban climate modeling study. *Geophysical Research Letters*, *51*(13), e2024GL109634. https://doi.org/10.1029/2024GL109634

Brozovsky, J., Simonsen, A., & Gaitani, N. (2021). Validation of a cfd model for the evaluation of urban microclimate at high latitudes: A case study in trondheim, norway. *Building and Environment*, *205*, 108175. https://doi.org/10.1016/j.buildenv.2021.108175

Bruse, M., & Fleer, H. (1998). Simulating surface–plant–air interactions inside urban environments with a three dimensional numerical model. *Environmental Modelling Software*, *13*(3), 373–384. https://doi.org/10.1016/S1364-8152(98)00042-5

Bruse, M., Simon, H., & Sinsel, T. (2023, October). *Development and implementation of a high-resolution dynamical wall and roof model for envi-met* (tech. rep.). https://doi.org/10.13140/RG.2.2.36020.83842

Bueno, B., Norford, L., Hidalgo, J., & Pigeon, G. (2012). The urban weather generator. *Journal of Building Performance Simulation*, *6*(4), 269–281. https://doi.org/10.1080/19401493.2012.718797

Cameron, R. W., Taylor, J. E., & Emmett, M. R. (2014). What's 'cool' in the world of green façades? how plant choice influences the cooling properties of green walls. *Building and Environment*, *73*, 198–207. https://doi.org/10.1016/j.buildenv.2013.12.005

Che-Ani, A. I., & Raman, S. N. (2019). Thermal environment accuracy investigation of integrated environmental solutions-virtual environment (ies-ve) software for double-story house simulation in malaysia. *Journal of Engineering and Applied Sciences*, *14*(11), 3659–3665. https://www.researchgate.net/publication/337652898_Thermal_Environment_Accuracy_Investigation_of_Integrated_Environmental_Solutions-Virtual_Environment_IES-VE_Software_for_Double-Story_House_Simulation_in_Malaysia

Chen, F., Kusaka, H., Bornstein, R., Ching, J., Grimmond, C. S. B., Grossman-Clarke, S., Loridan, T., Manning, K. W., Martilli, A., Miao, S., Sailor, D., Salamanca, F. P., Taha, H., Tewari, M., Wang, X., Wyszogrodzki,

A. A., & Zhang, C. (2011). The integrated wrf/urban modelling system: Development, evaluation, and applications to urban environmental problems. *International Journal of Climatology*, *31*(2), 273–288. https://doi.org/10.1002/joc.2158

Chen, Y., Hong, T., & Piette, M. A. (2017). Automatic generation and simulation of urban building energy models based on city datasets for city-scale building retrofit analysis. *Applied Energy*, *205*, 323–335. https://doi.org/10.1016/j.apenergy.2017.07.128

CIBSE. (2006). *Cibse guide a: Environmental design* (7th ed.). Chartered Institution of Building Services Engineers.

Climate.OneBuilding. (n.d.-a). *Netherlands (wmo region 6) – climate.onebuilding.org* [Accessed: 2025-07-18]. https://climate.onebuilding.org/WMO_Region_6_Europe/NLD_Netherlands/index.html

Climate.OneBuilding. (n.d.-b). *Repository of building simulation climate data* [Accessed: 2025-07-18]. https://climate.onebuilding.org/#:~:text=TMYx%20dataset%20are%20created%20by,the%20ERA5%20reanalysis%20data%20set.

Crawley, D. B., Lawrie, L. K., Winkelmann, F. C., Buhl, W. F., Huang, Y. J., Pedersen, C. O., Strand, R. K., Liesen, R. J., Fisher, D. E., Witte, M. J., & Glazer, J. (2008). Contrasting the capabilities of building energy performance simulation programs. *Building and Environment*, *43*(4), 661–673. https://doi.org/10.1016/j.buildenv.2006.10.027

Csáky, I., & Kalmár, F. (2015). Effects of thermal mass, ventilation, and glazing orientation on indoor air temperature in buildings. *Journal of Building Physics*, *39*(2), 189–204. https://doi.org/10.1177/1744259115579060

Daniel, R., Cortesão, J., Steeneveld, G.-J., Stremke, S., & Lenzholzer, S. (2023). Performance of urban climate-responsive design interventions in combining climate adaptation and mitigation. *Building and Environment*, *236*, 110227. https://doi.org/10.1016/j.buildenv.2023.110227

Defraeye, T., Blocken, B., & Carmeliet, J. (2011). Convective heat transfer coefficients for exterior building surfaces: Existing correlations and cfd modelling. *Energy Conversion and Management*, *52*(1), 512–522. https://doi.org/10.1016/j.enconman.2010.07.026

DGMR Software BV. (2025). *Dgmr software – rekensoftware voor geluid, luchtkwaliteit en gebouwprestaties* [Accessed: 2025-09-09]. https://dgmrsoftware.nl

Ding, X., Zhao, Y., Strebel, D., Fan, Y., Ge, J., & Carmeliet, J. (2024). A wrf-ucm-solweig framework for mapping thermal comfort and quantifying urban climate drivers: Advancing spatial and temporal resolutions at city scale. *Sustainable Cities and Society*, *112*, 105628. https://doi.org/10.1016/j.scs.2024.105628

Djedjig, R., Bozonnet, E., & Belarbi, R. (2016). Modeling green wall interactions with street canyons for building energy simulation in urban context. *Urban Climate*, *16*, 75–85. https://doi.org/10.1016/j.uclim.2015.12.003

Djedjig, R., Ouldboukhitine, S.-E., Belarbi, R., & Bozonnet, E. (2012). Development and validation of a coupled heat and mass transfer model for green roofs. *International Communications in Heat and Mass Transfer*, *39*(6), 752–761. https://doi.org/10.1016/j.icheatmasstransfer.2012.03.024

Droste, A. M., Heusinkveld, B. G., Fenner, D., & Steeneveld, G.-J. (2020). Assessing the potential and application of crowdsourced urban wind data. *Quarterly Journal of the Royal Meteorological Society*, *146*(731), 2671–2688. https://doi.org/https://doi.org/10.1002/qj.3811

E+E Elektronik Ges.m.b.H. (2023). *Humidity / temperature sensor for high humidity and chemical applications*. E+E Elektronik Ges.m.b.H. https://www.epluse.com/fileadmin/data/product/ee33

Eingrüber, N., Domm, A., Korres, W., & Schneider, K. (2025). Simulation of the heat mitigation potential of unsealing measures in cities by parameterizing grass grid pavers for urban microclimate modelling with envi-met (v5). *Geoscientific Model Development*, *18*. https://doi.org/10.5194/gmd-18-141-2025

ENVI-met. (2025, May). *Envi-met (version 5.8.0)* (Computer software). https://www.envi-met.com

ENVI-met. (n.d.). *Running envi-met* [Accessed: 2025-06-11]. https://envi-met.info/doku.php?id=kb:compute

ENVI-met Support Center. (2022). *Re: Questions about simulation results* [Accessed: 2025-06-11]. https://www.envi-hq.com/viewtopic.php?f=3&t=3840&p=13070

Erell, E., Pearlmutter, D., Boneh, D., & Kutiel, P. B. (2014). Effect of high-albedo materials on pedestrian heat stress in urban street canyons [ICUC8: The 8th International Conference on Urban Climate and the 10th Symposium on the Urban Environment]. *Urban Climate*, *10*, 367–386. https://doi.org/10.1016/j.uclim.2013.10.005

Feng, Y., Wang, J., Zhou, W., Li, X., & Yu, X. (2022). Evaluating the cooling performance of green roofs under extreme heat conditions. *Frontiers in Environmental Science*, *10*. https://doi.org/10.3389/fenvs.2022.874614

Frayssinet, L., Merlier, L., Kuznik, F., Hubert, J.-L., Milliez, M., & Roux, J.-J. (2018). Modeling the heating and cooling energy demand of urban buildings at city scale. *Renewable and Sustainable Energy Reviews*, *81*, 2318–2327. https://doi.org/10.1016/j.rser.2017.06.040

GGD Twente. (n.d.). *Gezond binnenmilieu in kindercentra* [Accessed: 2025-10-24]. https://www.ggdtwente.nl/professionals/voor-onderwijs-en-kinderopvang/gezonde-scholen-en-kinderopvang/folder-gezond-binnenmilieu-in-kindercentra

Gobakis, K., & Kolokotsa, D. (2017). Coupling building energy simulation software with microclimatic simulation for the evaluation of the impact of urban outdoor conditions on the energy consumption and indoor environmental quality. *Energy and Buildings*, *157*, 101–115. https://doi.org/10.1016/j.enbuild.2017.02.020

Gomes, M. G., M. Silva, C., Valadas, A. S., & Silva, M. (2019). Impact of vegetation, substrate, and irrigation on the energy performance of green roofs in a mediterranean climate. *Water*, *11*(10). https://doi.org/10.3390/w11102016

Groenblauwe Netwerken. (n.d.). *Groene daken* [Accessed: 2025-06-09]. https://groenblauwenetwerken.nl/measures/groene-daken/#:~:text=Hellende%20groene%20daken,tot%207%C2%B0%20het%20effici%C3%ABntst

Guzman, E. (2023). Evaluating the impact of trees on residential thermal conditions in los angeles using community science. *Cities and the Environment*, *16*. https://doi.org/10.15365/cate.2023.160208

Habib, M. M., van Esch, M., van Ham, M., & Timmermans, W. J. (2025). High-resolution datasets for urban heat vulnerability assessment in urbanized areas of the netherlands. *Data in Brief*, *60*, 111525. https://doi.org/10.1016/j.dib.2025.111525

Heisler, G. M. (1986). Energy savings with trees. *Journal of Arboriculture*, *12*(5), 113–125. https://doi.org/10.48044/jauf.1986.026

Henderson, H., & Harley, B. (2022). *Infiltration guidance for buildings at design conditions* (tech. rep.). NYS Clean Heat Program.

Hensen, J. L. M., & Lamberts, R. (2019). *Building performance simulation for design and operation* (2nd ed.). Routledge. https://research-ebsco-com.tudelft.idm.oclc.org/linkprocessor/plink?id=0b8aa8a6-b665-36b6-afc0-832fb75685f8

Hirons, A., & Sjöman, H. (2019). *Tree species selection for green infrastructure - a guide for specifiers*.

Hoelscher, M.-T., Nehls, T., Jänicke, B., & Wessolek, G. (2016). Quantifying cooling effects of facade greening: Shading, transpiration and insulation. *Energy and Buildings*, *114*, 283–290. https://doi.org/10.1016/j.enbuild.2015.06.047

Höppe, P. (1999a). The physiological equivalent temperature – a universal index for the biometeorological assessment of the thermal environment. *International Journal of Biometeorology*, *43*(2), 71–75. https://doi.org/10.1007/s004840050118

Höppe, P. (1999b). The physiological equivalent temperature — a universal index for the biometeorological assessment of the thermal environment. *International Journal of Biometeorology*, *43*(2), 71–75. https://doi.org/10.1007/s004840050118

Huang, K.-T., & Li, Y.-J. (2017). Impact of street canyon typology on building's peak cooling energy demand: A parametric analysis using orthogonal experiment. *Energy and Buildings*, *154*, 448–464. https://doi.org/10.1016/j.enbuild.2017.08.054

Huttner, S. (2012). *Further development and application of the 3d microclimate simulation envi-met* [Doctoral dissertation, Johannes Gutenberg-Universität Mainz]. https://doi.org/10.25358/openscience-2022

Huynen, M. M., Martens, P., Schram, D., Weijenberg, M. P., & Kunst, A. E. (2001). The impact of heat waves and cold spells on mortality rates in the dutch population. *Environmental Health Perspectives*, *109*(5), 463–470. https://doi.org/10.1289/ehp.01109463

IES-VE. (2021a). *Apachesim methods*. https://help.iesve.com/ve2021/apachecalc_methods.htm

IES-VE. (2021b). *Table 22: Outside surface resistance (table a3.6 cibse guide)* [Accessed: 2025-08- 21]]. https://help.iesve.com/ve2021/table_22_outside_surface_resistance__table_a3_6_cibse_guide_.htm

IES-VE. (2021c). *Table 6: Thermal conductivity, specific heat capacity and density* [Accessed: 2025-05-29]. https://help.iesve.com/ve2021/table_6_thermal_conductivity__specific_heat_capacity_and_density.htm

IES-VE. (2025). *Integrated environmental solutions virtual environment, version 2025.0.0.0*. https://www.iesve.com/software/virtual-environment

International Organization for Standardization. (2007). *Bs en iso 6946:2007 building components and building elements—thermal resistance and thermal transmittance—calculation method* (tech. rep. No. EN ISO

6946:2007) (British Standard adopted from ISO 6946:2007). International Organization for Standardization. Geneva, Switzerland.

Irmak, M., Yılmaz, S., & Dursun, D. (2017). Effect of different pavements on human thermal comfort conditions. *Atmosfera*, *30*, 355–366. https://doi.org/10.20937/ATM.2017.30.04.06

Jalilzadeh, A., Rafiee, A., De Graaf, S., Konstantinou, T., & van Oosterom, P. J. M. (2025). Automated district-level energy demand modeling using energyplus empowered by digital twin technology. *ISPRS Annals of the Photogrammetry, Remote Sensing and Spatial Information Sciences*, *X-G-2025*, 397–404. https://doi.org/10.5194/isprs-annals-X-G-2025-397-2025

Jamei, E., & Rajagopalan, P. (2019). Effect of street design on pedestrian thermal comfort. *Architectural Science Review*, *62*(2), 92–111. https://doi.org/10.1080/00038628.2018.1537236

Ji, Y., Lee, A., & Swan, W. (2019). Building dynamic thermal model calibration using the energy house facility at salford. *Energy and Buildings*, *191*, 224–234. https://doi.org/https://doi.org/10.1016/j.enbuild.2019.03.001

Jin, L., Schubert, S., Hefny Salim, M., & Schneider, C. (2020). Impact of air conditioning systems on the outdoor thermal environment during summer in berlin, germany. *International Journal of Environmental Research and Public Health*, *17*(13). https://doi.org/10.3390/ijerph17134645

Kipp & Zonen B.V. (2001a). *Instruction manual pyrgeometer cg 4*. Röntgenweg 1, 2624 BD Delft, The Netherlands. http://www.kippzonen.com

Kipp & Zonen B.V. (2001b). *Instruction manual pyrheliometer ch 1*. Delftechpark 36, 2628 XH Delft, The Netherlands. http://www.kippzonen.com

Kipp & Zonen B.V. (n.d.). *Cmp22 pyranometer* [Accessed: 2025-05-03]. https://www.kippzonen.com/Product/15/CMP22-Pyranometer#:~:text=The%20CMP22%20has%20all%20the,response%20and%20reduced%20thermal%20offsets.'

Klinger, J., Westover, T., Saha, N., Sibbett, C., & Williams, C. L. (2025). Thermal properties of native and densified hardwood, softwoods, and agricultural residue. *Biomass and Bioenergy*, *195*, 107711. https://doi.org/10.1016/j.biombioe.2025.107711

Kluck, J., Klok, L., Solcerová, A., Kleerekoper, L., Wilschut, L., Jacobs, C., & Loeve, R. (2020, May). *De hittebestendige stad-een koele kijk op de inrichting van de buitenruimte* (tech. rep.). Amsterdam University of Applied Sciences.

Knap, W. (2019). *Basic and other measurements of radiation at station Cabauw (2019-08)* [In: Knap, W (2022): Basic and other measurements of radiation at station Cabauw (2005-02 et seq) [dataset publication series]. Koninklijk Nederlands Meteorologisch Instituut, De Bilt, PANGAEA, https://doi.org/10.1594/PANGAEA.940531]. Koninklijk Nederlands Meteorologisch Instituut, De Bilt. https://doi.org/10.1594/PANGAEA.905898

Knight, T., Price, S., Bowler, D., et al. (2021). How effective is 'greening' of urban areas in reducing human exposure to ground-level ozone concentrations, uv exposure and the 'urban heat island effect'? an updated systematic review. *Environmental Evidence*, *10*(12). https://doi.org/10.1186/s13750-021-00226-y

KNMI. (2019). *Meteo surface - validated and gapfilled observations of common atmospheric variables at 10 minute interval at cabauw* (1.0). https://dataplatform.knmi.nl/dataset/cesar-surface-meteo-lc1-t10-v1-0

KNMI. (2023). *Knmi '23 klimaatscenario's voor nederland* (8th ed.).

KNMI. (2025). *Uurgegevens van het weer in nederland: Klimatologie* [Gevalideerde uurlijkse meteorologische data per station]. Retrieved July 18, 2025, from https://www.daggegevens.knmi.nl/klimatologie/uurgegevens

KNMI. (n.d.-a). *Knmi research - observations & data technology - baseline surface radiation network (bsrn)* [Accessed: 2025-05-03]. https://www.knmi.nl/research/observations-data-technology/projects/baseline-surface-radiation-network-bsrn

KNMI. (n.d.-b). *Uitleg over temperatuur* [Accessed: 2025-09-06]. www.knmi.nl/kennis-en-datacentrum/uitleg/temperatuur

Kolokotroni, M., Ren, X., Davies, M., & Mavrogianni, A. (2012). London's urban heat island: Impact on current and future energy consumption in office buildings. *Energy and Buildings*, *47*, 302–311. https://doi.org/10.1016/j.enbuild.2011.12.019

Köppen, W. (1931). *Klimakarte der erde* (2nd ed.). Grundriss derKlimakunde, Berlin.

Kranen, R. H. M. (2021, April). *Exploring scenarios for mixed-use high-rise buildings as frontrunner in meeting (future) energy performance requirements* [Master thesis, TU Eindhoven].

Langewen, J., Holstein, A. N., Spaan, K., Haer, T., de Moel, H., Solcerova, A., Drukker, E., van den Buuse, D., van Winden, W., Switzer, A., Morel, M., van der Grijp, N., Tigelaar, J. H., Logjes, P., Braat, W., Nieuwesteeg, R., Jacobi, J., & Molenaar, A. (2022). *Resilio final report: A roof journey* (Project report). https://resilio.amsterdam/wp-content/uploads/2022/03/Final-Report-RESILIO.pdf

Larsen, T. S. (2006). *Natural ventilation driven by wind and temperature difference* [Doctoral dissertation, Department of Civil Engineering, Aalborg University].

Lauzet, N., Rodler, A., Musy, M., Azam, M.-H., Guernouti, S., Mauree, D., & Colinart, T. (2019). How building energy models take the local climate into account in an urban context – a review. *Renewable and Sustainable Energy Reviews*, *116*, 109390. https://doi.org/10.1016/j.rser.2019.109390

Le, A.-V., & Chan, Y.-C. (2023). Comparison between envi-met and ansys-fluent when used for microclimate simulation. *Journal of Physics: Conference Series*, *2600*(8), 082019. https://doi.org/10.1088/1742-6596/2600/8/082019

Li, H., Zhao, Y., Wang, C., Ürge-Vorsatz, D., Carmeliet, J., & Bardhan, R. (2024). Cooling efficacy of trees across cities is determined by background climate, urban morphology, and tree trait. *Communications Earth & Environment*, *5*, 754. https://doi.org/10.1038/s43247-024-01908-4

Li, J., Zheng, B., Bedra, K. B., Li, Z., & Chen, X. (2021). Evaluating the effect of window-to-wall ratios on cooling-energy demand on a typical summer day. *International Journal of Environmental Research and Public Health*, *18*(16). https://doi.org/10.3390/ijerph18168411

Li, J., Zheng, B., Ouyang, X., Chen, X., & Bedra, K. B. (2021). Does shrub benefit the thermal comfort at pedestrian height in singapore? *Sustainable Cities and Society*, *75*, 103333. https://doi.org/10.1016/j.scs.2021.103333

Li, X., Zhou, Y., Yu, S., Jia, G., Li, H., & Li, W. (2019). Urban heat island impacts on building energy consumption: A review of approaches and findings. *Energy*, *174*, 407–419. https://doi.org/10.1016/j.energy.2019.02.183

Licón-Portillo, J. A., Martínez-Torres, K. E., Chung-Alonso, P., & Herrera Peraza, E. F. (2024). From block to city scale: Greenery's contribution to cooling the urban environment. *Urban Science*, *8*(2). https://doi.org/10.3390/urbansci8020041

Lindberg, F., Grimmond, C., Gabey, A., Huang, B., Kent, C. W., Sun, T., Theeuwes, N. E., Järvi, L., Ward, H. C., Capel-Timms, I., Chang, Y., Jonsson, P., Krave, N., Liu, D., Meyer, D., Olofson, K. F. G., Tan, J., Wästberg, D., Xue, L., & Zhang, Z. (2018). Urban multi-scale environmental predictor (umep): An integrated tool for city-based climate services. *Environmental Modelling Software*, *99*, 70–87. https://doi.org/10.1016/j.envsoft.2017.09.020

Liu, Z., Zheng, S., & Zhao, L. (2018). Evaluation of the envi-met vegetation model of four common tree species in a subtropical hot-humid area. *Atmosphere*, *9*(5). https://doi.org/10.3390/atmos9050198

Lobaccaro, G., & Acero, J. A. (2015). Comparative analysis of green actions to improve outdoor thermal comfort inside typical urban street canyons. *Urban Climate*, *14*, 251–267. https://doi.org/10.1016/j.uclim.2015.10.002

López-Guerrero, R. E., Verichev, K., Moncada-Morales, G. A., & Carpio, M. (2022). How do urban heat islands affect the thermo-energy performance of buildings? *Journal of Cleaner Production*, *373*, 133713. https://doi.org/10.1016/j.jclepro.2022.133713

Lundgren-Kownacki, K., Hornyanszky, E. D., Chu, T. A., Olsson, J. A., & Becker, P. (2018). Challenges of using air conditioning in an increasingly hot climate. *International Journal of Biometeorology*, *62*(3), 401–412. https://doi.org/10.1007/s00484-017-1493-z

Luo, X., Wang, J., & Li, J. (2022). Study on the effect of vegetation coverage on urban cooling and energy conservation: A case study of a typical hilly city, chenzhou, china. *Buildings*, *12*(5). https://doi.org/10.3390/buildings12050640

Manapragada, N. V. S. K., & Natanian, J. (2025). Urban microclimate and energy modeling: A review of integration approaches. *Sustainability*, *17*(7). https://doi.org/10.3390/su17073025

Manickathan, L., Kubilay, A., Defraeye, T., Allegrini, J., Derome, D., & Carmeliet, J. (2018). Integrated vegetation model for studying the cooling potential of trees in urban street canyons. *International Building Physics Conference 2018. 3.* https://doi.org/10.14305/IBPC.2018.GB-2.03

Manso, M., Teotónio, I., Silva, C. M., & Cruz, C. O. (2021). Green roof and green wall benefits and costs: A review of the quantitative evidence. *Renewable and Sustainable Energy Reviews*, *135*, 110111. https://doi.org/10.1016/j.rser.2020.110111

Maronga, B., Gryschka, M., Heinze, R., Hoffmann, F., Kanani-Sühring, F., Keck, M., Ketelsen, K., Letzel, M. O., Sühring, M., & Raasch, S. (2015). The parallelized large-eddy simulation model (palm) version 4.0 for atmospheric and oceanic flows: Model formulation, recent developments, and future perspectives. *Geoscientific Model Development*, *8*(8), 2515–2551. https://doi.org/10.5194/gmd-8-2515-2015

Mata, É., & Sasic Kalagasidis, A. (2009). *Calculation of energy use in the swedish housing: Description of the building energy simulation model eabs (energy assessment of building stocks)* (tech. rep. No. Report 2009:4). Chalmers University of Technology. Göteborg, Sweden.

Matzarakis, A., Rutz, F., & Mayer, H. (2007). Modelling radiation fluxes in simple and complex environments—application of the rayman model. *International Journal of Biometeorology*, *51*(4), 323–334. https://doi.org/10.1007/s00484-006-0061-8

Michael, P. R., Johnston, D. E., & Moreno, W. (2020). A conversion guide: Solar irradiance and lux illuminance. *Journal of Measurements in Engineering*, *8*(4), 153–166. https://doi.org/10.21595/jme.2020.21667

Mihalakakou, G., Souliotis, M., Papadaki, M., Menounou, P., Dimopoulos, P., Kolokotsa, D., Paravantis, J. A., Tsangrassoulis, A., Panaras, G., Giannakopoulos, E., & Papaefthimiou, S. (2023). Green roofs as a nature-based solution for improving urban sustainability: Progress and perspectives. *Renewable and Sustainable Energy Reviews*, *180*, 113306. https://doi.org/10.1016/j.rser.2023.113306

Ministerie van Infrastructuur en Waterstaat. (2016). *De nationale klimaatadaptatiestrategie (nas)* (tech. rep.) (Accessed: 2025-03-04). Ministerie van Infrastructuur en Waterstaat. https://zoek.officielebekendmakingen.nl/blg-791816.pdf

Ministerie van Klimaat en Groene Groei. (2025). *Nederland gaat stap voor stap over op duurzame energie* [Accessed: 2025-08-22]. https://www.rijksoverheid.nl/onderwerpen/duurzame-energie/nederland-gaat-stap-voor-stap-over-op-duurzame-energie

Mirzaei, P. A., & Haghighat, F. (2010). Approaches to study urban heat island – abilities and limitations. *Building and Environment*, *45*(10), 2192–2201. https://doi.org/10.1016/j.buildenv.2010.04.001

Mohapatra, S., Verma, S., Chowdhury, S., Dwivedi, G., & Harish, V. (2021). A critical appraisal of green vegetated roofs: Energy and environment in focus. *Materials Today: Proceedings*, *46*, 5703–5710. https://doi.org/https://doi.org/10.1016/j.matpr.2020.09.843

Molnár, G., Kovács, A., & Gál, T. (2020). How does anthropogenic heating affect the thermal environment in a medium-sized central european city? a case study in szeged, hungary. *Urban Climate*, *34*, 100673. https://doi.org/10.1016/j.uclim.2020.100673

Morakinyo, T. E., Dahanayake, K. K. C., Adegun, O. B., & Balogun, A. A. (2016). Modelling the effect of tree-shading on summer indoor and outdoor thermal condition of two similar buildings in a nigerian university. *Energy and Buildings*, *130*, 721–732. https://doi.org/10.1016/j.enbuild.2016.08.087

Morakinyo, T. E., Dahanayake, K., Ng, E., & Chow, C. L. (2017). Temperature and cooling demand reduction by green-roof types in different climates and urban densities: A co-simulation parametric study. *Energy and Buildings*, *145*, 226–237. https://doi.org/10.1016/j.enbuild.2017.03.066

Morakinyo, T. E., Lai, A., Lau, K. K.-L., & Ng, E. (2019). Thermal benefits of vertical greening in a high-density city: Case study of hong kong [Green Infrastructures: Nature Based Solutions for sustainable and resilient cities]. *Urban Forestry Urban Greening*, *37*, 42–55. https://doi.org/10.1016/j.ufug.2017.11.010

Morakinyo, T. E., & Lam, Y. F. (2016). Simulation study on the impact of tree-configuration, planting pattern and wind condition on street-canyon's micro-climate and thermal comfort. *Building and Environment*, *103*, 262–275. https://doi.org/10.1016/j.buildenv.2016.04.025

Morakinyo, T. E., Lau, K. K.-L., Ren, C., & Ng, E. (2018). Performance of hong kong's common trees species for outdoor temperature regulation, thermal comfort and energy saving. *Building and Environment*, *137*, 157–170. https://doi.org/10.1016/j.buildenv.2018.04.012

Mosteiro-Romero, M., Maiullari, D., Pijpers-van Esch, M., & Schlueter, A. (2020). An integrated microclimate-energy demand simulation method for the assessment of urban districts. *Frontiers in Built Environment*, *6 - 2020*. https://doi.org/10.3389/fbuil.2020.553946

Musy, M., Malys, L., Morille, B., & Inard, C. (2015). The use of solene-microclimat model to assess adaptation strategies at the district scale. *Urban Climate*, *14*, 213–223. https://doi.org/10.1016/j.uclim.2015.07.004

Nationale Dakenplan. (2021). *Handreiking groen geel dak* (tech. rep.) (Accessed: 2025-06-09). Nationaal Dakenplan. https://dakenplan.nl/storage/pdfs/ndp-handreiking-groen-geel.pdf

NETZSCH. (2025). *Pe-ld: Polyethylene low density* [Accessed: 2025-08-26]. https://analyzing-testing.netzsch.com/en/polymers-netzsch-com/commodity-thermoplastics/pe-ld-polyethylene-low-density

Ng, E., Chen, L., Wang, Y., & Yuan, C. (2012). A study on the cooling effects of greening in a high-density city: An experience from hong kong [International Workshop on Ventilation, Comfort, and Health in Transport Vehicles]. *Building and Environment*, *47*, 256–271. https://doi.org/10.1016/j.buildenv.2011.07.014

Nguyen, J. L., Schwartz, J., & Dockery, D. W. (2014). The relationship between indoor and outdoor temperature, apparent temperature, relative humidity, and absolute humidity. *Indoor Air*, *24*(1), 103–112. https://doi.org/10.1111/ina.12052

Noome, W., Feijen, A., Brolsma, R., Moens, M., Verhagen, F., Föllmi, D., Meeuwissen, S., Sahit, F., Veldkamp, T., & Heuvelink, D. (2023). *Praktische handvatten voor een droogtebestendigere inrichting van stedelijk groen: Achtergronddocument* (tech. rep. No. Versie 1.0). Sweco / Tauw / Deltares / Arcadis / Royal

HaskoningDHV / Hogeschool van Amsterdam. https://klimaatadaptatienederland.nl/actueel/actueel/nieuws/2023/praktische-handvatten-droogtebestendig-groen-stad/

Ochsner, T. E. (2019). *Rain or shine: An introduction to soil physical properties and processes*. Oklahoma State University Libraries. https://doi.org/10.22488/okstate.21.000000

Oke, T. R., Mills, G., Christen, A., & Voogt, J. A. (2017). *Urban climates*. Cambridge University Press. https://doi.org/10.1017/9781139016476

Ottelé, M., & Perini, K. (2017). Comparative experimental approach to investigate the thermal behaviour of vertical greened façades of buildings. *Ecological Engineering*, *108*, 152–161. https://doi.org/10.1016/j.ecoleng.2017.08.016

Ottelé, M., Perini, K., Fraaij, A., Haas, E., & Raiteri, R. (2011). Comparative life cycle analysis for green façades and living wall systems. *Energy and Buildings*, *43*(12), 3419–3429. https://doi.org/10.1016/j.enbuild.2011.09.010

Ouyang, W., Sinsel, T., Simon, H., Morakinyo, T. E., Liu, H., & Ng, E. (2022). Evaluating the thermal-radiative performance of envi-met model for green infrastructure typologies: Experience from a subtropical climate. *Building and Environment*, *207*, 108427. https://doi.org/10.1016/j.buildenv.2021.108427

Palme, M., Inostroza, L., Villacreses, G., Lobato, A., & Carrasco, C. (2017). Urban weather data and building models for the inclusion of the urban heat island effect in building performance simulation. *Data in Brief*, *14*, 671–675. https://doi.org/10.1016/j.dib.2017.08.035

Pan, Y., Zhu, M., Lv, Y., Yang, Y., Liang, Y., Yin, R., Yang, Y., Jia, X., Wang, X., Zeng, F., Huang, S., Hou, D., Xu, L., Yin, R., & Yuan, X. (2023). Building energy simulation and its application for building performance optimization: A review of methods, tools, and case studies. *Advances in Applied Energy*, *10*, 100135. https://doi.org/10.1016/j.adapen.2023.100135

Pantavou, K., Koletsis, I., Tseliou, A., Lykoudis, S., Tsiros, I., Lagouvardos, K., Psiloglou, B., & Founda, D. (2022). Validation of envi-met microscale model with in-situ measurements in warm thermal conditions across athens area. *17 th International Conference on Environmental Science and Technology*. https://doi.org/10.30955/gnc2021.00261

Parizotto, S., & Lamberts, R. (2011). Investigation of green roof thermal performance in temperate climate: A case study of an experimental building in florianópolis city, southern brazil. *Energy and Buildings*, *43*(7), 1712–1722. https://doi.org/10.1016/j.enbuild.2011.03.014

Pasandi, L., Qian, Z., & Woo, W. L. (2025). Quantifying urban microclimate feedback on building energy use using a coupled simulation workflow. *Building and Environment*, *285*, 113657. https://doi.org/10.1016/j.buildenv.2025.113657

Pasandi, L., Qian, Z., Woo, W. L., & Palacin, R. (2024). A comprehensive review of applications and feedback impact of microclimate on building operation and energy. *Building and Environment*, *263*, 111855. https://doi.org/10.1016/j.buildenv.2024.111855

Pastore, L., Corrao, R., & Heiselberg, P. K. (2017). The effects of vegetation on indoor thermal comfort: The application of a multi-scale simulation methodology on a residential neighborhood renovation case study. *Energy and Buildings*, *146*, 1–11. https://doi.org/10.1016/j.enbuild.2017.04.022

Peel, M. C., Finlayson, B. L., & McMahon, T. A. (2007). Updated world map of the köppen-geiger climate classification. *Hydrology and Earth System Sciences*, *11*(5), 1633–1644. https://doi.org/10.5194/hess-11-1633-2007

Peng, S., Piao, S., Ciais, P., Friedlingstein, P., Ottlé, C., Bréon, F.-M., Nan, H., Zhou, L., & Myneni, R. B. (2012). Surface urban heat island across 419 global big cities. *Environmental Science & Technology*, *46*(2), 696–703. https://doi.org/10.1021/es2030438

Perez, R., Webster, K., Seals, R., Stewart, R., & Barron, J. (1987). Variations of the luminous efficacy of global and diffuse radiation and zenith luminance with weather conditions—description of a potential method to generate key daylight availability data from existing solar radiation data bases. *Solar Energy*, *38*(1), 33–44. https://doi.org/10.1016/0038-092X(87)90068-5

Pérez, G., Coma, J., Chàfer, M., & Cabeza, L. F. (2022). Seasonal influence of leaf area index (lai) on the energy performance of a green facade. *Building and Environment*, *207*, 108497. https://doi.org/10.1016/j.buildenv.2021.108497

Perini, K., Chokhachian, A., Dong, S., & Auer, T. (2017). Modeling and simulating urban outdoor comfort: Coupling envi-met and trnsys by grasshopper. *Energy and Buildings*, *152*, 373–384. https://doi.org/10.1016/j.enbuild.2017.07.061

Perini, K., Ottelé, M., Fraaij, A., Haas, E., & Raiteri, R. (2011). Vertical greening systems and the effect on air flow and temperature on the building envelope. *Building and Environment*, *46*(11), 2287–2294. https://doi.org/10.1016/j.buildenv.2011.05.009

Perini, K., & Rosasco, P. (2013). Cost–benefit analysis for green façades and living wall systems. *Building and Environment*, *70*, 110–121. https://doi.org/10.1016/j.buildenv.2013.08.012

Rallapalli, H. S. (2010). *A comparison of energyplus and equest: Whole building energy simulation results for a medium sized office building* [Master thesis]. Arizona State University.

Reeves, T., Olbina, S., & Issa, R. R. A. (2012). Validation of building energy modeling tools: Ecotect™, green building studio™ and ies<ve>™. *Proceedings of the 2012 Winter Simulation Conference*, 581–593. https://doi.org/10.1109/WSC.2012.6465223

Reinhart, C., Dogan, T., Jakubiec, A., Rakha, T., & Sang, A. (2013). Umi â€“ an urban simulation environment for building energy use, daylighting and walkability. *Proceedings of Building Simulation 2013: 13th Conference of IBPSA*, *13*, 476–483. https://doi.org/10.26868/25222708.2013.1404

Reinhart, C. F., & Cerezo Davila, C. (2016). Urban building energy modeling – a review of a nascent field. *Building and Environment*, *97*, 196–202. https://doi.org/10.1016/j.buildenv.2015.12.001

RIVM. (2022). *Thermisch comfort* [Accessed: 2025-10-24]. https://www.rivm.nl/binnenmilieu/thermisch-comfort

RIVM. (2023). *Achtergronddocument "Warm weer in Nederland" behorend bij de GGD richtlijn Hitte en Gezondheid* (tech. rep.). Rijksinstituut voor Volksgezondheid en Milieu (RIVM). https://www.rivm.nl/sites/default/files/2023-06/Achtergrond_Warm_weer_in_NL_Richtlijn_Hitte_Gezondheid.pdf

Rosenfelder, M., Koppe, C., Pfafferott, J., & Matzarakis, A. (2016). Effects of ventilation behaviour on indoor heat load based on test reference years. *International journal of biometeorology*, *60*(2), 277–287. https://doi.org/10.1007/s00484-015-1024-8

Rovers, V., Bosch, P., Albers, R., Hove, B., Blocken, B., Dobbelsteen, A., Spit, T. J. M., Dikmans, M., Boonstra, B., Brolsma, R. J., Daanen, H., Echevarria, L., Groot, A., Hartogensis, O., Hensen, J., Heusinkveld, B., Hofman, J., Hutjes, R., Jacobs, C., & Zevenbergen, C. (2015). *Climate proof cities – final report*. Knowledge for Climate Programme. Utrecht, The Netherlands.

RVO. (2017). *Referentiegebouwen beng (bijna energie-neutrale gebouwen)* (tech. rep.) (Version 002a). Rijksdienst voor Ondernemend Nederland and DGMR Bouw B.V. Den Haag / Arnhem, Nederland. https://www.rvo.nl/sites/default/files/2017/02/Referentiegebouwen%20BENG.pdf

RVO. (2018). *Temperatuuroverschrijding in nieuwe woningen in relatie tot voorgenomen beng-eisen* (tech. rep.). Rijksdienst voor Ondernemend Nederland. https://www.rvo.nl/sites/default/files/2019/05/Temperatuuroverschrijding%20in%20nieuwe%20woningen%20in%20relatie%20tot%20voorgenomen.pdf

Sadineni, S. B., Madala, S., & Boehm, R. F. (2011). Passive building energy savings: A review of building envelope components. *Renewable and Sustainable Energy Reviews*, *15*(8), 3617–3631. https://doi.org/10.1016/j.rser.2011.07.014

Sailor, D. J. (2011). A review of methods for estimating anthropogenic heat and moisture emissions in the urban environment. *International Journal of Climatology*, *31*(2), 189–199. https://doi.org/10.1002/joc.2106

Sailor, D. J., Elley, T. B., & Gibson, M. (2012). Exploring the building energy impacts of green roof design decisions – a modeling study of buildings in four distinct climates. *Journal of Building Physics*, *35*(4), 372–391. https://doi.org/10.1177/1744259111420076

Salvati, A., Palme, M., Chiesa, G., & Kolokotroni, M. (2020). Built form, urban climate and building energy modelling: Case-studies in rome and antofagasta. *Journal of Building Performance Simulation*, *13*(2), 209–225. https://doi.org/10.1080/19401493.2019.1707876

Santamouris, M. (2001). *Energy and climate in the urban built environment*. James & James Science Publishers.

Santamouris, M. (2014). Cooling the cities – a review of reflective and green roof mitigation technologies to fight heat island and improve comfort in urban environments. *Solar Energy*, *103*, 682–703. https://doi.org/10.1016/j.solener.2012.07.003

Santamouris, M., Cartalis, C., Synnefa, A., & Kolokotsa, D. (2015). On the impact of urban heat island and global warming on the power demand and electricity consumption of buildings—a review. *Energy and Buildings*, *98*, 119–124. https://doi.org/10.1016/j.enbuild.2014.09.052

Santamouris, M., Ding, L., Fiorito, F., Oldfield, P., Osmond, P., Paolini, R., Prasad, D., & Synnefa, A. (2017). Passive and active cooling for the outdoor built environment – analysis and assessment of the cooling potential of mitigation technologies using performance data from 220 large scale projects. *Solar Energy*, *154*, 14–33. https://doi.org/10.1016/j.solener.2016.12.006

Santamouris, M., & Osmond, P. (2020). Increasing green infrastructure in cities: Impact on ambient temperature, air quality and heat-related mortality and morbidity. *Buildings*, *10*(12). https://doi.org/10.3390/buildings10120233

Santamouris, M., Haddad, S., Saliari, M., Vasilakopoulou, K., Synnefa, A., Paolini, R., Ulpiani, G., Garshasbi, S., & Fiorito, F. (2018). On the energy impact of urban heat island in sydney: Climate and energy potential of mitigation technologies. *Energy and Buildings*, *166*, 154–164. https://doi.org/10.1016/j.enbuild.2018.02.007

Schinasi, L. H., Benmarhnia, T., & De Roos, A. J. (2018). Modification of the association between high ambient temperature and health by urban microclimate indicators: A systematic review and meta-analysis. *Environmental Research*, *161*, 168–180. https://doi.org/10.1016/j.envres.2017.11.004

Sedumspecialist. (n.d.). *Groendak: Alles over aanleg en voordelen* [Accessed: 2025-06-09]. https://www.sedumspecialist.nl/groendak/#:~:text=Heb%20je%20een%20dak%20met,op%20hun%20plek%20blijven%20zitten

Seto, K. C., Güneralp, B., & Hutyra, L. R. (2012). Global forecasts of urban expansion to 2030 and direct impacts on biodiversity and carbon pools. *Proceedings of the National Academy of Sciences*, *109*(40), 16083–16088. https://doi.org/10.1073/pnas.1211658109

Sezer, N., Yoonus, H., Zhan, D., Wang, L. (, Hassan, I. G., & Rahman, M. A. (2023). Urban microclimate and building energy models: A review of the latest progress in coupling strategies. *Renewable and Sustainable Energy Reviews*, *184*, 113577. https://doi.org/10.1016/j.rser.2023.113577

Shaik, S., Gorantla, K., Ghosh, A., Arumugam, C., & Maduru, V. R. (2021). Energy savings and carbon emission mitigation prospective of building's glazing variety, window-to-wall ratio and wall thickness. *Energies*, *14*(23), 8020. https://doi.org/10.3390/en14238020

Shareef, S. (2021). The impact of urban morphology and building's height diversity on energy consumption at urban scale. the case study of dubai. *Building and Environment*, *194*, 107675. https://doi.org/10.1016/j.buildenv.2021.107675

Shareef, S., & Altan, H. (2022). Urban block configuration and the impact on energy consumption: A case study of sinuous morphology. *Renewable and Sustainable Energy Reviews*, *163*, 112507. https://doi.org/10.1016/j.rser.2022.112507

Sharmin, T., Steemers, K., & Matzarakis, A. (2017). Microclimatic modelling in assessing the impact of urban geometry on urban thermal environment. *Sustainable Cities and Society*, *34*, 293–308. https://doi.org/10.1016/j.scs.2017.07.006

Sharples, S. (1984). Full-scale measurements of convective energy losses from exterior building surfaces. *Building and Environment*, *19*(1), 31–39. https://doi.org/https://doi.org/10.1016/0360-1323(84)90011-8

Shashua-Bar, L., Pearlmutter, D., & Erell, E. (2009). The cooling efficiency of urban landscape strategies in a hot dry climate. *Landscape and Urban Planning*, *92*(3), 179–186. https://doi.org/10.1016/j.landurbplan.2009.04.005

Simon, H. (2016). *Modeling urban microclimate: Development, implementation and evaluation of new and improved calculation methods for the urban microclimate model envi-met* [Doctoral dissertation, Johannes Gutenberg-Universität Mainz]. https://doi.org/10.25358/openscience-4042

Singh, N., Singh, S., & Mall, R. (2020). Chapter 17 - urban ecology and human health: Implications of urban heat island, air pollution and climate change nexus. In *Urban ecology* (pp. 317–334). Elsevier. https://doi.org/10.1016/B978-0-12-820730-7.00017-3

Smith, I. A., Fabian, M. P., & Hutyra, L. R. (2023). Urban green space and albedo impacts on surface temperature across seven united states cities. *Science of The Total Environment*, *857*, 159663. https://doi.org/10.1016/j.scitotenv.2022.159663

Sola, A., Corchero, C., Salom, J., & Sanmarti, M. (2018). Simulation tools to build urban-scale energy models: A review. *Energies*, *11*(12). https://doi.org/10.3390/en11123269

Solcerova, A., Klok, L., & Kluck, J. (2022). *Effect of blue-green roofs on outdoor temperature in the city of amsterdam* (Report). Amsterdam University of Applied Sciences.

Spanjar, G., Bartlett, D., Schramkó, S., Kluck, J., van Zandbrink, L., & Föllmi, D. (2023). *Cool towns intervention catalogue: Proven solutions to mitigate heat stress at street-level* (Report). CoE City Net Zero, Faculty of Technology, Amsterdam University of Applied Sciences.

Spijker, J. H., Ravesloot, M. B. M., de Vries, S., Hiemstra, J. A., & Voeten, J. G. W. F. (2024). *Groen in de stad: De meerwaarde van groen in de stedelijke omgeving* (Rep.). Wageningen Environmental Research. https://edepot.wur.nl/412084

Steeneveld, G.-J., Koopmans, S., Heusinkveld, B. G., Hove, L., & Holtslag, A. A. M. (2011). Quantifying urban heat island effects and human comfort for cities of variable size and urban morphology in the netherlands. *Journal of Geophysical Research*, *116*. https://doi.org/10.1029/2011JD015988

Steeneveld, G.-J., & Peerlings, E. (2025). Unravelling indoor temperature response to summer heat through long-term crowdsourced observations in dutch residences [Under review]. *Quarterly Journal of the Royal Meteorological Society*.

Suleiman, B. M., Larfeldt, J., Leckner, B., & Gustavsson, M. (1999). Thermal conductivity and diffusivity of wood. *Wood Science and Technology*, *33*(6), 465–473. https://doi.org/10.1007/s002260050130

Sun, C. Y., Lee, K. P., Lin, T. P., & Lee, S. H. (2012). Vegetation as a material of roof and city to cool down the temperature. *461*, 552–556. https://doi.org/10.4028/www.scientific.net/AMR.461.552

Sun, F., Zhang, J., Takeda, S., Cui, J., & Yang, R. (2024). Vertical plant configuration: Its impact on microclimate and thermal comfort in urban small green spaces. *Land*, *13*(10). https://doi.org/10.3390/land13101715

Tamerius, J. D., Perzanowski, M. S., Acosta, L. M., Jacobson, J. S., Goldstein, I. F., Quinn, J. W., Rundle, A. G., & Shaman, J. (2013). Socioeconomic and outdoor meteorological determinants of indoor temperature and humidity in new york city dwellings. *Weather, Climate, and Society*, *5*(2), 168–179. https://doi.org/10.1175/WCAS-D-12-00030.1

Tate, C., Wang, R., Akaraci, S., Burns, C., Garcia, L., Clarke, M., & Hunter, R. (2024). The contribution of urban green and blue spaces to the united nation's sustainable development goals: An evidence gap map. *Cities*. https://api.semanticscholar.org/CorpusID:266070164

Teuling, A. J., Seneviratne, S. I., Stöckli, R., Reichstein, M., Moors, E., Ciais, P., Luyssaert, S., van den Hurk, B., Ammann, C., Bernhofer, C., Dellwik, E., Gianelle, D., Gielen, B., Grünwald, T., Klumpp, K., Montagnani, L., Moureaux, C., Sottocornola, M., & Wohlfahrt, G. (2010). Contrasting response of european forest and grassland energy exchange to heatwaves. *Nature Geoscience*, *3*, 722–727. https://doi.org/10.1038/ngeo950

Tilley, D. (2012, May). *Vegetated walls: Thermal and growth properties of structured green facades*. https://doi.org/10.13140/RG.2.2.24238.56646

Toparlar, Y., Blocken, B., Maiheu, B., & van Heijst, G. (2017). A review on the cfd analysis of urban microclimate. *Renewable and Sustainable Energy Reviews*, *80*, 1613–1640. https://doi.org/10.1016/j.rser.2017.05.248

Tsoka, S., Tsikaloudaki, A., & Theodosiou, T. (2018). Analyzing the envi-met microclimate model's performance and assessing cool materials and urban vegetation applications–a review. *Sustainable Cities and Society*, *43*, 55–76. https://doi.org/10.1016/j.scs.2018.08.009

Tsoka, S., Leduc, T., & Rodler, A. (2021). Assessing the effects of urban street trees on building cooling energy needs: The role of foliage density and planting pattern. *Sustainable Cities and Society*, *65*, 102633. https://doi.org/10.1016/j.scs.2020.102633

TU Delft OpenCourseWare. (2016). *Bebouwing - TU Delft OCW* [Accessed: 2025-06-07]. https://ocw.tudelft.nl/course-readings/bebouwing/

UN-Habitat. (2024). *World Cities Report 2024: Cities and Climate Action* (tech. rep.). United Nations Human Settlements Programme (UN-Habitat). Nairobi, Kenya. https://unhabitat.org/sites/default/files/2024/11/wcr2024_-_full_report.pdf

Uniec 3. (2025). *Uniec 3 – beng indicatoren berekenen volgens de nta 8800* [Accessed: 2025-09-09]. https://uniec3.nl

U.S. Geological Survey. (2022). *Urban heat islands* [Accessed: 2025-07-24]. https://www.usgs.gov/media/images/urban-heat-islands

Vabi. (2025). *Vabi elements – 3d rekensoftware voor installateur & adviseur*. Retrieved September 9, 2025, from https://www.vabi.nl/producten/vabi-elements/

Vadiee, A., Dodoo, A., & Gustavsson, L. (2019). A comparison between four dynamic energy modeling tools for simulation of space heating demand of buildings. *Cold Climate HVAC 2018*, 701–711. https://doi.org/10.1007/978-3-030-00662-4_59

van Hove, L., Steeneveld, G., Jacobs, C., Heusinkveld, B., Elbers, J., Moors, E., & Holtslag, A. (2011). *Exploring the urban heat island intensity of dutch cities: Assessment based on a literature review, recent meteorological observation and datasets provided by hobby meteorologists* [Alterra report; No. 2170]. Alterra.

van Loenhout, J. A. F., Delbiso, T. D., Kiriliouk, A., Rodriguez-Llanes, J. M., Segers, J., & Guha-Sapir, D. (2018). Heat and emergency room admissions in the netherlands. *BMC Public Health*, *18*(1), 108. https://doi.org/10.1186/s12889-017-5021-1

van der Velde, J., Price, R., Maiullari, D., van Esch, M., Hartmeyer, L., Pouderoijen, M., Batenburg, W., Schoon, P., & Aktürk Hauser, G. (2023). *I-tree 2.0 nl: Next-generation metrics and methodologies for urban forestry and climate resilience in dutch cities* (tech. rep.). TU Delft / Partners i-Tree NL. https://filelist.tudelft.nl/IO/Actueel/Nieuwsberichten/2025/27%20-%202025/i-Tree%202.0%20NL_final%20report_2024.pdf

van der Werf, M., van der Windt, S., Svejda, A., & Nottrot, J. (2024). *Revitalising urban curaçao: A climate resilient plan for wilhelminaplein in punda* (Student report). Delft University of Technology. https://repository.tudelft.nl/record/uuid:a66b05fa-ad1a-41b6-899c-9161e993d575

van Loenhout, J., le Grand, A., Duijm, F., Greven, F., Vink, N., Hoek, G., & Zuurbier, M. (2016). The effect of high indoor temperatures on self-perceived health of elderly persons. *Environmental Research*, *146*, 27–34. https://doi.org/10.1016/j.envres.2015.12.012

Van Ulden, A. P., & Wieringa, J. (1996). Atmospheric boundary layer research at cabauw. In J. R. Garratt & P. A. Taylor (Eds.), *Boundary-layer meteorology 25th anniversary volume, 1970–1995: Invited reviews and selected contributions to recognise ted munn's contribution as editor over the past 25 years* (pp. 39–69). Springer Netherlands. https://doi.org/10.1007/978-94-017-0944-6_3

Vant-Hull, B., Ramamurthy, P., Havlik, B., Jusino, C., Corbin-Mark, C., Schuerman, M., Keefe, J., Drapkin, J. K., & Glenn, A. A. (2018). The harlem heat project: A unique media–community collaboration to study indoor heat waves. *Bulletin of the American Meteorological Society*, *99*(12), 2491–2506. https://doi.org/10.1175/BAMS-D-16-0280.1

Verkaik, J. W., & Holtslag, A. A. M. (2007). Wind profiles, momentum fluxes and roughness lengths at cabauw revisited. *Boundary-Layer Meteorology*, *122*(3), 701–719. https://doi.org/10.1007/s10546-006-9121-1

Vurro, G., & Carlucci, S. (2024). Contrasting the features and functionalities of urban microclimate simulation tools. *Energy and Buildings*, *311*, 114042. https://doi.org/10.1016/j.enbuild.2024.114042

Wang, Y., Ma, Y.-F., Muñoz-Esparza, D., Dai, J., Li, C. W. Y., Lichtig, P., Tsang, R. C.-W., Liu, C.-H., Wang, T., & Brasseur, G. P. (2023). Coupled mesoscale–microscale modeling of air quality in a polluted city using wrf-les-chem. *Atmospheric Chemistry and Physics*, *23*(10), 5905–5927. https://doi.org/10.5194/acp-23-5905-2023

Watkins, R., Palmer, J., & Kolokotroni, M. (2002). Increased temperature and intensification of the urban heat island: Implications for human comfort and urban design. *Built Environment*, *28*(1), 85–96. https://doi.org/10.2148/benv.33.1.85

Wilcox, S., & Marion, W. (2008). *Users manual for tmy3 data sets (revised)* (tech. rep.). National Renewable Energy Lab. (NREL), Golden, CO (United States). https://doi.org/10.2172/928611

Wong, N. H., Kwang Tan, A. Y., Chen, Y., Sekar, K., Tan, P. Y., Chan, D., Chiang, K., & Wong, N. C. (2010). Thermal evaluation of vertical greenery systems for building walls. *Building and Environment*, *45*(3), 663–672. https://doi.org/10.1016/j.buildenv.2009.08.005

WRMC. (2022). *Wrmc-bsrn* [Accessed: 2025-05-03]. https://bsrn.awi.de/

Xu, G., Li, J., Shi, Y., Feng, X., & Zhang, Y. (2022). Improvements, extensions, and validation of the urban weather generator (uwg) for performance-oriented neighborhood planning. *Urban Climate*, *45*, 101247. https://doi.org/10.1016/j.uclim.2022.101247

Yang, J., Hu, X., Feng, H., & Marvin, S. (2021). Verifying an envi-met simulation of the thermal environment of yanzhong square park in shanghai. *Urban Forestry Urban Greening*, *66*, 127384. https://doi.org/10.1016/j.ufug.2021.127384

Yang, S., Wang, L. L., Stathopoulos, T., & Marey, A. M. (2023). Urban microclimate and its impact on built environment – a review. *Building and Environment*, *238*, 110334. https://doi.org/10.1016/j.buildenv.2023.110334

Yang, X., Zhao, L., Bruse, M., & Meng, Q. (2012). An integrated simulation method for building energy performance assessment in urban environments. *Energy and Buildings*, *54*, 243–251. https://doi.org/10.1016/j.enbuild.2012.07.042

Yang, Z., & Becerik-Gerber, B. (2014). Coupling occupancy information with hvac energy simulation: A systematic review of simulation programs. *Proceedings of the winter simulation conference 2014*, 3212–3223. https://doi.org/10.1109/WSC.2014.7020157

Zhang, R., Mirzaei, P. A., & Jones, B. (2018). Development of a dynamic external cfd and bes coupling framework for application of urban neighbourhoods energy modelling. *Building and Environment*, *146*, 37–49. https://doi.org/10.1016/j.buildenv.2018.09.006

Appendices

A

Physiological Equivalent Temperature

In this study, both outdoor air temperature and Physiological Equivalent Temperature (PET) are evaluated. PET is a widely used thermal comfort index that expresses the perceived temperature of the human body as an equivalent air temperature in a standardised indoor environment (Höppe, 1999b). The reference indoor conditions are defined as a wind speed of 0.1 m s^{-1} and a water vapour pressure of 12 hPa.

Unlike air temperature alone, PET integrates the combined effects of air temperature, wind speed, humidity, and radiation, thereby providing a more comprehensive measure of thermal comfort. By translating complex outdoor conditions into an equivalent indoor temperature scale, PET allows for an intuitive interpretation of heat stress and is therefore useful in urban climate studies.

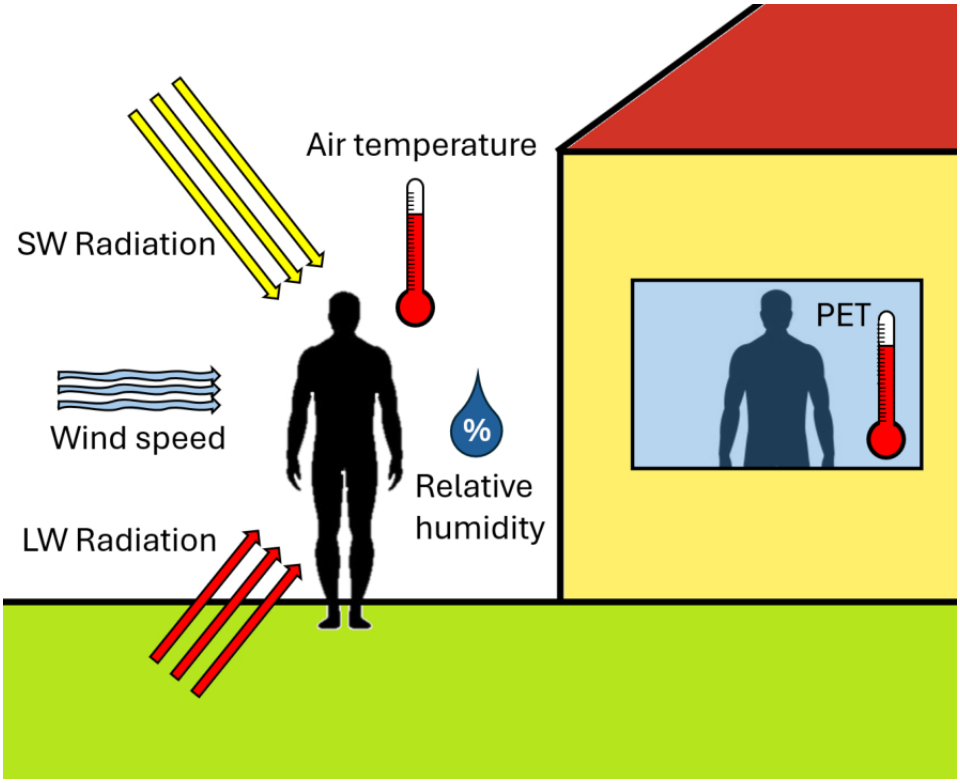

Figure A.1: Conceptual representation of PET: two individuals experience the same level of heat stress, one under multiple meteorological influences outdoors and the other in a standardised indoor setting (van der Werf et al., 2024).

B

Inputs ENVI-met

B.1. Radiation input

Radiation input for ENVI-met was derived from BSRN irradiance data at a 1-minute interval at Cabauw (Knap, 2019). These data are part of the Baseline Surface Radiation Network (BSRN), a global initiative for high-quality radiation observations (KNMI, n.d.-a).

BSRN is a project of the Data and Analysis Panel of the Global Energy and Water Exchange (GEWEX) and aims to detect important changes in the Earth's surface radiation budget that may be related to climate change (WRMC, 2022). Data for August were extracted, converted from UTC to UTC+1 (CET), and resampled to 10-minute intervals to match the temporal resolution of the meteorological input dataset. Measurements were taken at a height of 2 m. The direct, diffuse, and longwave radiation inputs are visualised in Figure B.1.

Direct radiation

Direct radiation (DIR) [W m^{-2}] is measured using a Pyrheliometer (CH1) by Kipp & Zonen, operated by KNMI (Kipp & Zonen B.V., 2001b; Knap, 2019). The measurement accuracy of this instrument is influenced by several factors. The zero offset, which accounts for systematic errors caused by ambient temperature changes, is less than ±3 W m^{-2} for a 5 K h^{-1} temperature variation. Sensor non-stability is below 1% per year, ensuring long-term reliability. Non-linearity remains within ±0.2% for irradiance levels up to 1000 W m^{-2}, minimising deviations at high radiation levels. As direct radiation is not measured on a horizontal plane, ENVI-met internally converts it using the solar elevation angle.

Diffuse radiation

Diffuse radiation (DIF) [W m^{-2}] is measured using a Pyranometer (CMP22) by Kipp Zonen, also operated by KNMI (Kipp & Zonen B.V., n.d. Knap, 2019). The accuracy of these measurements is influenced by several instrumental and environmental factors. The zero offset is less than ±3 W m^{-2} (Offset A) and less than ±1 W m^{-2} (Offset B). The directional response introduces a maximum deviation of ±5 W m^{-2} for solar radiation at incident angles up to 80°. The temperature response of the sensor remains within ±0.5% over a temperature range from -20°C to +50°C.

Long-wave downward radiation

Long-wave downward radiation [W m^{-2}] is measured using a Pyrgeometer (CG4) by Kipp & Zonen, operated by KNMI (Kipp & Zonen B.V., 2001a; Knap, 2019). The estimated uncertainty of this instrument is below 7.5 W m^{-2}.

B.2. Meteorological input

Meteorological input for temperature, relative humidity, wind speed, wind direction, and precipitation is derived from the CESAR Meteo Surface dataset (lc1) (KNMI, 2019). This dataset contains validated and gap-filled observations of standard atmospheric variables at 10-minute intervals for the Cabauw site (KNMI, 2019). Compared to the non-gap-filled dataset (lb1), differences are minor: <1.2% for relative humidity and <0.01 mm for precipitation, while other parameters remain unchanged. Data from August 2019 were extracted, with the period from 23 to 27 August selected for simulation. Each 10-minute value represents the mean over that interval.

Wind speed and direction

Wind direction is measured using a KNMI wind vane containing an 8-bit coded disk, providing a resolution of 1.5°. The WMO accuracy requirement is 3°, though in practice the accuracy is substantially better (Bosveld, 2020).

Wind speed is measured with a KNMI cup anemometer. The WMO accuracy requirement of 0.5 m s^{-1} is satisfied; however, the effective accuracy is the greater of either 1% or 0.1 m s^{-1}. The threshold velocity is below 0.5 m s^{-1}. Instruments that do not meet these criteria are rejected (Bosveld, 2020). Wind speed and direction for 23–28 August are visualised in Figure B.2.

To stabilise the ENVI-met model and ensure comparability between scenarios, both wind speed and direction were standardised in ENVI-met to ensure stable and comparable simulations. A constant wind speed of 1.5 m s^{-1} at 10 m height and a constant wind direction of 85° were applied. The applied wind speed was reduced relative to Cabauw observations to better represent typical urban wind conditions.

Temperature and humidity

Temperature and humidity are measured using an EPLUSE EE33 dew point sensor (E+E Elektronik Ges.m.b.H., 2023). Both parameters are recorded at 2 m height. The accuracy and resolution for temperature are 0.1 °C, while for relative humidity, the accuracy is 1.5% RH with a resolution of 0.1% RH (Bosveld, 2020). The temperature and relative humidity inputs used in ENVI-met are shown in Figure B.3 and Figure B.4, respectively.

Precipitation

Precipitation is set to 0 mm h^{-1} for the entire heatwave period, consistent with the Cabauw dataset.

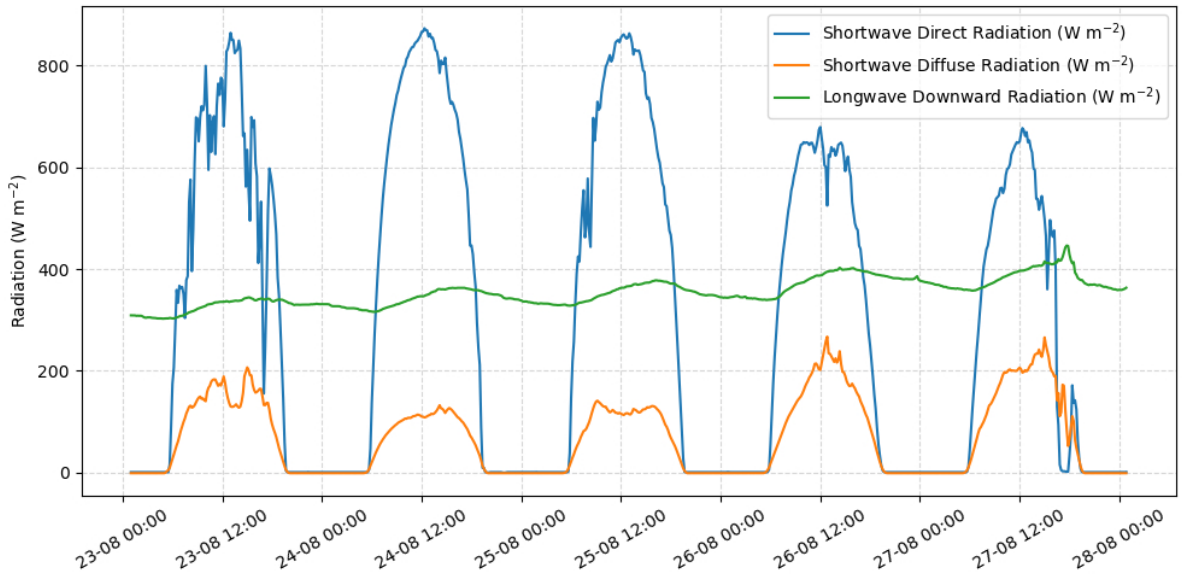

Figure B.1: Radiation data from 23-28 August 2019 from Cabauw (Knap, 2019)

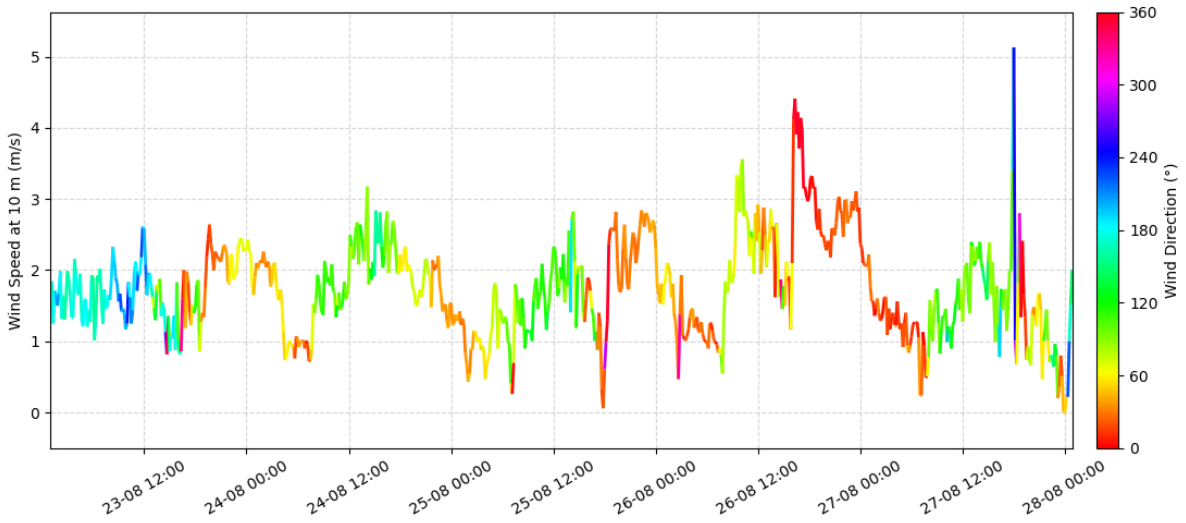

Figure B.2: Wind speed and direction from 23-28 August 2019 from Cabauw (KNMI, 2019). These data is overruled in ENVI-met with wind speed 1.5 m s^{-1} and wind direction 85°

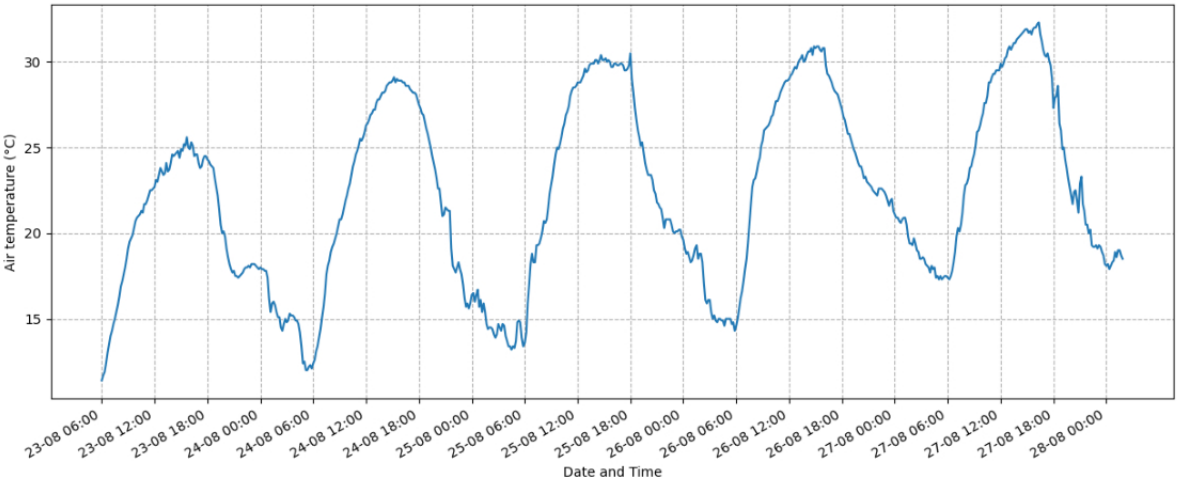

Figure B.3: Temperature data from 23-28 August 2019 from Cabauw (KNMI, 2019)

B.3. Other simulation input

Time step

The standard ENVI-met time step is used: 2 seconds for solar angles below 40°, 2 seconds for 40–50°, and 1 second for angles above 50°.

Duration of simulation

The simulation runs from 23 August 06:00 until 28 August 00:00 (UTC +1).

Roughness length

The roughness length defines the aerodynamic surface roughness at the location where wind speed is measured at 10 m height. At the Cabauw measurement tower, this value is defined as 0.01 m (Oke et al., 2017; Van Ulden & Wieringa, 1996; Verkaik & Holtslag, 2007).

Soil parameters

The soil type defined in ENVI-met is *Default Sandy Loam*, characterised by the following physical properties:

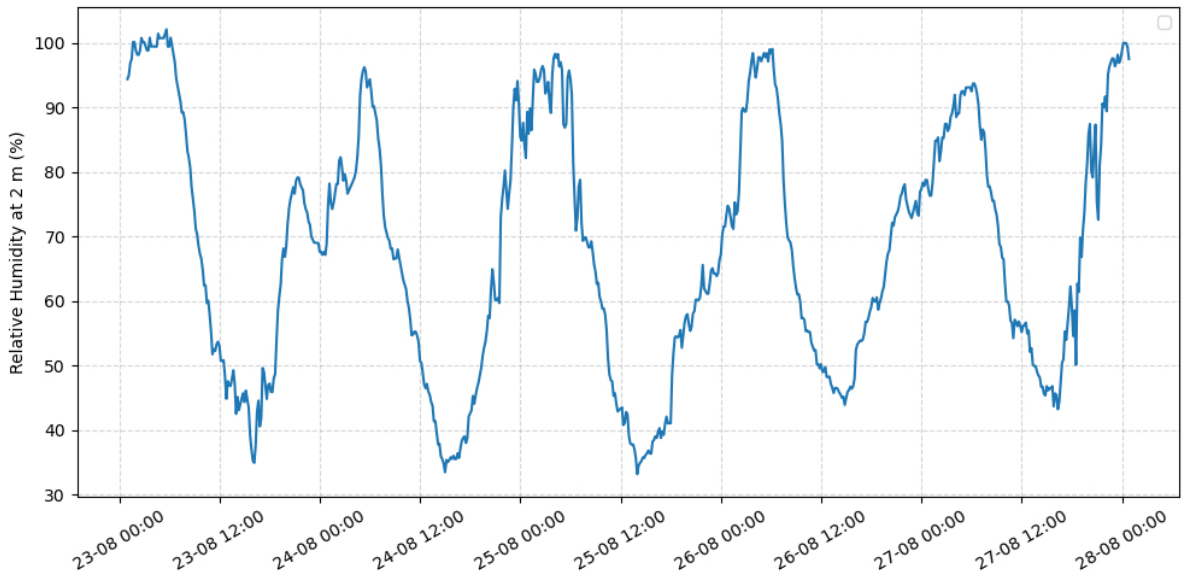

Figure B.4: Relative humidity data from 23-28 August 2019 from Cabauw (KNMI, 2019)

- Roughness length (z_0): 0.015 m
- Albedo: 0.2
- Emissivity: 0.9
- Water mixing coefficient: 0.001 m^2 s^{-1}
- Water turbidity/extinction: 2.1 m^{-1}

B.4. Building input

B.4.1. Low-rise building

The building used in ENVI-met for the low-rise building typology is described below. It consists of three adjoining houses, each 6.1 m wide. A visual representation is provided in Appendix I. The building comprises three main components: glass, walls, and roof.

The glazing material selected from the standard ENVI-met database is *clear float glass*. The wall structure consists of an outer leaf, an air cavity, and an inner leaf. The wall configuration used in ENVI-met is illustrated in Figure B.6a. The roof structure is composed of roof tiles, an air cavity, and a timber framework. Roof battens, purlins, laths, and trusses are excluded, as their contribution to overall thermal resistance is assumed negligible. Although the actual roof has a slope of 24.8°, ENVI-met only allows block-shaped geometry. Therefore, the lower roof cells are defined at 6 m height and the upper roof cells at 8 m, as shown in Figure B.5. The ENVI-met roof representation is shown in Figure B.6b. The specifications of all building materials are summarised in Table B.1.

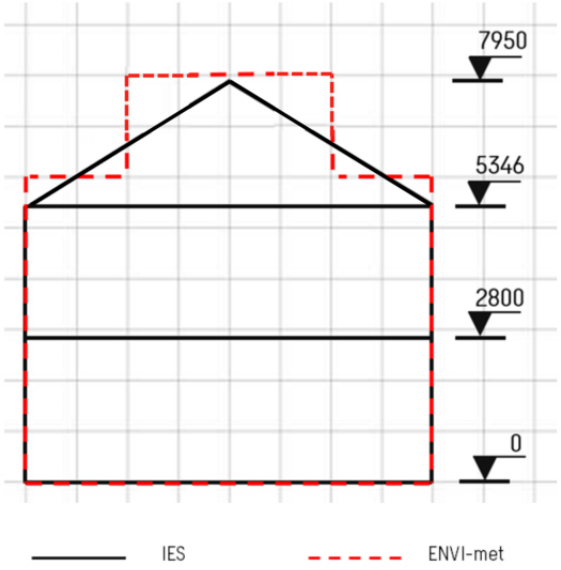

Figure B.5: Comparison of geometry between low-rise building and ENVI-met

Table B.1: ENVI-met input parameters for: External wall for low-, mid- and high-rise, Roof for low-rise (LR), Roof for mid- and high-rise (MHR), and glass for low, mid- and high-rise material inputs.

Property	Wall: Outer leaf	Wall: Inner leaf	Roof LR: Tiles	Roof LR: Timber roof	Roof MHR: Bitu-men	Roof MHR: Insula-tion	Roof MHR: Con-crete	Glass: Clear float glass
Thickness [m]	0.100	0.100	0.040	0.120	0.100	0.040	0.010	0.020
Absorption	0.70[a]	0.70[a]	0.80[a]	0.80[a]	0.85[a]	0.60[b]	0.70[b]	0.05[c]
Transmission	0.00[a]	0.00[a]	0.00[a]	0.00[a]	0.00[a]	0.00[a]	0.00[a]	0.90[c]
Reflection	0.30[a]	0.30[a]	0.20[a]	0.20[a]	0.15[a]	0.40[b]	0.30[b]	0.05[c]
Emissivity	0.90[a]	0.90[a]	0.90[a]	0.90[a]	0.92[a]	0.90[b]	0.94[b]	0.90[c]
Specific Heat [J kg^{-1} K^{-1}]	800[b]	800[b]	837[b]	1200[b]	1200[b]	14000[b]	850[b]	750[c]
Thermal Conductivity [W m^{-1} K^{-1}]	0.84[b]	0.62[b]	1.10[b]	0.12[b]	0.18[b]	0.024[b]	1.60[b]	1.05[c]
Density [kg m^{-3}]	1700[b]	1700[b]	2100[b]	540[b]	1200[b]	32[b]	2220[b]	2500[c]

[a] Data from Oke et al. (2017) (Oke et al., 2017)
[b] Data from IES Ltd. (2021) (IES-VE, 2021c)
[c] Data from ENVI-met (2025) (ENVI-met, 2025)

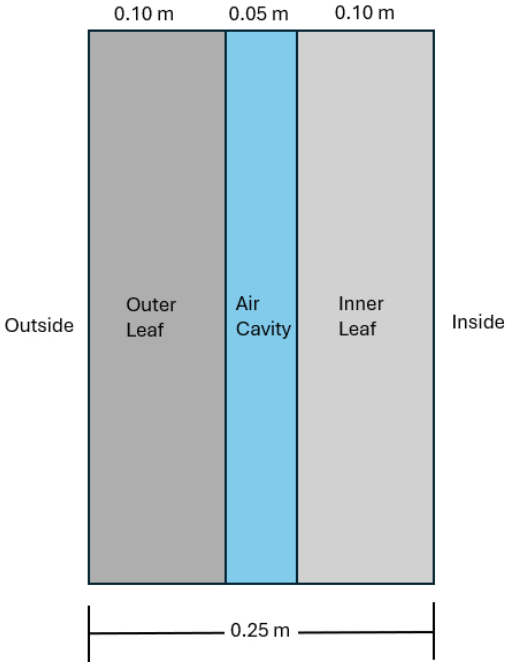

(a) ENVI-met representation of the wall for low-, mid-, and high-rise.

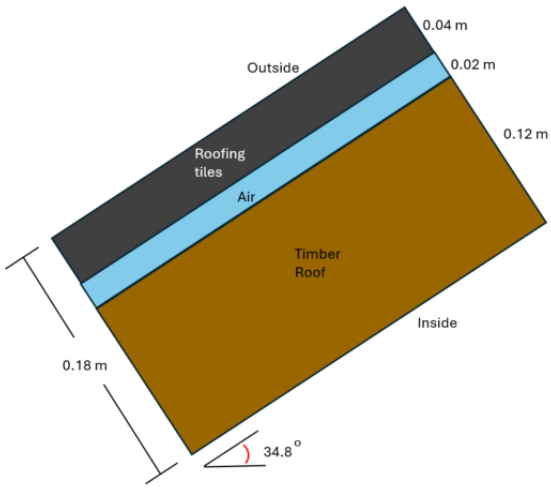

(b) Representation of the low-rise roof; roof slope represented in ENVI-met in block form.

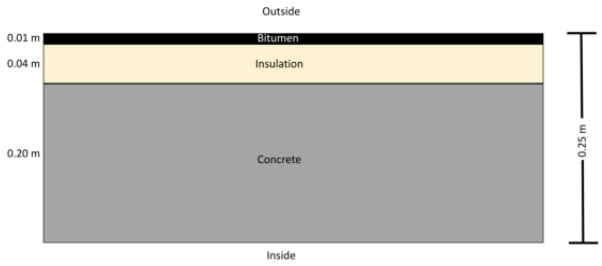

(c) ENVI-met representation of the roof for mid- and high-rise.

Figure B.6: ENVI-met representations of (a) wall for all typologies, (b) low-rise roof, and (c) mid- and high-rise roof.

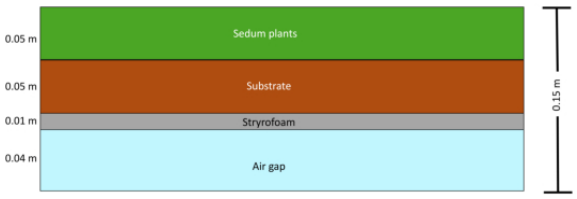

(a) Representation of extensive green roof in ENVI-met.

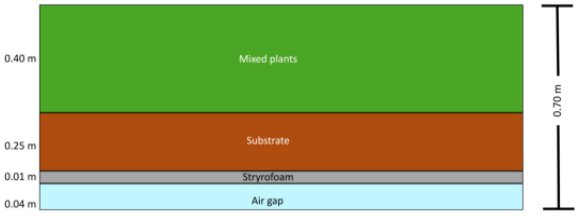

(b) Representation of intensive green roof in ENVI-met.

Figure B.7: Representation of (a) extensive and (b) intensive green roof, scale is not exactly similar. The drainage layer cannot be modelled exactly similar to an actual green roof. Therefore a styrofoam layer is modelled for plastic and air gap for air. In ENVI-met this has no effect on the results.

Glazing percentage calculation

To realistically model the glazing ratios of the Green Village houses in ENVI-met, the blueprint values for both the north and south façades were translated into equivalent surface areas in the simulation model. Due to ENVI-met's resolution grid (1 m, 2 m, or 3 m), only certain discrete configurations are possible. The aim is to reproduce the glass-to-wall ratio from the blueprint as closely as possible.

North-facing façade

- From the blueprint:
  - Glass surface per house: $8.77\,\text{m}^2$
    - Ground floor $4.66\,\text{m}^2$
    - First floor $4.11\,\text{m}^2$
  - For three houses: $3 \times 8.77 = 26.31\,\text{m}^2$
  - Total façade surface (3 houses): $98.05\,\text{m}^2$
  - Glazing ratio: $\frac{26.31}{98.05} = 26.8\%$
- In ENVI-met:
  - ENVI-met façade surface: $108\,\text{m}^2$
  - Required glass area for same ratio: $0.268 \times 108 = 28.94\,\text{m}^2$
  - Closest practical glass area achievable: $28.8\,\text{m}^2$
  - Realisation: $12 + 12 + 2.4 \times 2 = 28.8\,\text{m}^2$
- Resolution scenarios for grid sensitivity check:
  - 1 m, 2 m and 3 m resolution: $12\,\text{m} + 12\,\text{m} + 2.4\,\text{m} \times 2 = 28.8\,\text{m}^2$ (All resolutions can be used for 28.8 m^2)

South-facing façade

- From the blueprint:
  - Glass surface per house: $9.64\,\text{m}^2$
    - Ground floor $5.56\,\text{m}^2$
    - First floor $4.08\,\text{m}^2$
  - For three houses: $3 \times 9.64 = 28.92\,\text{m}^2$
  - Total façade surface (3 houses): $98.05\,\text{m}^2$
  - Glazing ratio: $\dfrac{28.92}{98.05} = 29.5\%$
- In ENVI-met:
  - ENVI-met façade surface: $108\,\text{m}^2$
  - Required glass area for same ratio: $0.295 \times 108 = 31.9\,\text{m}^2$
  - Closest practical glass area achievable: $31.2\,\text{m}^2$
  - Realisation: $12 + 12 + 2.4 \times 3 = 31.2\,\text{m}^2$
- Resolution scenarios for grid sensitivity check:
  - 1 m, 2 m and 3 m resolution: $12\,\text{m} + 12\,\text{m} + 2.4\,\text{m} \times 3 = 31.2\,\text{m}^2$ (All resolutions can be used for 28.8 m^2)

B.4.2. Mid-rise building

The mid-rise typology consists of a standardised five-storey building. Every storey is 3 m high, making it 15 m in height. The building consists of three units in total, with dimensions of 18 m (x) and 8 m (y). Meteorological boundary conditions are identical to those used for the low-rise model. A glazing percentage of 33.3% is used for the south and north façades. The glazing material is *clear float glass* from the standard ENVI-met database, as in the low-rise case. The wall construction is identical to that of the low-rise building. The roof structure is different from low-rise. The roof consists of a 20 cm concrete slab, topped with a 4 cm insulation layer and a 1 cm bitumen layer, visualised in Figure B.6c. All material input parameters are summarised in Table B.1.

B.4.3. High-rise building

High-rise building typology consist of a standardised building with 8 storeys. Every storey is 3 m high, making it 24 m in height. The building consists of three units in total, with dimensions of 18 m (x) and 8 m (y). Meteorological boundary conditions are identical to those used for the low-rise model. A glazing percentage of 33.3% is used for the south and north façades. "The glazing material is *clear float glass* from the standard ENVI-met database, as in the low- and mid-rise. The wall construction is identical to that of the low- and mid-rise building. The roof structure is similar as in mid-rise. The roof consists of a 20 cm concrete slab, topped with a 4 cm insulation layer and a 1 cm bitumen layer, visualised in Figure B.6c. All material input parameters are summarised in Table B.1.

B.5. Green intervention input

This section presents the ENVI-met input parameters for each green intervention. An overview of all inputs is stated in Table B.3.

Extensive green roof low-rise

The extensive sedum green roof was modelled in ENVI-met using the parameters listed in Table B.3. A representation is visualised in Figure B.7a. For the low-rise case, 67% of the roof surface was modelled as green roof. As often only 70% of a roof can be used for green, based on a study in Den Haag. As often there is space needed for air-conditioning or other installations and green is not used close to the edge of the roof (Personal communication Sweco).

Because ENVI-met represents green roofs as block geometries, exact blueprint dimensions cannot be replicated. Therefore the roof area in ENVI-met is 216 m^2 which is higher than the roof area of the blueprint m^2.

Green roof area adjustment:

- Roof length 18.5 m
- Roof width = $\sqrt{height \times height + length \times length} = \sqrt{2.606 \times 2.606 + 3.75 \times 3.75} = 4.57$ m
- Reference roof size: $18.5 \times 4.57 \times 2 = 169.09\,m^2$
- Target green roof coverage (70%): $0.7 \times 169.09 = 118.4\,m^2$
- ENVI-met roof area: $8 \times 18 + 2 \times 2 \times 18 = 144 + 72 = 216\,m^2$
- Required green roof area in ENVI-met: $151.2\,m^2$ to match 70 procent green roof
- Realised green area: $36 \times 4 = 144\,m^2$
- Resulting green roof percentage in ENVI-met: $\frac{144}{216} = 66.7\%$

Extensive and intensive green roof mid-rise

The differences between extensive and intensive green roofs were evaluated through separate ENVI-met simulations (MID-GR-EXT & MID-GR-INT). A 100% coverage is used in the mid-rise simulations for both roof types, with the extensive roof parameters identical to those in the low-rise case. A full (100%) roof coverage was applied in the mid-rise scenario, using identical parameters as the low-rise case. At 70% coverage, uncovered grid cells would alter local spatial effects, reducing comparability between the extensive and intensive cases. All parameters are stated in Table B.3. A representation is visualised in Figure B.7a and Figure B.7b.

Green wall

Standard *0200IV Ivy (Hedera helix)* in ENVI-met used, glazing was excluded from the greening surface. The north facing wall includes 28.8 m^2 of glazing and 79.2 m^2 of green wall coverage. The south facing wall includes 31.2 m^2 of glazing and 76.8 m^2 of green wall coverage.

Hedera Helix with thickness 0.2 m is used, LAI is 3 m^2 m^{-2} and Leaf Angle Distribution is 0.3. All inputs are visualised in Table B.3.

Low vegetation
A simple plant *0200XX Grass 25 cm aver. dense* is used for low vegetation. Inputs in ENVI-met are visualised in Table B.3.

Medium vegetation
A simple plant *0200H1 Hedge dense 1m* is used for medium vegetation.

Inputs in ENVI-met are visualised in Table B.3.

High vegetation
Two types of field maple trees are used with height 5.59 m and 11.08 m. First, *Field Maple (young)* is used with a scaling factor of 0.4, representing a small garden tree. Exact dimensions:

- 010020 Field Maple Young
- height 5.59 m
- width 2.99 x 3.55 m

Second a *Field maple middle* is used in ENVI-met with a scaling factor of 0.75, so it becomes a larger tree which is possible in gardens. Exact dimensions:

- 010020 Field Maple Middle
- medium age scaled with 0.75 in envi-met
- 11.08 height
- 6.30 x 6.90 m width

Both trees have full foliage in August. Other inputs use ENVI-met defaults and are listed in Table B.2.

Table B.2: ENVI-met input parameters for foliage properties of field maple (ENVI-met, 2025)

Parameter	Value
Foliage Shortwave Albedo	0.18
Foliage Shortwave Transmittance	0.30
Emissivity of Leaves	0.96
Leaf Weight [g m^{-2}]	100.00
Isoprene Capacity	12.00

Table B.3: Overview ENVI-met input parameters for low (grass, 0.25 m), medium (hedge, 1 m), extensive green roof (sedum, 0.05 m), intensive green roof (Mixed plants, 0.40 m), and green wall (Hedera Helix 0.20 m) (ENVI-met, 2025; Gomes et al., 2019; Groenblauwe Netwerken, n.d. Nationale Dakenplan, 2021; Ottelé et al., 2011; Perez et al., 1987; Perini et al., 2011; Sedumspecialist, n.d.)

Parameter	**Low vegetation (grass, 0.25 m)**	**Medium vegetation (hedge, 1 m)**	**Extensive green roof (0.15 m)**	**Intensive green roof (0.70 m)**	**Green wall (0.40 m)**
Greening	Grass 25 cm aver. dense	Hedge dense, 1 m	Sedum (5 cm)	Plants (40 cm)	Ivy (Hedera Helix)
Leaf Type	Grass	Deciduous	Deciduous	Deciduous	Deciduous
Albedo [-]	0.20	0.20	0.25	0.25	0.20
Emissivity [-]	0.97	0.97	0.96	0.96	0.97
Transmittance [-]	0.30	0.30	0.05	0.05	0.30
Plant Height [m]	0.25	1.00	0.05	0.40	0.25
Root Zone Depth [m]	0.20	1.00	0.05	0.25	0.50
Leaf Area Index (LAI) [m^2/m^2]	-	-	1.0	3.0	3.0
Leaf Angle Distribution [-]	0.30	0.30	0.30	0.30	0.30
Leaf Area Density Profile	0.30, 0.30, ..., 0.30	1.00, 1.00, ..., 1.00	0.15, 0.15, ..., 0.15	0.15, 0.15, ..., 0.15	0.15, 0.15, ..., 0.15
Root Area Density Profile	0.10, 0.10, ..., 0.00	0.10, 0.10, ..., 0.00	0.00, 0.10, ..., 0.00	0.10, 0.10, ..., 0.00	0.10, 0.10, ..., 0.00
Season Profile	1.00, 1.00, ..., 1.00	1.00, 1.00, ..., 1.00	1.00, 1.00, ..., 1.00	1.00, 1.00, ..., 1.00	1.00, 1.00, ..., 1.00
Substrate Type	—	—	Sandy Loam (substrate 5 cm) + Styrofoam (1 cm) + Air gap(4 cm)	Sandy Loam (substrate 25 cm) + Styrofoam (1 cm) + Air gap (4 cm)	—
Substrate Thickness [m]	—	—	0.10	0.30	—
Substrate Albedo [-]	—	—	0.30	0.30	—
Substrate Emissivity [-]	—	—	0.96	0.96	—
Water Coefficient of Substrate [-]	—	—	0.50	0.50	—

C

Inputs IES-VE

C.1. Radiation and meteorological input

IES-VE requires a complete EPW file containing all environmental inputs to calculate indoor climate and energy use. The EPW climate file used originates from Cabauw, NLD_UT_Cabauw.Tower.063480_TMYx.2009-2023 (Climate.OneBuilding, n.d.-a).

The EPW climate data files used for IES-VE simulations are based on the Typical Meteorological Year (TMY). The TMY consists of hourly averaged meteorological variables derived from a long-term climate data record (Wilcox & Marion, 2008). TMYx files are derived from hourly weather data through 2023 in the ISD (US NOAA's Integrated Surface Database) using the TMY/ISO 15927-4:2005 methodologies (Climate.OneBuilding, n.d.-b). For each month of the TMY, data from the month that best represent the long-term climatic conditions are selected. For example, this TMY dataset uses the climate data from Jan=2015; Feb=2016; Mar=2020; Apr=2022; May=2009; Jun=2020; Jul=2015; Aug=2013; Sep=2009; Oct=2013; Nov=2023; Dec=2018. Since the TMY uses data from 2013 for August, all August parameters were replaced with 2019 data for this study. Because the TMY data do not reflect the actual conditions during the simulated period, the EPW file was modified accordingly. An example of the difference in dry-bulb temperature is shown in Figure C.1.

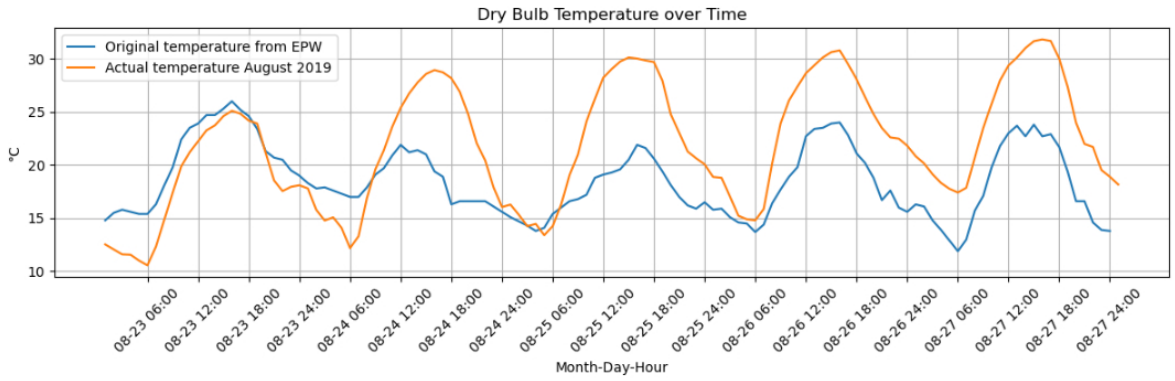

Figure C.1: Original dry-bulb temperature in EPW from Cabauw versus actual temperature on 23–28 August

The EPW inputs were updated hourly using KNMI data for August 2019 or outputs from ENVI-met. KNMI climate data from 2019 were used to replace the month of August in the EPW file. Figure C.1 shows the temperature differences for 23–28 August used in this study. Table C.17 states the source for each parameter in the updated EPW file. In Figure C.2, a flow diagram illustrates which parameters are used in which model.

Extraterrestrial radiation is calculated from the solar constant and is assumed to be the same each year. Dry-bulb temperature, wind speed, and relative humidity were extracted from the cells around the building and used as inputs for IES-VE. Dew-point temperature was calculated using the following steps in the Python code:

Given:

$E_0 = 0.611\,\text{kPa}$ (Reference vapour pressure at $T_0 = 273\,\text{K}$)

$\frac{L}{R_v} = 5423\,\text{K}$ (Latent heat of vaporisation over gas constant for water vapour)

$T_0 = 273.15\,\text{K}$ (Reference temperature)

$T_a = T_{\text{dry, ENVI-met}} + 273.15$ (Air temperature in [K] from ENVI-met)

$RH = RH_{\text{ENVI-met}}$ (Relative humidity in % from ENVI-met)

Step 1: Calculate saturation vapour pressure E_s :

$$E_s = E_0 \cdot \exp\left(\frac{L}{R_v}\left(\frac{1}{T_0} - \frac{1}{T_a}\right)\right) \tag{C.1}$$

Step 2: Calculate actual vapour pressure E :

$$E = \frac{RH}{100} \cdot E_s \tag{C.2}$$

Step 3: Calculate dew-point temperature T_d :

$$T_d = \left(\frac{1}{\frac{1}{T_0} - \frac{1}{L/R_v} \cdot \ln\left(\frac{E}{E_0}\right)}\right) \tag{C.3}$$

Step 4: Convert to degrees Celsius:

$$T_d[°\text{C}] = T_d[\text{K}] - 273.15 \tag{C.4}$$

Other meteorological data were gathered from the Cabauw CESAR Meteo Surface dataset LC1 (KNMI, 2019). This dataset consists of validated and gap-filled observations of common atmospheric variables at a 10-minute interval at Cabauw (KNMI, 2019). Radiation data were obtained from BSRN irradiance measurements at a 1-minute interval at Cabauw (Knap, 2019). These data are part of the Baseline Surface Radiation Network (BSRN), a global initiative for high-quality radiation observations (KNMI, n.d.-a). These data were aggregated to hourly radiation output in the EPW file.

The EPW file provides an overview of various parameters, some of which are not used by IES-VE. These were set to zero or NaN. Illuminance values were estimated from radiation by multiplying by a factor of 120 for global horizontal illuminance, a factor of 110 for direct normal illuminance, and a factor of 110 for diffuse horizontal illuminance (Arveson, 2017; Michael et al., 2020; Perez et al., 1987).

Wind direction was fixed at 85°, consistent with the ENVI-met configuration. Visibility and ceiling height were set to 10 km and 1500 m, respectively. Aerosol optical depth was set to 0.15, and the ground albedo was set to 0.2, identical to ENVI-met. All other inputs were set to 0, NaN, or missing values, as they do not influence the IES-VE model.

C.2. Building parameters

The outside resistance of each wall and window was calculated from the convective and radiative heat-transfer coefficients. These coefficients were derived from wind speed and from air and surface temperatures provided by ENVI-met. The specific coupling approach is stated in section 4.2.

Wall absorption, emissivity, conductivity, density, and thickness are identical to those in ENVI-met. These values can be found in Table B.1. As indoor walls and floors are not modelled in ENVI-met, they were modelled using the buildings' blueprints. All inputs for walls, roofs, windows, and floors are provided in subsection C.2.4.

C.2.1. Ventilation and infiltration

Ventilation and infiltration were kept constant per room. An average window opening was assumed for every room. Ventilation and infiltration were identical across all rooms and building typologies. Ventilation was calculated using the following equation (Larsen, 2006):

$$Q_{window} = 0.1 \cdot A_{\text{eff}} \cdot v_s \tag{C.5}$$

where Q_{window} is the ventilation for a window in [m^3/s], A_{eff} is the effective open window area in [m^2], and v_s is the average wind speed in [m s^{-1}] at 1 m from the wall. The average wind speed over all walls and the roof was used. In this case:

$A_{\text{eff}} = h_{opening} * w_{opening} = 1.3 * 0.3 = 0.39$ m^2 (window opening area, 30 cm opened)
$v_s = 0.51$ m s^{-1}

This results in 0.020 m^3 s^{-1} per room, equivalent to 20 l s^{-1}. No distinction was made between upstairs and downstairs rooms. Total ventilation for the house is 160 l s^{-1}. The attic contains no windows; therefore, no natural ventilation was modelled.

The infiltration rate was assumed to be 0.4 air changes per hour (ACH), consistent with values from the literature (Henderson & Harley, 2022; Sailor, 2011).

C.2.2. Internal gains

A household of four persons (two adults and two children) was assumed. Standard IES-VE metabolic rates were applied per person. Four persons per house correspond to an average of 0.5 person per room. In reality, occupancy would differ by room, but accounting for this would introduce an additional variable and complicate the analysis. Each person emits 90 W sensible and 60 W latent heat (IES-VE, 2025).

Internal heat gains from household equipment were also assumed to be uniform across all rooms. Average internal equipment gains were estimated at 2.5 W m^{-2} (Mata & Sasic Kalagasidis, 2009).

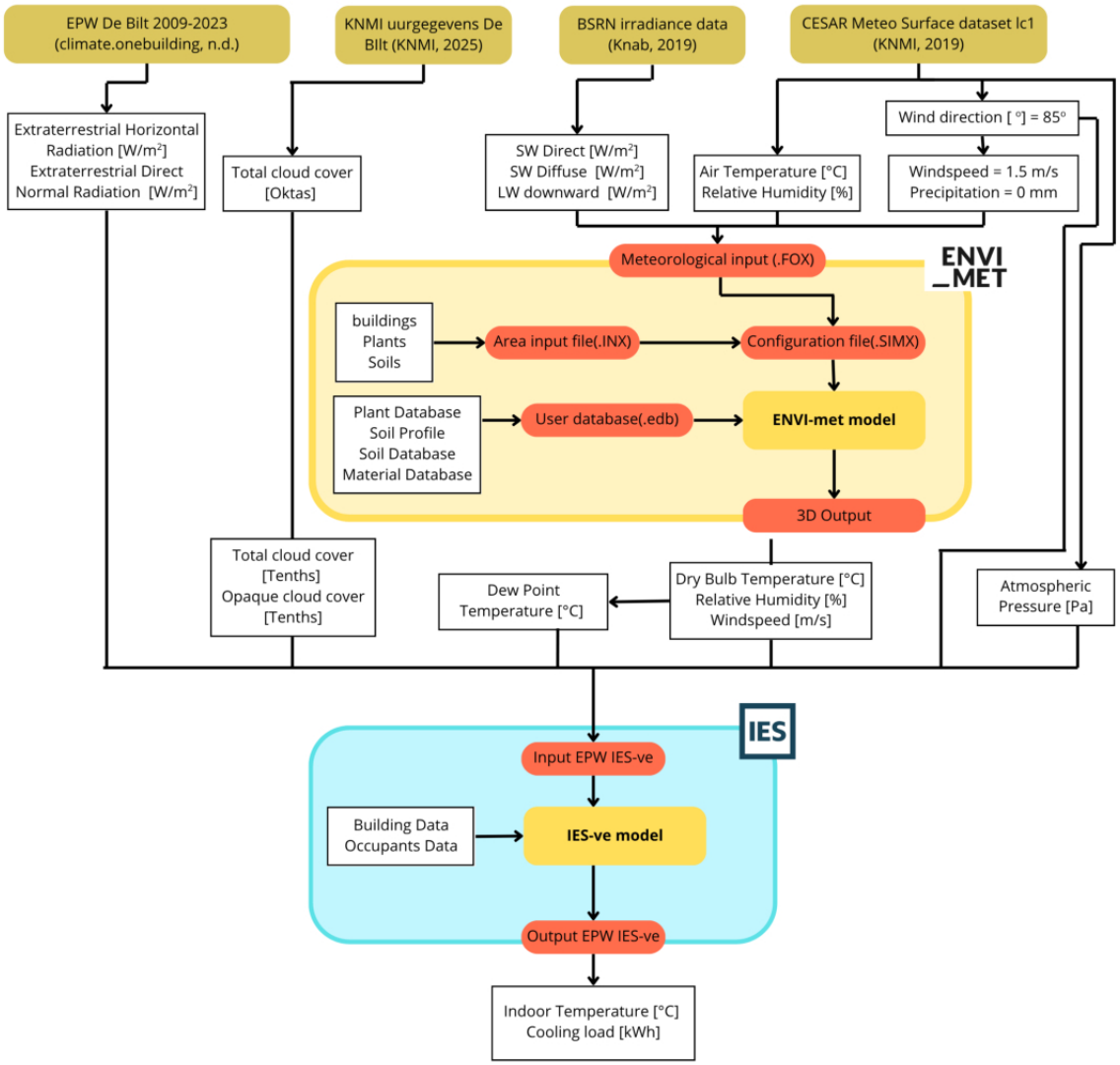

Figure C.2: Flow diagram of meteorological parameters

C.2.3. Glazing percentage calculation

To represent the glazing ratios in IES-VE consistently with the architectural blueprints, the window and door areas were recalculated and adjusted to match the effective glass surface as closely as possible. The height from the blueprints was always used, while the width was sometimes modified to make the geometry implementable in IES-VE. As IES-VE assigns a percentage of each window and door area to the frame, this additional calculation was necessary. The frame accounts for all wooden elements in and around the door and window structures.

North-facing façade

- From the blueprint:
  - Glass surface per house: 8.77 m^2
    - Ground floor 4.66 m^2
    - First floor 4.11 m^2
- Ground floor:
  - Blueprint total: 4.66 m^2
  - 2 Doors: 50% glass 50% frame (softwood) from blueprint
  - Both Doors: 2.2 m height, 1 m width
    - $2 \times 1 \times 2.2 = 4.4\,m^2$ (50% glass = 2.2 m^2)
  - 2 Windows: 60% glass 40% frame (softwood)
  - Both Windows: 2.2 m height, 0.9 m width
    - $2 \times 2.2 \times 0.9 = 3.96\,m^2$ (60% glass = 2.38 m^2)
  - Total IES-VE effective glass surface: 4.48 m^2
- First floor:
  - Blueprint total: 4.11 m^2
  - 2 Windows: 85% glass 15% frame (softwood)
  - Both Windows: 1.3 m height, 1.9 m width
    - $2 \times 1.3 \times 1.9 = 4.94\,m^2$ (85% glass = 4.20 m^2)
  - Total IES-VE effective glass surface: 4.20 m^2
- Total IES-VE glass surface 8.68 m^2 (per house)

South-facing façade

- From the blueprint:
  - Glass surface per house: 9.64 m^2
    - Ground floor 5.56 m^2
    - First floor 4.08 m^2
- Ground floor:
  - Blueprint total: 5.56 m^2
  - 2 Doors: 50% glass 50% frame (softwood) from blueprint
  - Both Doors: 2.2 m height, 1 m width
    - $2 \times 1 \times 2.2 = 4.4\,m^2$ (50% glass = 2.2 m^2)
  - 2 Windows: 85% glass 15% frame (softwood)
  - Both Windows: 2.2 m height, 0.9 m width
    - $2 \times 2.2 \times 0.9 = 3.96\,m^2$ (85% glass = 3.37 m^2)
  - Total IES-VE effective glass surface: 5.57 m^2

- First floor:
  - Blueprint total: 4.08 m^2
  - 2 Windows: 85% glass 15% frame (softwood)
  - Both Windows: 1.3 m height, 1.9 m width
    - $2 \times 1.3 \times 1.9 = 4.94\,m^2$ (85% glass = $4.20\,m^2$)
  - Total IES-VE effective glass surface: $4.20\,m^2$
- Total IES-VE glass surface $9.77\,m^2$ (per house)

C.2.4. Parameters per building element

For each building element described in this section, the construction details and parameters are provided. Only unique building elements are included. Below is a list of all building elements, with the building typologies in which they are used indicated in parentheses. All parameters are stated, except for the external resistances, which are shown in Table C.13. The U-values of all building elements are presented in subsection C.2.5. The U-values are not input parameters but the result of the combined external resistance, material thermal resistance, and internal resistance.

Internal Ceiling/Floor

- Internal floors (low & mid-rise) — see Table C.1
- Internal floor (high-rise) — see Table C.2

Ground/Exposed Floor

- Ground/exposed floor (all) — see Table C.3

Internal Partition

- Internal partition wall (all) - see Table C.4
- Internal partition wall between houses (all) - see Table C.5

Roof

- Roof (low-rise, no greening) — see Table C.6
- Green roof, extensive (low-rise) — see Table C.7
- Roof (mid/high-rise, no greening) — see Table C.8
- Green roof, extensive (mid-rise) — see Table C.9
- Green roof, intensive (mid-rise) — see Table C.10

External Wall

- External wall (all façades) — see Table C.11

External Window / Door

- All glazing and doors — see Table C.12

Internal floors (low and mid-rise)

Outside: Emissivity = 0.900, Absorptance = 0.55
Inside: Emissivity = 0.900, Absorptance = 0.55, Resistance = $0.1000\,m^2\,K\,W^{-1}$

Table C.1: Construction layers – internal floor (low- and mid-rise) (IES-VE, 2025)

Material	Thickness (mm)	Conductivity ($W\,m^{-1}\,K^{-1}$)	Density ($kg\,m^{-3}$)	Spec. Heat ($J\,kg^{-1}\,K^{-1}$)	Resistance ($m^2\,K\,W^{-1}$)
Particleboard low density	18	0.102	590	1300	0.1765
Cavity	150	–	–	–	0.2100
Plywood sheeting	12	0.140	530	1800	0.0857
Gypsum plasterboard	10	0.160	950	840	0.0625

Internal floors (high-rise)

Outside: Emissivity = 0.900, Absorptance = 0.55
Inside: Emissivity = 0.900, Absorptance = 0.55, Resistance = 0.1000 $m^2\,K\,W^{-1}$

Table C.2: Construction layers – Internal floor (high-rise) (IES-VE, 2025)

Material	Thickness (mm)	Conductivity ($W\,m^{-1}\,K^{-1}$)	Density ($kg\,m^{-3}$)	Spec. Heat ($J\,kg^{-1}\,K^{-1}$)	Resistance ($m^2\,K\,W^{-1}$)
Concrete deck	30	2.000	2400	1000	0.0150
Cast concrete (medium)	150	1.400	2100	840	0.1071

Ground exposed floor (all)

Outside: Emissivity = 0.900, Absorptance = 0.55
Inside: Emissivity = 0.900, Absorptance = 0.55, Resistance = 0.0700 $m^2\,K\,W^{-1}$

Table C.3: Construction layers – Ground/exposed floor (IES-VE, 2025)

Material	Thickness (mm)	Conductivity ($W\,m^{-1}\,K^{-1}$)	Density ($kg\,m^{-3}$)	Spec. Heat ($J\,kg^{-1}\,K^{-1}$)	Resistance ($m^2\,K\,W^{-1}$)
Reinforced concrete	200	2.300	2300	1000	0.0870
Cavity	600	–	–	–	0.2100
Cast concrete (lightweight)	170	0.380	1200	1000	0.4474
Screed	30	0.410	1200	840	0.0732

Internal partition wall (all)

Outside: Emissivity = 0.90, Absorptance = 0.70
Inside: Emissivity = 0.90, Absorptance = 0.70, Resistance = 0.0700 $m^2\,K\,W^{-1}$

Table C.4: Construction layers – Internal partition wall (standard) (IES-VE, 2025)

Material	Thickness (mm)	Conductivity ($W\,m^{-1}\,K^{-1}$)	Density ($kg\,m^{-3}$)	Spec. Heat ($J\,kg^{-1}\,K^{-1}$)	Resistance ($m^2\,K\,W^{-1}$)
Gypsum plasterboard	100	0.160	950	840	0.6250

Internal partition wall between houses (all)

Outside: Emissivity = 0.90, Absorptance = 0.70
Inside: Emissivity = 0.90, Absorptance = 0.70, Resistance = 0.1300 $m^2\,K\,W^{-1}$

Table C.5: Construction layers – Internal partition wall (between houses) (IES-VE, 2025)

Material	Thickness (mm)	Conductivity ($W\,m^{-1}\,K^{-1}$)	Density ($kg\,m^{-3}$)	Spec. Heat ($J\,kg^{-1}\,K^{-1}$)	Resistance ($m^2\,K\,W^{-1}$)
Gypsum plasterboard	100	0.160	950	840	0.6250
Gypsum plasterboard	100	0.160	950	840	0.6250

Roof without greening (low-rise)

Outside: Emissivity = 0.90, Absorptance = 0.80
Inside: Emissivity = 0.90, Absorptance = 0.70, Resistance = 0.1000 $m^2\,K\,W^{-1}$

Table C.6: Construction layers – Roof (low-rise) (IES-VE, 2025)

Material	Thickness (mm)	Conductivity ($W\,m^{-1}\,K^{-1}$)	Density ($kg\,m^{-3}$)	Spec. Heat ($J\,kg^{-1}\,K^{-1}$)	Resistance ($m^2\,K\,W^{-1}$)
Concrete Tiles	40.0	1.1000	2100	837	0.0364
Cavity	20.0	–	–	–	0.1800
Plywood – Douglas Fir (ASHRAE)	120.0	0.1200	540	1200	1.0000

Green roof, extensive (low-rise)

Outside: Emissivity = 0.96, Absorptance = 0.75
Inside: Emissivity = 0.9, Absorptance = 0.8, Resistance = 0.1000 $m^2\,K\,W^{-1}$

Table C.7: Construction layers – Green roof: extensive (low-rise) (IES-VE, 2025)

Material	Thickness (mm)	Conductivity ($W\,m^{-1}\,K^{-1}$)	Density ($kg\,m^{-3}$)	Spec. Heat ($J\,kg^{-1}\,K^{-1}$)	Resistance ($m^2\,K\,W^{-1}$)
Cultivated clay soil (25% D.W. Moisture) (Ochsner, 2019; Oke et al., 2017)	50.0	0.500	2000	1550	0.100
Polyethylene (NETZSCH, 2025)	10.0	0.320	920	2600	0.0313
Cavity	40.0	–	–	–	0.1800
Concrete Tiles	40.0	1.1000	2100	837	0.0364
Cavity	20.0	–	–	–	0.1800
Plywood – Douglas Fir (ASHRAE)	120.0	0.1200	540	1200	1.0000

Roof without greening (mid and high-rise)

Outside: Emissivity = 0.92, Absorptance = 0.85
Inside: Emissivity = 0.90, Absorptance = 0.80, Resistance = 0.1000 $m^2\,K\,W^{-1}$

Table C.8: Construction layers – Roof without greening (mid- and high-rise) (IES-VE, 2025)

Material	Thickness (mm)	Conductivity ($W\,m^{-1}\,K^{-1}$)	Density ($kg\,m^{-3}$)	Spec. Heat ($J\,kg^{-1}\,K^{-1}$)	Resistance ($m^2\,K\,W^{-1}$)
Felt/bitumen layers	10	0.500	1700	1000	0.0200
Insulation (EPS)	40	0.025	20	1030	1.6000
Cast concrete (medium)	200	1.400	2100	840	0.1429

Green roof; extensive (mid-rise)

Outside: Emissivity = 0.96, Absorptance = 0.75
Inside: Emissivity = 0.90, Absorptance = 0.80, Resistance = 0.1000 $m^2\,K\,W^{-1}$

Table C.9: Construction layers – Green roof; extensive (mid-rise) (IES-VE, 2025)

Material	Thickness (mm)	Conductivity ($W\,m^{-1}\,K^{-1}$)	Density ($kg\,m^{-3}$)	Spec. Heat ($J\,kg^{-1}\,K^{-1}$)	Resistance ($m^2\,K\,W^{-1}$)
Cultivated clay soil 25% d.w. moisture	50	0.500	2000	1550	0.1000
Felt/bitumen layers	10	0.500	1700	1000	0.0200
Insulation (EPS)	40	0.025	20	1030	1.6000
Cast concrete (medium)	200	1.400	2100	840	0.1429

Green roof; intensive (mid-rise)

Outside: Emissivity = 0.96, Absorptance = 0.75
Inside: Emissivity = 0.90, Absorptance = 0.80, Resistance = 0.1000 $m^2\,K\,W^{-1}$

Table C.10: Construction layers – Green roof: intensive (IES-VE, 2025)

Material	Thickness (mm)	Conductivity ($W\,m^{-1}\,K^{-1}$)	Density ($kg\,m^{-3}$)	Spec. Heat ($J\,kg^{-1}\,K^{-1}$)	Resistance ($m^2\,K\,W^{-1}$)
Cultivated clay soil 25% d.w. moisture	250	0.500	2000	1550	0.5000
Felt/bitumen layers	10	0.500	1700	1000	0.0200
Insulation (EPS)	40	0.025	20	1030	1.6000
Cast concrete (medium)	200	1.400	2100	840	0.1429

External wall (south/north/east/west) all

All external walls share the same construction layers; only the outside resistance differs, leading to small U-value variations.
Outside: Emissivity = 0.90, Absorptance = 0.70
Inside: Emissivity = 0.90, Absorptance = 0.70, Resistance = 0.1300 $m^2\,K\,W^{-1}$

Table C.11: Construction layers – external wall (IES-VE, 2025)

Material	Thickness (mm)	Conductivity ($W\,m^{-1}\,K^{-1}$)	Density ($kg\,m^{-3}$)	Spec. Heat ($J\,kg^{-1}\,K^{-1}$)	Resistance ($m^2\,K\,W^{-1}$)
Brickwork (Outer Leaf)	100.0	0.840	1700	800	0.1190
Cavity	25.0	–	–	–	0.1800
Expanded polystyrene (CIBSE)	25.0	0.035	25	1400	0.7143
Brickwork (Inner Leaf)	100.0	0.620	1700	800	0.1613
Plasterboard	12.5	0.210	700	1000	0.0595

Window ground floor South (low-rise)

Inside: Resistance = 0.1300 $m^2\,K\,W^{-1}$
Frame: Frame percentage 15%, absorptance 0.7, resistance 0.42 $m^2\,K\,W^{-1}$ (IES-VE, 2025)

Window ground floor North (low-rise)

Inside: Resistance = 0.1300 $m^2\,K\,W^{-1}$
Frame: Frame percentage 40%, absorptance 0.7, resistance 0.42 $m^2\,K\,W^{-1}$ (IES-VE, 2025)

Window first floor South (low-rise)
Inside: Resistance = 0.1300 $m^2\,K\,W^{-1}$
Frame: Frame percentage 15%, absorptance 0.7, resistance 0.42 $m^2\,K\,W^{-1}$ (IES-VE, 2025)

Window first floor North (low-rise)
Inside: Resistance = 0.1300 $m^2\,K\,W^{-1}$
Frame: Frame percentage 15%, absorptance 0.7, resistance 0.42 $m^2\,K\,W^{-1}$ (IES-VE, 2025)

Door ground floor South (low-rise)
Inside: Resistance = 0.1300 $m^2\,K\,W^{-1}$
Frame: Frame percentage 50%, absorptance 0.7, resistance 0.42 $m^2\,K\,W^{-1}$ (IES-VE, 2025)

Door ground floor North (low-rise)
Inside: Resistance = 0.1300 $m^2\,K\,W^{-1}$
Frame: Frame percentage 50%, absorptance 0.7, resistance 0.42 $m^2\,K\,W^{-1}$ (IES-VE, 2025)

Door ground floor South (mid and high-rise)
Inside: Resistance = 0.1300 $m^2\,K\,W^{-1}$
Frame: Frame percentage 10%, absorptance 0.7, resistance 0.42 $m^2\,K\,W^{-1}$ (IES-VE, 2025)

Door ground floor North (mid and high-rise)
Inside: Resistance = 0.1300 $m^2\,K\,W^{-1}$
Frame: Frame percentage 10%, absorptance 0.7, resistance 0.42 $m^2\,K\,W^{-1}$ (IES-VE, 2025)

Table C.12: Construction layers – All glazing and doors (low-, mid- and high-rise) (IES-VE, 2025)

Material	Thickness (mm)	Conductivity ($W\,m^{-1}\,K^{-1}$)	Resistance ($m^2\,K\,W^{-1}$)	Transmittan	Reflectance (Out/In)	Emissivity (Out/In)
STO_GW01 Outer Plate	4.0	1.060	0.409	0.805	0.289 / 0.837	0.042
Cavity (Argon)	16.0	–	0.7279	–	–	–
STO_GW01 Inner Pane	4.0	1.060	0.783	0.805	0.109 / 0.837	0.837

C.2.5. U-values per building element for every scenario

In this section, the final external resistances and U-values for each building element and scenario are presented. The U-values were calculated in IES-VE based on the external resistance, the resistance of each construction layer, and the internal resistance. Table C.13 lists all external resistance values for each scenario. Subsequently, Table C.14, Table C.15, and Table C.16 present the U-values of all building elements for the low-rise, mid-rise, and high-rise typologies, respectively. For every unique building component, the corresponding materials and properties are described in subsection C.2.4.

Table C.13: Outdoor resistance R_e of wall and window façades for all scenarios. Values are calculated from windspeed (v_s) at 1 m of the façade, emissivity ϵ, surface temperature (T_s) of the wall, and outdoor air temperature (T_a) using the formulas in subsection 4.2.2.

façade	LOW-REF	LOW-GR-EXT	LOW-GW-N	LOW-GW-S	LOW-GW-S-N	LOW-GRASS	LOW-SHRUBS	LOW-TREE-6m-N3S9	LOW-TREE-6m-N9S3	LOW-TREE-11m-N9S5	LOW-TREE-11m-N9S5 + SHRUB + GRASS	LOW-INTEGRATED	MID-REF	MID-TREE-11m-N9S5	MID-GR-EXT	MID-GR-INT	HIGH-REF	HIGH-TREE-11m-N9S5
Wall N	0.0863	0.0864	0.0846	0.0863	0.0847	0.0864	0.0868	0.0869	0.0863	0.0862	0.0866	0.0851	0.0851	0.0850	0.0852	0.0852	0.0844	0.0843
Wall S	0.0860	0.0861	0.0860	0.0854	0.0855	0.0869	0.0869	0.0860	0.0865	0.0861	0.0882	0.0862	0.0853	0.0860	0.0854	0.0854	0.0849	0.0852
Wall E	0.0908	0.0909	0.0909	0.0909	0.0909	0.0910	0.0910	0.0909	0.0909	0.0910	0.0912	0.0913	0.0901	0.0903	0.0901	0.0901	0.0888	0.0889
Wall W	0.0933	0.0935	0.0933	0.0934	0.0935	0.0935	0.0934	0.0934	0.0933	0.0934	0.0936	0.0938	0.0929	0.0931	0.0931	0.0930	0.0933	0.0935
Roof	0.0847	0.0831	0.0847	0.0847	0.0847	0.0848	0.0847	0.0847	0.0847	0.0846	0.0848	0.0832	0.0835	0.0834	0.0830	0.0840	0.0830	0.0829
Window N	0.0891	0.0892	0.0896	0.0892	0.0897	0.0893	0.0897	0.0898	0.0891	0.0890	0.0895	0.0901	0.0879	0.0878	0.0880	0.0880	0.0872	0.0871
Window S	0.0889	0.0891	0.0890	0.0905	0.0906	0.0898	0.0899	0.0889	0.0895	0.0890	0.0912	0.0913	0.0882	0.0889	0.0883	0.0883	0.0878	0.0881

Table C.14: U-value (W $m^{-2}K^{-1}$) for every building element from IES-VE model for low-rise scenarios

Category	Description	LOW-REF	LOW-GR-EXT	LOW-GW-N	LOW-GW-S	LOW-GW-S-N	LOW-GRASS	LOW-SHRUB	LOW-TREE-6m-N3S9	LOW-TREE-6m-N9S3	LOW-TREE-11m-N9S5	LOW-TREE-11m- N9S5 + SHRUB + GRASS	LOW-INTEGRATED
Internal Ceiling/Floor	Internal floors (low and mid-rise)	1.3611	1.3611	1.3611	1.3611	1.3611	1.3611	1.3611	1.3611	1.3611	1.3611	1.3611	1.3611
Ground/Exposed Floor	Ground Exposed Floor (all)	1.0336	1.0336	1.0336	1.0336	1.0336	1.0336	1.0336	1.0336	1.0336	1.0336	1.0336	1.0336
External Window	Window ground floor South (low-rise)	1.1255	1.1252	1.1253	1.1253	1.1233	1.1243	1.1242	1.1255	1.1247	1.1253	1.1225	1.1224
External Window	Window ground floor North (low-rise)	1.2545	1.2543	1.2537	1.2537	1.2535	1.2541	1.2535	1.2533	1.2545	1.2546	1.2538	1.2528
External Window	Window first floor North (low-rise)	1.1252	1.1251	1.1246	1.1246	1.1244	1.1250	1.1244	1.1243	1.1252	1.1253	1.1247	1.1239
External Window	Door ground floor North (low-rise)	1.3062	1.3060	1.3053	1.3053	1.3051	1.3058	1.3051	1.3049	1.3062	1.3064	1.3055	1.3044
External Window	Window first floor South (low-rise)	1.1255	1.1252	1.1253	1.1253	1.1233	1.1243	1.1242	1.1255	1.1247	1.1253	1.1225	1.1224
External Window	Door ground floor South (low-rise)	1.3065	1.3062	1.3064	1.3035	1.3064	1.3049	1.3048	1.3065	1.3055	1.3064	1.3024	1.3023
Internal Partition	Internal Partition wall (all)	1.3072	1.3072	1.3072	1.3072	1.3072	1.3072	1.3072	1.3072	1.3072	1.3072	1.3072	1.3072
Internal Partition	Internal Partition wall between houses (all)	0.6623	0.6623	0.6623	0.6623	0.6623	0.6623	0.6623	0.6623	0.6623	0.6623	0.6623	0.6623
Roof	Roof without greening (low-rise)	0.7137	-	0.7137	0.7137	0.7137	0.7137	0.7137	0.7137	0.7137	0.7137	0.7137	-
Roof	Green Roof; extensive (low-rise)	-	0.5846	-	-	-	-	-	-	-	-		0.5845
External Wall	External Wall South (all)	0.6896	0.6896	0.6896	0.6896	0.6898	0.6892	0.6892	0.6896	0.6893	0.6896	0.6885	0.6895
External Wall	External Wall North (all)	0.6894	0.6894	0.6903	0.6903	0.6902	0.6894	0.6892	0.6992	0.6994	0.6992	0.6993	0.6900
External Wall	External Wall East (all)	0.6873	0.6873	0.6873	0.6873	0.6873	0.6872	0.6872	0.6873	0.6873	0.6873	0.6871	0.6871
External Wall	External Wall West (all)	0.6861	0.6861	0.6861	0.6861	0.6861	0.6860	0.6861	0.6861	0.6861	0.6861	0.6860	0.6859

Table C.15: U-values (W $m^{-2}K^{-1}$) for every building element from IES-VE model for mid-rise scenarios

Category	Description	MID-REF	MID-TREE-11m-N9S5	MID-GR-EXT	MID-GR-INT
Internal Ceiling/Floor	Internal floors (low and mid-rise)	1.3611	1.3611	1.3611	1.3611
External Window	Windows South façade (mid and high-rise)	1.1008	1.1010	1.1007	1.1007
External Window	Windows North façade (mid and high-rise)	1.1005	1.0996	1.1004	1.1004
Ground/Exposed Floor	Ground Exposed Floor (all)	1.0336	1.0336	1.0336	1.0336
Internal Partition	Internal Partition wall (all)	1.3072	1.3072	1.3072	1.3072
Internal Partition	Internal Partition wall between houses (all)	0.6623	0.6623	0.6623	0.6623
Roof	Roof without greening (mid and high-rise)	0.5138	-	-	0.5138
Roof	Green Roof; extensive (mid-rise)	-	0.4887	-	-
Roof	Green Roof; intensive (mid-rise)	-	-	0.4088	-
External Wall	External Wall South (all)	0.6899	0.6896	0.6899	0.6899
External Wall	External Wall North (all)	0.6900	0.6901	0.6900	0.6900
External Wall	External Wall East (all)	0.6876	0.6875	0.6876	0.6876
External Wall	External Wall West (all)	0.6863	0.6862	0.6862	0.6863

Table C.16: U-values (W $m^{-2}K^{-1}$) for every building element from IES-VE model for high-rise scenarios

Category	Description	HIGH-REF	HIGH-TREE-11m- N9S5
Internal Ceiling/Floor	Internal floor (high-rise)	3.1042	3.1042
External Window	Windows north (mid and high-rise)	1.1017	1.1018
External Window	Windows south (mid and high-rise)	1.1010	1.1006
Ground/Exposed Floor	Ground exposed floor (all)	1.0336	1.0336
Internal Partition	Internal Partition wall (all)	1.3072	1.3072
Internal Partition	Internal Partition between houses (all)	0.6623	0.6623
Roof	Roof without greening (mid and high-rise)	0.5139	0.5139
External Wall	External wall south (all)	0.6901	0.6900
External Wall	External wall north (all)	0.6903	0.6904
External Wall	External wall east (all)	0.6883	0.6882
External Wall	External wall west (all)	0.6861	0.6860

Table C.17: Overview of EPW weather input fields

EPW Field Name	Source
Month, Day, Hour, Minute	-
Data Source and Uncertainty Flags	EPW 2009-2023 Cabauw[a]
Dry Bulb Temperature [°C]	ENVI-met
Dew Point Temperature [°C]	Calculated from ENVI-met output with Equation C.1
Relative Humidity [%]	ENVI-met
Atmospheric Station Pressure [Pa]	CESAR Meteo Surface dataset lc1[b]
Extraterrestrial Horizontal Radiation [Wh/m^2]	EPW 2009-2023 Cabauw[a]
Extraterrestrial Direct Normal Radiation [Wh/m^2]	EPW 2009-2023 Cabauw[a]
Horizontal Infrared Radiation Intensity [Wh/m^2]	BSRN Cabauw[c]
Global Horizontal Radiation [Wh/m^2]	BSRN Cabauw[c]
Direct Normal Radiation [Wh/m^2]	BSRN Cabauw[c]
Diffuse Horizontal Radiation [Wh/m^2]	BSRN Cabauw[c]
Global Horizontal Illuminance [lux]	Radiation *120
Direct Normal Illuminance [lux]	Radiation * 110
Diffuse Horizontal Illuminance [lux]	Radiation * 110
Zenith Luminance [Cd/m^2]	NaN
Wind Direction [°]	constant 85°
Wind Speed [m/s]	ENVI-met
Total Sky Cover [tenths]	KNMI file * 1.25[d]
Opaque Sky Cover [tenths]	NaN
Visibility [km]	10
Ceiling Height [m]	1500
Present Weather Observation	9
Present Weather Codes	NaN
Precipitable Water [mm]	30
Aerosol Optical Depth	0.15 (Boers et al., 2015)
Snow Depth [cm]	0
Days Since Last Snowfall	99
Albedo	identical to ENVI-met
Liquid Precipitation Depth [mm]	0
Liquid Precipitation Quantity [hr]	0

[a] Data from NLD_UT_Cabauw.Tower.063480_TMYx.2009-2023 (Climate.OneBuilding, n.d.-a)
[b] Data from CESAR Meteo surface dataset lc1 (KNMI, 2019)
[c] Data from BSRN irradiance data (Knap, 2019)
[d] Data from KNMI de Bilt (KNMI, 2025)

D

IES-VE model explanation

This appendix provides a detailed explanation of the equations used by IES-VE to calculate the indoor thermal environment. In IES-VE, the *ApacheSim* module is employed for indoor climate calculation. ApacheSim uses a dynamic heat balance model that computes the thermal response of a building zone based on the first law of thermodynamics. The fundamental governing equation is:

$$\frac{dE_{\text{zone}}}{dt} = \sum Q_{\text{in}} - \sum Q_{\text{out}} \tag{D.1}$$

Where:

- dE_{zone}: Change in internal energy of the zone air [J]
- dt: Time step (10 min) over which the energy balance is evaluated [s]
- Q_{in}: Total incoming heat fluxes per zone, including solar gains, internal gains, and heating system input [W]
- Q_{out}: Total outgoing heat fluxes per zone, such as convective, conductive, and ventilation losses [W]

This net energy change drives the zone air temperature. The main heat transfer terms contributing to the balance are as follows:

$$\frac{dE_{\text{zone}}}{dt} = Q_{\text{cond}} + Q_{\text{conv}} + Q_{\text{LW}} + Q_{\text{vent}} + Q_{\text{int}} + Q_{\text{SW}} + Q_{\text{HVAC}} \tag{D.2}$$

Where:

- dE_{zone}: Change in internal energy of the zone air [J]
- dt: Time step (10 min) over which the energy balance is evaluated [s]
- Q_{cond}: Heat flux through building fabric (walls, roof, floor) [W]
- Q_{conv}: Convective exchange with indoor surfaces [W]
- Q_{LW}: Net longwave radiative exchange between surfaces [W]
- Q_{vent}: Infiltration or mechanical ventilation exchange [W]
- Q_{int}: Internal latent + sensible gains (occupants, lighting, equipment) [W]
- Q_{SW}: Shortwave radiation from sun through windows or absorbed by surfaces) [W]
- Q_{HVAC}: Heating or cooling supplied by the building system [W]

ApacheSim solves this energy balance at each simulation time step to determine the zone air temperature and HVAC loads. The model employs a nodal network for surface and air nodes, typically assuming one well-mixed air node per zone (IES-VE, 2021a). The following sections provide further details on each heat transfer component.

Heat Conduction and Storage

Heat transfer through building elements (walls, roofs, and floors) is governed by the one-dimensional transient heat diffusion equation (CIBSE, 2006):

$$\rho c \frac{\partial T}{\partial t} = \lambda \frac{\partial^2 T}{\partial x^2} \tag{D.3}$$

$$\rho \ [\mathrm{kg\,m^{-3}}], \quad c \ [\mathrm{J\,kg^{-1}\,K^{-1}}], \quad T \ [\mathrm{K}], \quad t \ [\mathrm{s}], \quad \lambda \ [\mathrm{W\,m^{-1}\,K^{-1}}], \quad x \ [\mathrm{m}]$$

Air temperature dynamics within zones are described by:

$$Q_{\text{net}} = \rho_{\text{air}} c_p V \frac{dT_{\text{air}}}{dt} \tag{D.4}$$

$$Q_{\text{net}} \ [\mathrm{W}], \quad \rho_{\text{air}} \ [\mathrm{kg\,m^{-3}}], \quad c_p \ [\mathrm{J\,kg^{-1}\,K^{-1}}], \quad V \ [\mathrm{m^3}], \quad T_{\text{air}} \ [\mathrm{K}], \quad t \ [\mathrm{s}]$$

In IES-VE, the default values for air properties are:

$$\rho_{\text{air}} = 1.2 \ [\mathrm{kg\,m^{-3}}], \quad c_p = 1006 \ [\mathrm{J\,kg^{-1}\,K^{-1}}]$$

These values represent dry air at 20 °C and 1 atm, as used in the ApacheSim module for dynamic thermal simulations (CIBSE, 2006; IES-VE, 2021a).

Convective Heat Transfer

ApacheSim distinguishes between natural and forced convection. Convective heat exchange is generally expressed as:

$$q_{\text{conv}} = h_c (T_{\text{air}} - T_{\text{surface}}) \tag{D.5}$$

$$q_{\text{conv}} \ [\mathrm{W\,m^{-2}}], \quad h_c \ [\mathrm{W\,m^{-2}\,K^{-1}}], \quad T_{\text{air}}, T_{\text{surface}} \ [\mathrm{K}]$$

Convective heat transfer coefficients (h_c) can be fixed or calculated dynamically using empirical correlations, such as those proposed by Alamdari and Hammond (1983).

Radiative Heat Transfer

Long-wave thermal radiation between interior surfaces is simplified using a mean radiant temperature (MRT) approach:

$$q_{\text{rad}} = h_r (T_{\text{surface}} - T_{\text{MRT}}) \tag{D.6}$$

$$q_{\text{rad}} \ [\mathrm{W\,m^{-2}}], \quad h_r \ [\mathrm{W\,m^{-2}\,K^{-1}}], \quad T_{\text{surface}}, T_{\text{MRT}} \ [\mathrm{K}]$$

Radiative heat transfer coefficients and MRT are computed assuming uniform emissivity and well-mixed surface conditions (CIBSE, 2006).

Ventilation and Infiltration

Ventilation and infiltration heat transfer is modelled using the mass flow rate and temperature difference between supply and room air:

$$Q_{\text{vent}} = \dot{m} c_p (T_{\text{sup}} - T_{\text{room}}) \tag{D.7}$$

$$Q_{\text{vent}}\ [\text{W}], \quad \dot{m}\ [\text{kg s}^{-1}], \quad c_p\ [\text{J kg}^{-1}\,\text{K}^{-1}], \quad T_{\text{sup}}, T_{\text{room}}\ [\text{K}]$$

These flows can be constant, scheduled, demand-controlled, or driven by pressure differences (IES-VE, 2021a).

Internal Heat Gains and HVAC Control

Internal gains from occupants, lighting, and equipment are defined through schedules and consist of both sensible and latent loads. Heating and cooling are controlled by temperature setpoints and the system's capacity limits:

$$T_{\text{room}} \leq T_{\text{heat,set}} \ \rightarrow \ Q_{\text{heat,max}} T_{\text{room}} \geq T_{\text{cool,set}} \ \rightarrow \ Q_{\text{cool,max}}$$

$$T_{\text{room}}\ [\text{K}], \quad T_{\text{heat,set}}, T_{\text{cool,set}}\ [\text{K}], \quad Q_{\text{heat,max}}, Q_{\text{cool,max}}\ [\text{W}]$$

Setpoints ensure that indoor temperatures remain within defined comfort limits. In this thesis, these are used solely for predicting cooling loads in the building. For Hypothesis 3, which concerns the determination of the cooling load for each scenario, a cooling setpoint temperature $T_{\text{cool,set}}$ of 25 °C (298.15 K) was applied.

Solar Gains

Solar radiation incident on building surfaces is computed from weather data and accounts for surface orientation, tilt, shading, and material optical properties (IES-VE, 2021a). Direct solar irradiance on a surface is calculated as:

$$I_{\text{direct,surface}} = I_{\text{beam}} \cdot \cos(\theta) \tag{D.8}$$

$$I_{\text{direct,surface}}, I_{\text{beam}}\ [\text{W m}^{-2}], \quad \theta\ [\text{rad}]$$

E

ENVI-met code

In this Appendix the python code used in Leonardo 5.8.0 is stated. This code is used to extract average data for outdoor air temperature and PET for Area 1 and 2.

```
""" title=Compare Locations"""
""" category=Atmosphere Data """
""" description=This script takes two areas, a file path and a data index as input and
    creates a comparison between these two areas for the selected variable """
""" app=Leonardo """
""" context=GridExplor_AT,GridExplor_POLU """
""" output=svg """
""" datafile1=Atmosphere EDX File, Atmosphere EDX|*.EDX """

from envimet import DataFile
from envimet import EDXFile
from envimet import EDXFileSeries
from envimet import datastudio
from envimet import svgimage

import numpy as np
import matplotlib.pyplot as plt
from io import StringIO
import csv

# if two figures are generated, we need two figfile streams
figfile = StringIO()
figfile2 = StringIO()

# ====================== SETTINGS ======================

# Location Area 1 bounding box
x1_from, x1_to = 12, 20
y1_from, y1_to = 8, 21
z1_from, z1_to = 5, 5

# Location Area 2 bounding box
x2_from, x2_to = 2, 30
y2_from, y2_to = 3, 26
z2_from, z2_to = 5, 5

# helper functions
identity = lambda x: x

def getDates(a, b, x):
    res = []
    for index in range(a, b+1, x):
        DataFile.LinkEDXfileInSeries(EDXFileSeries, index)
        res.append(DataFile.associatedEDXFile.simdate)
    return res

# ====================== INITIALIZE ======================

# Load selected EDX file
EDXFile.ReadFile(datafile.value)
```

```
folder = EDXFile.GetRootFolder()
EDXFileSeries.ReadFolder(folder, EDXFile.SimBaseID)

# Define timespan
time_from = 0
time_to = EDXFileSeries.CountEDXFiles()-1

print("-----------------------------------------------------")
print("Simulation Data ")
print("Base Folder: "+folder)
print("Sim ID: "+EDXFile.SimBaseID)
print("Title: "+ EDXFile.Title)
print("Simulated Time Steps: "+str(time_to))
print("-----------------------------------------------------")

# Initialize data arrays
data1 = np.empty([time_to - time_from + 1, (x1_to - x1_from + 1)*(y1_to - y1_from + 1)*(z1_to - z1_from + 1)], dtype=float)
data2 = np.empty([time_to - time_from + 1, (x2_to - x2_from + 1)*(y2_to - y2_from + 1)*(z2_to - z2_from + 1)], dtype=float)
timesteps = []

startEDXFile = EDXFileSeries.GetEDXFile(time_from)
startDate, startTime = startEDXFile.simdate, startEDXFile.simtime
endDate, endTime = EDXFileSeries.GetEDXFile(time_to).simdate, EDXFileSeries.GetEDXFile(time_to).simtime

print('Display Interval: ')
print('  From: '+startDate+'  '+startTime)
print('  To:   '+endDate+  '  '+endTime)
print("-----------------------------------------------------")

DataFile.LinkEDXFile(startEDXFile)

# Select variable
varlist = [DataFile.GetVarNameAndUnit(i) for i in range(DataFile.CountVariables())]
data_index = datastudio.SelectOptionsDlgIdx("Variable for Analysis","Select Variable to analyse:", varlist)

# ====================== LOAD DATA ======================
xTick_labels = []

for t in range(time_to - time_from + 1):
    DataFile.LinkEDXfileInSeries(EDXFileSeries, t + time_from)
    xTick_labels.append(DataFile.associatedEDXFile.simtime[0:5])
    timesteps.append(str(t))
    x = 0
    for i in range(x1_to - x1_from + 1):
        for j in range(y1_to - y1_from + 1):
            for k in range(z1_to - z1_from + 1):
                data1[t][x] = DataFile.GetDataPointValue(data_index, i + x1_from, j + y1_from, k + z1_from)
                x += 1
    x = 0
    for i in range(x2_to - x2_from + 1):
        for j in range(y2_to - y2_from + 1):
            for k in range(z2_to - z2_from + 1):
                data2[t][x] = DataFile.GetDataPointValue(data_index, i + x2_from, j + y2_from, k + z2_from)
                x += 1

# Calculate min, max, mean
min_vals1, max_vals1, mean_vals1 = np.nanmin(data1, axis=1), np.nanmax(data1, axis=1), np.nanmean(data1, axis=1)
min_vals2, max_vals2, mean_vals2 = np.nanmin(data2, axis=1), np.nanmax(data2, axis=1), np.nanmean(data2, axis=1)

diff_vals = mean_vals1 - mean_vals2

# ====================== PLOT 1 ======================
dTitle = 'Comparison of ' + DataFile.GetVarNameAndUnit(data_index) + ' between location A and
```

```
     B' if diagramtitle.value == '' else diagramtitle.value

figure = plt.figure(facecolor="lightblue")
ori = 210
plots1 = [[],[]]

count = 1
for i in plots1:
    i.append(figure.add_subplot(ori + count))
    count += 1

# Location A
ax1 = plots1[0][0]
ax1.plot(timesteps, min_vals1, color='blue',marker='o', label='Minimum values')
ax1.plot(timesteps, max_vals1, color='red', marker='x',label='Maximum values')
ax1.plot(timesteps, mean_vals1, color='green',marker='o' , label='Mean values')
ax1.fill_between(timesteps, max_vals1, min_vals1, alpha=0.2)
ax1.set(xlabel='Time', ylabel=DataFile.GetVarNameAndUnit(data_index), title='Location A : ' +
     DataFile.GetVarNameAndUnit(data_index) + f' ({startDate} {xTick_labels[0]}:00h - {
    endDate} {xTick_labels[-1]}:00h)')
ax1.legend(loc="upper right")
ax1.grid()

# Location B
ax1 = plots1[1][0]
ax1.plot(timesteps, min_vals2, color='blue', label='Minimum values')
ax1.plot(timesteps, max_vals2, color='red', label='Maximum values')
ax1.plot(timesteps, mean_vals2, color='green', label='Mean values')
ax1.fill_between(timesteps, max_vals2, min_vals2, alpha=0.2)
ax1.set(xlabel='Time', ylabel=DataFile.GetVarNameAndUnit(data_index), title='Location B : ' +
     DataFile.GetVarNameAndUnit(data_index) + f' ({startDate} {xTick_labels[0]}:00h - {
    xTick_labels[-1]}:00h)')
ax1.legend(loc="upper right")
ax1.grid()

figure.suptitle(dTitle)
figure.set_size_inches(20, 20)
plt.xticks(timesteps, xTick_labels)
plt.rcParams["figure.figsize"] = (75, 50)
plt.subplots_adjust(left = 0.125, right = 0.9, bottom = 0.1, top = 0.9, wspace = 0.2, hspace
    = 0.3)

plt.savefig(figfile, format="svg")
figdata_svg = figfile.getvalue()
svgimage.SvgText = figdata_svg
datastudio.AddSVGToLightbox('Locations Details')

# ====================== PLOT 2 ======================
figure2 = plt.figure(facecolor="lightyellow")
plots2 = [[],[]]
count = 1
for i in plots2:
    i.append(figure2.add_subplot(ori + count))
    count += 1

# Mean comparison
ax2 = plots2[0][0]
ax2.plot(timesteps, mean_vals1, color='green', label= 'Mean values Location A')
ax2.plot(timesteps, mean_vals2, color='blue', label= 'Mean values Location B ')
ax2.fill_between(timesteps, mean_vals1, mean_vals2, alpha=0.2)
ax2.set(xlabel='Time', ylabel=DataFile.GetVarNameAndUnit(data_index), title=DataFile.
    GetVarNameAndUnit(data_index) + f' ({startDate} {xTick_labels[0]}:00h - {endDate} {
    xTick_labels[-1]}:00h)')
ax2.legend(loc="upper right")
ax2.grid()

# Difference
ax2 = plots2[1][0]
ax2.bar(timesteps, diff_vals, zorder=3)
ax2.set(xlabel='Time', ylabel='Difference (A-B) ' + DataFile.GetVarNameAndUnit(data_index),
    title='Difference (A-B) ' + DataFile.GetVarNameAndUnit(data_index) + f' ({startDate} {
```

```
    xTick_labels[0]}:00h - {xTick_labels[-1]}:00h)')
ax2.grid(zorder=0)

figure2.suptitle(dTitle)
figure2.set_size_inches(20, 20)
plt.xticks(timesteps, xTick_labels)
plt.rcParams["figure.figsize"] = (75, 50)
plt.subplots_adjust(left = 0.125, right = 0.9, bottom = 0.1, top = 0.9, wspace = 0.2, hspace
    = 0.3)

plt.savefig(figfile2, format="svg")
figdata_svg = figfile2.getvalue()
svgimage.SvgText = figdata_svg
datastudio.AddSVGToLightbox('Locations Compared')
datastudio.MessageDlg("Compare Locations2","Finished! \nThe graphics are copied in your
    Lightbox!")

# ====================== EXPORT TO CSV ======================
csv_filename = "REF_comparison_potential_temperature.csv"
n_steps = time_to - time_from + 1

with open(csv_filename, mode="w", newline="") as f:
    writer = csv.writer(f)
    # header
    writer.writerow([
        "Datetime",
        "ScenarioA_Min",
        "ScenarioA_Mean",
        "ScenarioA_Max",
        "ScenarioB_Min",
        "ScenarioB_Mean",
        "ScenarioB_Max",
        "AbsoluteDifference"
    ])

    for t in range(n_steps):
        # link EDX file to get date and time
        DataFile.LinkEDXfileInSeries(EDXFileSeries, t + time_from)
        date_str = DataFile.associatedEDXFile.simdate
        time_str = DataFile.associatedEDXFile.simtime[0:5]
        datetime_str = f"{date_str} {time_str}"

        # write values
        writer.writerow([
            datetime_str,
            min_vals1[t],
            mean_vals1[t],
            max_vals1[t],
            min_vals2[t],
            mean_vals2[t],
            max_vals2[t],
            diff_vals[t]
        ])

datastudio.MessageDlg("CSV Export", f"CSV-bestand is opgeslagen als:\n{csv_filename}")
```

F

Additional output ENVI-met

This appendix presents additional ENVI-met outputs related to the grid sensitivity analysis.

F.1. Grid sensitivity analysis

The grid sensitivity analysis aims to determine the optimal spatial resolution (1 m, 2 m, or 3 m) in the x and y dimensions for the grid cells. In all scenarios, the z-resolution remains fixed at 1 m. The reference case employed involves a low-rise strip typology building combined with urban trees and road surfaces. A representation of the reference case can be seen in Figure F.1a. Sensitivity analysis for the three resolutions is conducted at three specific time points: 11:00, to evaluate the impact of grid resolution on the diurnal temperature increase; 14:00, commonly the peak temperature hour, although during very hot days this peak shift to a subsequent time (RIVM, 2023); and 17:00, to account for late afternoon temperatures. The sensitivity analysis focuses on the cells within 6 m of the building as these are the most important in this study, see Figure F.1b.

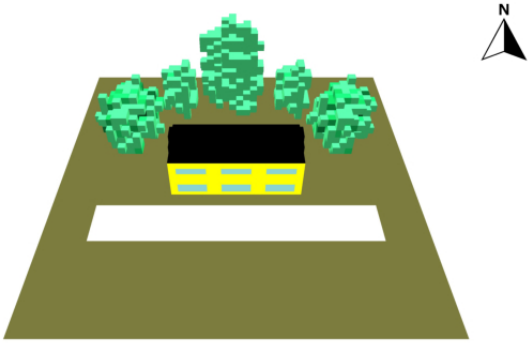

(a) Reference case in ENVI-met Spaces.

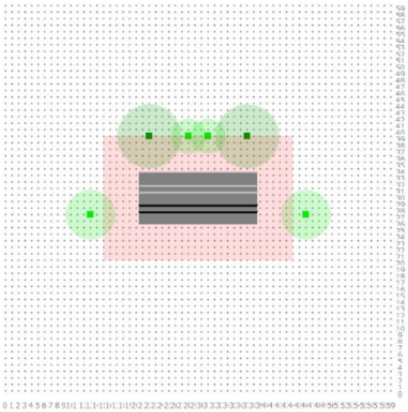

(b) Grid cells within 6 m of the building are used to compare resolution 1, 2 and 3 m.

The results of the grid analysis can be visualised in Figure F.2. It can be seen that the 1 m resolution catches the most detailed effects. The 3m resolution loses some detail in comparison with the 2 m resolution. As stated in chapter 4 a 2 m resolution was selected for this study. In figure Figure F.3a until Figure F.5c the grid sensitivity runs are visualised in a larger plot with a more detailed colorbar.

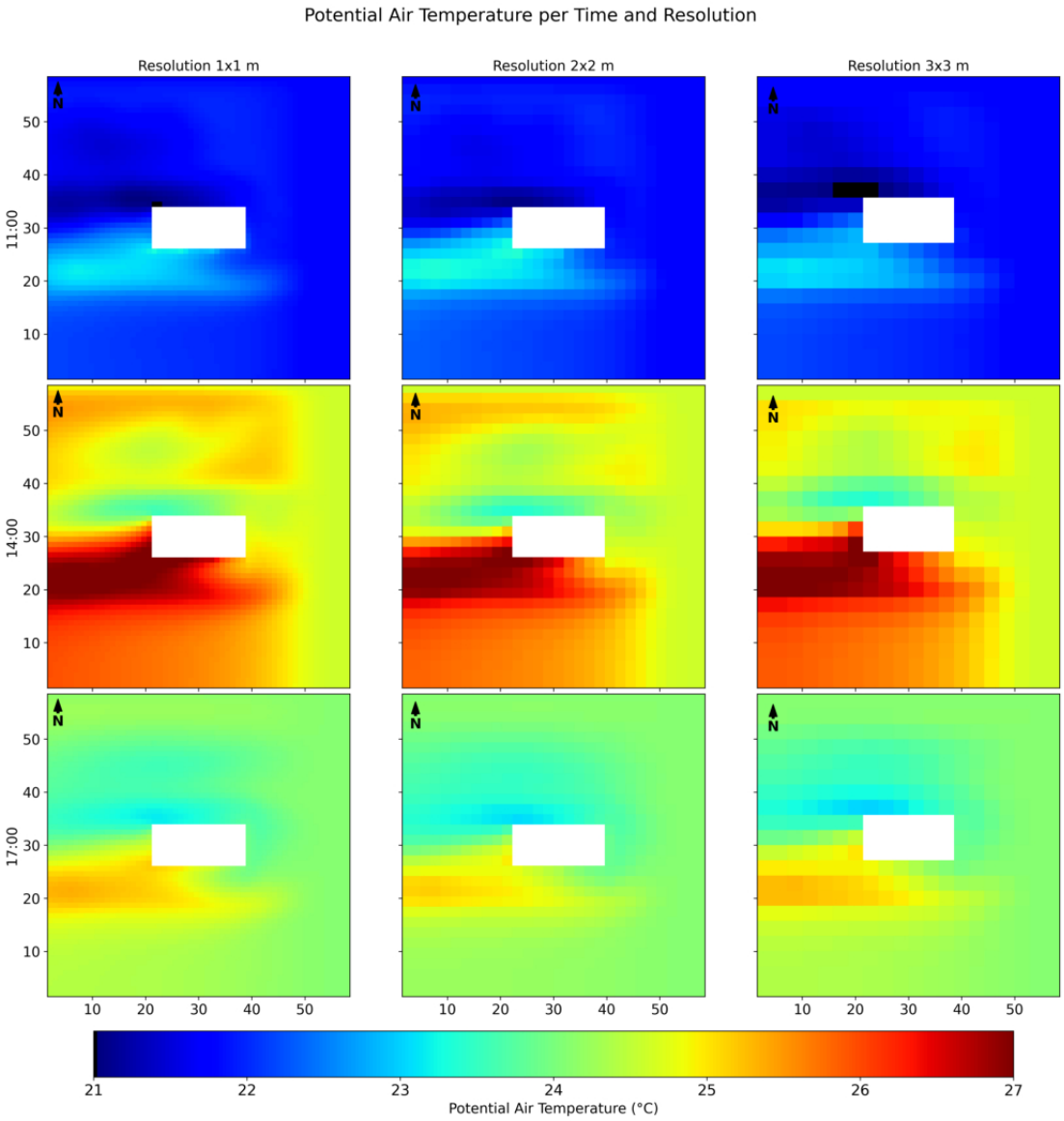

Figure F.2: Potential Air Temperature for 23-08-2019 at 11:00, 14:00 and 17:00 with resolution 1,2 and 3 m (height 1.5 m).

Grid sensitivity all plots

More detailed plots are visualised in this section.

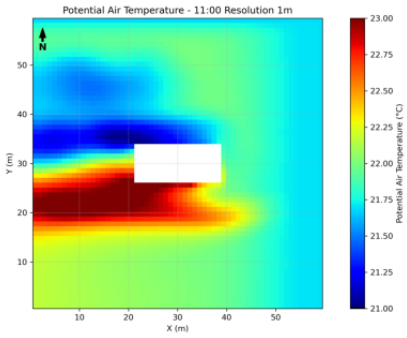

(a) 11:00 — Res 1 m

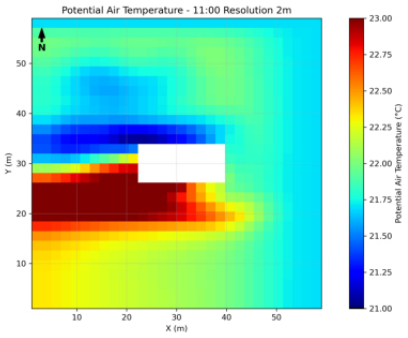

(b) 11:00 — Res 2 m

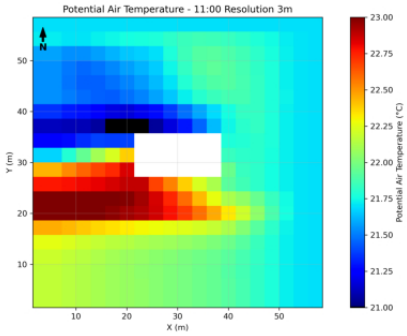

(c) 11:00 — Res 3 m

Figure F.3: Potential Air Temperature for 23-08-2019 at 11:00 (height 1.5 m).

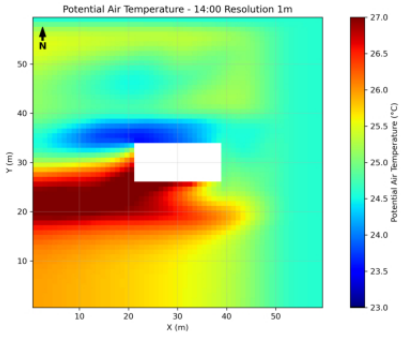

(a) 14:00 — Res 1 m

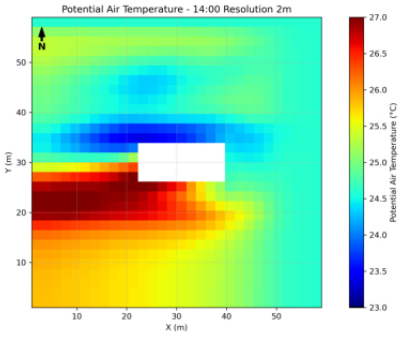

(b) 14:00 — Res 2 m

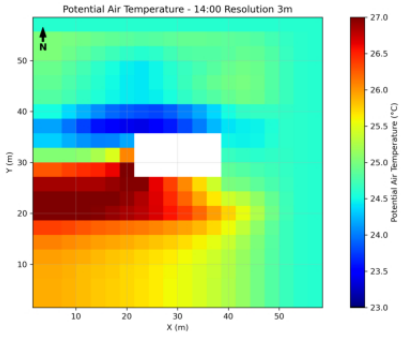

(c) 14:00 — Res 3 m

Figure F.4: Potential Air Temperature for 23-08-2019 at 14:00 (height 1.5 m).

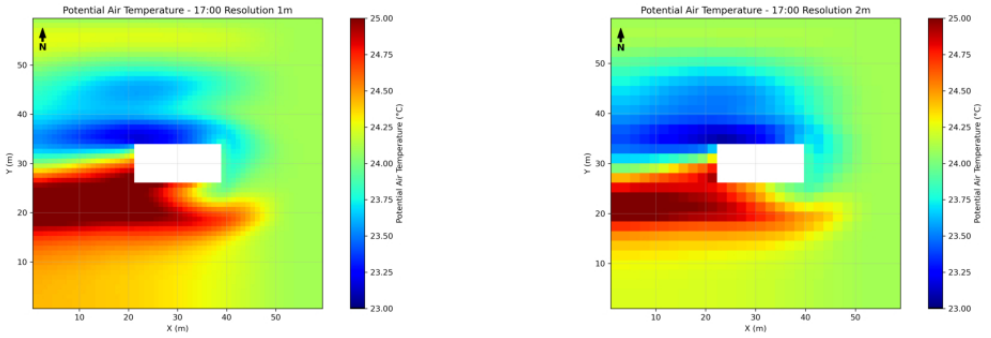

(a) 17:00 — Res 1 m

(b) 17:00 — Res 2 m

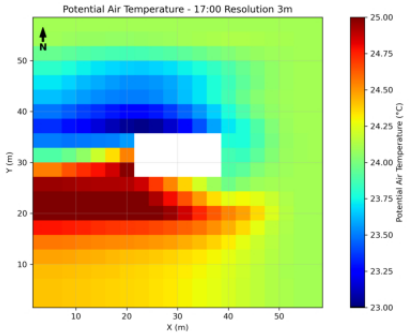

(c) 17:00 — Res 3 m

Figure F.5: Potential Air Temperature for 23-08-2019 at 17:00 (height 1.5 m).

G

Effect of shading structures

The low-rise building analysed in this study has a glazing percentage of 26.8% for the north facade and 29% for the south facade. Mid and high-rise both have a glazing percentage of 33.3%. This relatively high proportion of transparent façade allows substantial solar radiation to enter the building during a heatwave. To assess potential mitigation measures, additional scenarios incorporating shading structures were introduced. In this study, a sunshade of 1.5 m, inclined at 20° to the façade, was modelled. Such a sunshade reduces the amount of direct solar radiation entering the building, thereby lowering indoor air temperatures.

Three scenarios were compared to evaluate the additional effect of shading structures: LOW-REF, LOW-TREE-11m-N9S5, and LOW-INTEGRATED.

G.1. Indoor temperature

An additional simulation was conducted in which shading structures were added to every south-facing window of the reference scenario. For LOW-REF, the shading structures reduced the average indoor air temperature across all rooms by 1.05 °C, while the maximum indoor temperature reduction, occurring in a single room (S-M-R-2 or S-M-L-2), was 1.62 °C. This indicates that, for the low-rise building, shading structures are as effective as the integrated greening scenario in reducing average indoor temperatures and even more effective in lowering peak indoor temperatures.

The best-performing low-rise greening scenario, LOW-INTEGRATED, reduced the average and maximum indoor air temperatures by 1.12 °C and 1.20 °C, respectively. When shading structures were added, these reductions increased to 1.74 °C and 3.93 °C. This demonstrates that the combined effect of evaporative cooling from vegetation and direct solar blocking by shading provides the most substantial overall cooling. It also suggests that the 11 m trees used in the LOW-INTEGRATED scenario could not fully prevent direct solar radiation from entering the south-facing rooms on the second floor (S-M-R-2 and S-M-L-2), leading to very high peak temperature reductions. Higher trees or a combination with shading structures are needed to reduce this peak temperature in the building.

A similar pattern was observed in the LOW-TREE-11m-N9S5 scenario. The average and maximum indoor temperatures decreased by 0.62 °C and 0.95 °C, respectively. When shading structures were added, these reductions increased to 1.26 °C and 1.74 °C. Trees provide both shading and evaporative cooling, but in this case their influence on the second floor was limited: the height and placement of the trees prevented continuous shading of the windows throughout the day. Consequently, their cooling effect was smaller than that of dedicated shading structures.

The importance of shading structures is also evident in the high-rise scenario. As shown in Table 5.1, the average and maximum indoor air temperatures of the high-rise building were already substantially lower compared with low-rise (2.82 °C, 6.33 °C) and mid-rise (2.22 °C, 7.00 °C). This can be attributed to the gallery on the south façade, which effectively functions as a continuous shading element and significantly reduces solar gains.

In summary, greening measures reduce indoor air temperatures during heatwaves, but only when combined with shading structures can the indoor environment be cooled effectively.

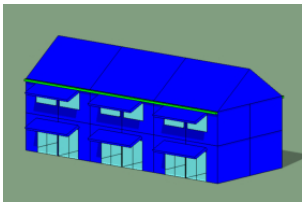

(a) Sunshade of 1.5 m with an angle of 20° visualised on the low-rise strip building.

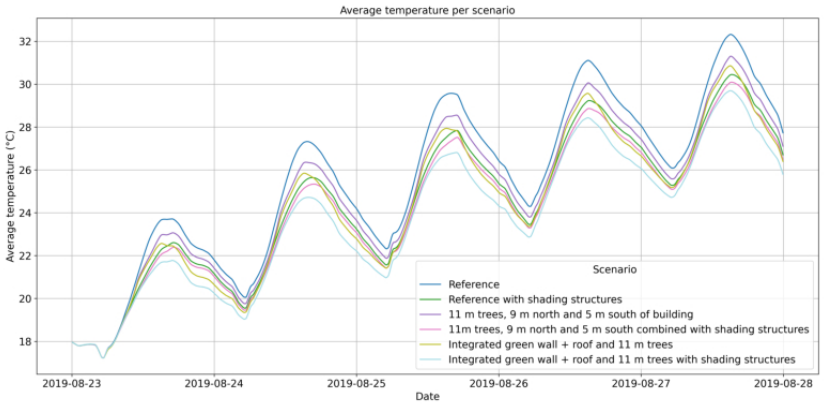

(b) Effect of the sunshade on average room temperature for the scenarios: reference, 11 m trees (9 m north, 5 m south), and integrated greening.

Figure G.1: Effect of shading structures on average indoor temperature.

G.2. Cooling load

For indoor air temperature, the addition of shading structures resulted in the largest reduction in both average and peak conditions. A similar pattern was observed for cooling energy demand:

- In the LOW-REF scenario, it decreased from 114.3 to 70.7 kWh.
- In the LOW-TREE-11M-N9S5 scenario, it decreased from 87.3 to 62.6 kWh.
- In the LOW-INTEGRATED scenario, the total cooling load decreased from 77.9 to 54.1 kWh.

These results show that while greening already considerably reduces the cooling load, the additional impact of shading structures is substantial. For the LOW-TREE-11M-N9S5 scenario, the cooling load reduction increased from 23.6% without shading to 45.2% with the sunshade applied. Similarly, for the LOW-INTEGRATED scenario, the reduction increased from 31.9% to 52.7% when shading structures were added. These findings highlight that, especially when combined, shading and greening provide a substantial reduction in both indoor air temperature and cooling energy demand.

H

AI statement

Artificial intelligence (AI) tools were used throughout this thesis to support the research and writing process. ChatGPT (OpenAI, GPT-5 model) was employed to improve readability and to check grammar and sentence structure. All edits suggested by ChatGPT were critically reviewed and manually implemented by the author.

Elicit was used alongside Scopus, the TU Delft Library, and Google Scholar used to find scientific papers, especially early in the project, during the literature review phase.

ChatGPT helped debug Python code used for data analysis and post-processing simulation findings. Furthermore, it was consulted for feedback on draft sections of the report, including the clarity of methods and the organisation of results.

No AI-generated text or figures were used as direct sources in this thesis, and all references and analyses were independently verified. At all times, the author remained fully responsible for the analytical reasoning, interpretation of results, and final content presented in this work.

I

Reference buildings

The low-rise reference building is shown in Figure I.1. Blueprints of the low-rise dwellings were available, enabling a detailed replication of the geometry and construction. These buildings, located at *The Green Village* in Delft, represent a typical 1970s terraced housing typology commonly found in the Netherlands. For the mid-rise and high-rise typologies, no specific buildings were modelled due to the unavailability of blueprints. Instead, average geometric and material parameters for a representative mid and high-rise Dutch residential buildings were used.

Figure I.1: Reference houses used for the low-rise typology. Blueprints of these dwellings were used to replicate the buildings as accurately as possible in ENVI-met and IES-VE.